UC Irvine
UC Irvine Electronic Theses and Dissertations

Title
Numerical modeling and remote sensing of global water management systems: Applications for land surface modeling, satellite missions, and sustainable water resources management

Permalink
https://escholarship.org/uc/item/17t791r6

Author
Solander, Kurt

Publication Date
2016

Peer reviewed|Thesis/dissertation

eScholarship.org Powered by the California Digital Library
University of California

UNIVERSITY OF CALIFORNIA, IRVINE

Numerical modeling and remote sensing of global water management systems: Applications for land surface modeling, satellite missions, and sustainable water resources management

DISSERTATION

submitted in partial satisfaction of the requirements
for the degree of

DOCTOR OF PHILOSOPHY

in
Earth System Science

by

Kurt C. Solander

Dissertation Committee:

Professor James S. Famiglietti, Chair
Professor James T. Randerson
Professor Charles Zender

2016

© 2016 Kurt C. Solander

DEDICATION

To

a better future for myself and humanity

TABLE OF CONTENTS

	Page
LIST OF FIGURES	**v**
LIST OF TABLES	**vii**
ACKNOWLEDGMENTS	**viii**
CURRICULUM VITAE	**ix**
ABSTRACT OF THE DISSERTATION	**xiii**
CHAPTER 1: Introduction	**1**
CHAPTER 2: Development of a reservoir model for a global Land Surface Model (LSM)	**9**
2.1 Introduction	**9**
2.2 Global and California Reservoir Modeling	**11**
2.3 Materials and Methods	**17**
2.3.1 California Study Area	**17**
2.3.2 Data Sources	**17**
2.3.3 Model Criteria	**18**
2.3.4 Model Development and Selection	**20**
2.3.5 Parameter Optimization	**25**
2.3.6 Parameter Generalization and Model Validation	**26**
2.4 Results	**27**
2.5 Discussion	**30**
2.5.1 Model Selection	**30**
2.5.2 Model Calibration and Generalization	**31**
2.5.3 Model Caveats and Omissions	**33**
2.5.4 Climate Adaptive Capability	**35**
2.5.5 Expected Utility in a Land-Surface Scheme	**38**
2.6 Conclusion	**40**
CHAPTER 3: How well will SWOT observe global reservoirs?	**58**
3.1 Introduction	**58**
3.2 Methods	**65**
3.2.1 Data Sources	**65**
3.2.2 Temporal Analysis	**65**
3.2.3 Spatial Analysis: Theoretical Reservoir Experiments	**66**
3.2.4 Spatial Analysis: Actual Reservoir Experiments	**71**

3.3 Results **72**
3.3.1 Temporal Analysis **72**
3.3.2 Spatial Analysis: Theoretical Reservoir Experiments **73**
3.3.3 Spatial Analysis: Actual Reservoir Experiments **74**
3.4 Discussion **75**
3.4.1 Temporal Analysis **75**
3.4.2 Spatial Analysis: Theoretical Reservoir Experiments **76**
3.4.3 Spatial Analysis: Actual Reservoir Experiments **80**
3.4.4 Study Limitations and Caveats **82**
3.5 Conclusions **84**

CHAPTER 4: Examining sustainable water use using observations from GRACE over the continental United States **103**

4.1 Introduction **103**
4.2 Methods **107**
4.3 Results **111**
4.4 Discussion **113**
4.4.1 Results Highlights and Comparisons **113**
4.4.2 Shortcomings and Limitations **115**
4.4.3 Ecological Implications **118**
4.5 Conclusions **119**

CHAPTER 5: Conclusions **130**

5.1 Summary of Results **131**
5.2 Implications for Future Work **133**

REFERENCES **135**

APPENDIX A: SWOTsim Instrument Simulator Settings and Parameters **143**

LIST OF FIGURES

Page

Chapter 2

Figure 2.1 Map of the study reservoirs 48

Figure 2.2 Conceptual diagram of reservoir flow behavior 49

Figure 2.3 Simulated and observed time series for calibration reservoirs 50

Figure 2.4 Simulated and observed climatology for calibration reservoirs 51

Figure 2.5 Parameter domain plots used in Nelder Mead optimization 52

Figure 2.6 Parameter pareto fronts from Nelder Mead optimization 53

Figure 2.7 Generalized parameter curves 54

Figure 2.8 Simulated and observed time series for generalized reservoirs 55

Figure 2.9 Simulated and observed climatology for generalized reservoirs 56

Figure 2.10 Equation usage and mean annual storage from climate adaptive experimental simulations 57

Chapter 3

Figure 3.1 Map of the study reservoirs and repeat orbit paths 91

Figure 3.2 Cumulative distribution function of global reservoir surface area 92

Figure 3.3 Temporal analysis time series for virtual and in-situ storage records 93

Figure 3.4 Temporal analysis RMSE and NSE results 94

Figure 3.5 Temporal analysis confidence interval results 95

Figure 3.6 Area and height bias based on reservoir size 96

Figure 3.7 Area and height bias based on reservoir shape and orientation 97

Figure 3.8 Area and height bias based on surrounding topography of reservoir 98

Figure 3.9 Area and height bias based on partial swath coverage of reservoir 99

Page

Chapter 3

Figure 3.10 Area and height bias for actual reservoir simulations 100

Figure 3.11 SWOT repeat orbit pass frequencies by reservoir area 101

Figure 3.12 Estimation of area from ellipses using theoretical reservoir results 102

Chapter 4

Figure 4.1 Conceptual diagram demonstrating how to calculate TWA 126

Figure 4.2 Annual 2003-2015 CWU:TWA over the continental United States 127

Figure 4.3 2003-2015 CWU:TWA time series and trends for the southwest two-digit HUC basins 128

Figure 4.4 2003-2015 CWU:TWA statistics over the continental United States 129

LIST OF TABLES

Page

Chapter 2

Table 2.1 Summary of reservoir hydrology and spatial information 42

Table 2.2 Reservoir outflow model description 43

Table 2.3 Reservoir outflow model performance 44

Table 2.4 Model performance statistics for optimized parameters 45

Table 2.5 Model performance statistics for generalized parameters 46

Table 2.6 Performance statistics and rank according to reservoir storage coefficient of variation and inflow to storage capacity 47

Chapter 3

Table 3.1 Summary of theoretical reservoir geospatial information 88

Table 3.2 Summary of actual reservoir hydrology and spatial information 89

Table 3.2 Reservoir shape and orientation test area and bias 90

Chapter 4

Table 4.1 Two-digit HUC basin areas over the continental United States 121

Table 4.2 CWU:TWA parameter sensitivity analysis 122

Table 4.3 CWU:TWA water balance statistics 124

Table 4.4 Maximum water use reductions to achieve sustainability 125

ACKNOWLEDGMENTS

Firstly, I would like to express the deepest appreciation to my committee chair, Professor James S. Famiglietti for his vision, support, and ongoing conversation inspiring hope that maybe this will be the Red Sox year!

I would also like to thank my other committee members Professor Charles Zender, Professor James T. Randerson, Professor Keith Moore, and Professor Brett Sanders for their help and intellectual support along the way. Thank you to my research group, and in particular, Hrishi Chandanpurkar, Aimée Gibbons, Jamiat Nanteza, and A. J. Purdy. This would not have been possible without all of you. Thanks to the faculty, staff, post-docs, and other graduate students of Earth System Science for their support and generally making for a fun work environment.

Thank you to research scientist staff members of the Jet Propulsion Laboratory Dr. Cédric David, Dr. Brian Thomas, and especially Dr. John T. Reager for his never-ending, mentally stimulating stream of ideas.

Lastly, I would like to thank my friends and family for their support.

CURRICULUM VITAE

Kurt C. Solander

Education

Ph.D. 2016 Earth System Science
University of California, Irvine, CA

M.S. 2013 Earth System Science
University of California, Irvine, CA

M.S. 2009 Hydrologic Sciences
University of Nevada, Reno, NV

B.A. 2003 Earth and Planetary Sciences and Environmental Studies
Washington University in St. Louis, MO

Research Experience

2011-2016 Graduate Research Assistant, Earth System Science, University of California, Irvine, CA

2007-2009 Graduate Research Assistant, Hydrologic Sciences, University of Nevada, Reno, NV

2003 Research Assistant, Earth and Planetary Science, Washington University in St. Louis, MO

External Funding and Awards

NASA Earth and Space Science Fellowship (2013-2015) for *How well will the NASA Surface Water and Ocean Topography (SWOT) mission observe global reservoirs?*

High Throughput Computing at the University of Wisconsin, Madison Open Science Grid User School (2015)

American Geophysical Union Chapman Conference on Drought at the University of California, Irvine (2015)

Jenkins Fellowship (2013) for *Developing a reservoir management model to understand the impacts on the climate system*

Peer-Reviewed Publications

Solander, K.C., J.T. Reager, J.S. Famiglietti, 2016, Evaluating the over-consumption of water through observations from GRACE over the continental United States, *in preparation*.

Solander, K.C., J.T. Reager, J.S. Famiglietti, 2016, How well will the NASA Surface Water and Ocean Topography (SWOT) mission observe global reservoirs? *Water Resour. Res.* 52, 1-18.

Solander, K.C., J.T. Reager, B.F. Thomas, C.H. David, and J.S. Famiglietti, 2016, Simulating human water regulation: the development of an optimal complexity, climate-adaptive reservoir management model for an LSM, *J. Hydrometeor*., 17, 725-744.

Solander, K.C., L. Saito, and F. Biondi, 2010, Streamflow simulation using a water balance model with annually-resolved inputs, *J. Hydrol.,* 387: 46-53.

Presentations

Solander, K.C., 2016, *Understanding human impacts on the terrestrial water cycle through numerical modeling and remote sensing of global water management systems (invited talk)*, Massachusetts Institute of Technology Center for Global Change Science, Cambridge, Mass., 29 Feb.

Solander, K.C., J.T. Reager, and J.S. Famiglietti, 2015, *Evaluating sustainable water use through observations from GRACE and in-situ water use records over the continental United States (Poster),* American Geophysical Union Fall Meeting, San Francisco, Calif., 14-18 Dec.

Solander, K.C., J.T. Reager, and J.S. Famiglietti, 2015, *Evaluation of Sustainable Water Use using GRACE over the Continental United States? (Oral Session),* UCLA Institute for the Environment Workshop: Towards Food, Energy, and Water Security in California, Los Angeles, Calif., 2-4 Dec.

Solander, K.C., J.T. Reager, J.S. Famiglietti, and K.M. Andreadis, 2015, *How well will the NASA surface water and ocean topography (SWOT) mission observe global reservoirs? (Poster),* SWOT Science Definition Team Meeting, Toulouse, France, 7-9 Jul.

Solander, K.C., J.S. Famiglietti, J.T. Reager, C.H. David, and K.M. Andreadis, 2015, *Simulating the uncertainty in NASA surface water and ocean topography (SWOT) observations of global reservoirs (Oral Session),* UCOWR/NIWR/ CUAHSI Annual Conference, Las Vegas, NV, 16-18 Jun.

Solander, K.C., J.S. Famiglietti, C.H. David, and J.T. Reager, 2014, *How well will the Surface Water and Ocean Topography (SWOT) mission observe global reservoirs? (Oral Session),* AGU, San Francisco, Calif., 15-19 Dec.

Solander, K.C., J.S. Famiglietti, and J.T. Reager, 2014, *Development of a climate-adaptive, reservoir management model for a GCM (Oral Session),* UCOWR/NIWR/CUAHSI Annual Conference, Medford, MA, 18-20 Jun.

Solander, K.C., J.T. Reager, J.S. Famiglietti, and C.H. David, 2013, *The Development of a Simple, Climate-Change Adaptive Model to Represent Reservoir Management in California with Global-Scale Applications (Poster),* AGU, San Francisco, Calif., 9-13 Dec.

Solander, K.C., J. Edman, M.-H. Lo, J.T. Reager, C.H. David, B.F. Thomas, J.S. Famiglietti, R.S. Singh, and N.L. Miller, 2012, *Simulating reservoir operations in California for use in a coupled LSM and human impacts model (CLM-HUM) (Poster),* AGU, San Francisco, Calif., 3-7 Dec.

Solander, K.C., L. Saito, J. Salas, and *F. Biondi, 2009*. The Application of a Dendro-Hydrologic Model to the Upper Meadow Valley Wash Watershed, Lincoln County, Nevada. *Annual Meeting of the Association of American Geographers*, Paper Session on "Climate, Wildfire, and Woodland Dynamics in the Great Basin of North America - II", Las Vegas, NV.

Teaching

ESS 1 – *Introduction to Earth System Science* (Summer 2014, Instructor)
ESS 19 – *Modeling of the Earth* (Spring 2016, Teaching Assistant)
ESS 1 – *Introduction to Earth System Science* (Fall 2013, Teaching Assistant)
ESS 15 – *Introduction to Global Climate Change* (Spring 2013, Teaching Assistant)
ESS 60B – *Regional Environmental Issues* (Winter 2013, Teaching Assistant)
ESS 7 – *Physical Geology* (Fall 2012, Teaching Assistant)
ESS 272 – Directed development of graduate-level course in Science Communication (Fall and Winter 2012)
CLEAN Education (Climate, Literacy, Empowerment, and Inquiry) 501(c)(3) non-profit in education and outreach: Lead Instructor

Industry Experience

2009-2011 VESTRA Resources, Inc., Redding, CA
Associate Hydrologist

2005-2007 SECOR International, Inc., Carson City, NV
Staff Hydrologist

2004-2005 City of Tucson – Environmental Services, Tucson, AZ
Hydrologic Technician

2003-2004 Great Basin Institute, Reno, NV
Land Restoration Technician and Water Quality Intern

Leadership and Extracurricular

Reviewer for *Journal of Hydrometeorology* and *Water Resources Research* (2015 – current)

Director of CLEAN Education 501 (c)(3) non-profit dedicated to teaching climate science education to under-represented students (2014 – current)

Teacher of water quality and quantity field methods to Native American high school students (2012-2013)

Graduate Student Representative for Earth System Science Department (2012-2013)

Professional Affiliations

Jet Propulsion Laboratory (JPL) Water Group (2014 – current)

American Geophysical Union (AGU) (2011 – current)

Universities Council on Water Resources (UCOWR) (2014 – current)

American Association of Geographers (AAG) (2009)

ABSTRACT OF THE DISSERTATION

Numerical modeling and remote sensing of global water management systems: applications for land surface modeling future satellite missions, and sustainable water resources management

By

Kurt C. Solander

Doctor of Philosophy in Earth System Science

University of California, Irvine, 2016

Professor James S. Famiglietti, Chair

The ability to accurately quantify water storages and fluxes in water management systems through observations or models is of increasing importance due to the expected impacts from climate change and population growth worldwide. Here, I describe three innovative techniques developed to better understand this problem. First, a model was created to represent reservoir storage and outflow with the objective of integration into a Land Surface Model (LSM) to simulate the impacts of reservoir management on the climate system. Given this goal, storage capacity represented the lone model input required that is not already available to an LSM user. Model parameterization was linked to air temperature to allow future simulations to adapt to a changing climate, making it the first such model to mimic the potential response of a reservoir operator to climate change. Second, spatial and temporal error properties of future NASA Surface Water and Ocean Topography (SWOT) satellite reservoir operations were quantified. This work invoked the use of the SWOTsim instrument simulator, which was run over a number of synthetic and actual reservoirs so the resulting error properties could be extrapolated to the global scale.

The results provide eventual users of SWOT data with a blueprint of expected reservoir error properties so such characteristics can be determined a priori for a reservoir given knowledge about its topology and anticipated repeat orbit pass over its location. Finally, data from the Gravity Recovery and Climate Experiment (GRACE) satellite mission was used in conjunction with in-situ water use records to evaluate sustainable water use at the two-digit HUC basin scale over the contiguous United States. Results indicate that the least sustainable water management region is centered in the southwest, where consumptive water use exceeded water availability by over 100% on average for some of these basins. This work represents the first attempt at evaluating sustainable water use using exclusively remote sensing and in-situ observations at the continental scale, and offers a framework for future similar studies attempting to evaluate water use sustainability at large scales.

Chapter 1

Introduction

Historically, the perspective on water use has been the same as any other natural resource – water exists on the planet for the exclusive benefit of humans. From a water quantity standpoint, this means that all accessible water to a given area is eligible for human use to satisfy domestic, industrial, or agricultural demands with little to no concern for the needs of the environment. Thus, water demand to support cities, farms, or industries often outstrips the supplies of a given area. As soon as the water is over-allocated locally, users simply target the next closest water source still considered economically feasible to acquire new water supplies for increased development. Often, this has played out through abandoning the collection of additional surface water reserves in favor of groundwater, assuming the aquifer targeted for groundwater extraction is deemed productive enough for this to be a financially viable decision. Alternatively, more water is acquired through surface water imports that have been captured and stored in a series of dams and reservoirs and transported through aqueducts to serve areas of up to several hundred miles away from the source. More recently, now that the technology has become economically practicable, some developers have turned to desalination techniques and wastewater treatment and recycling methods to satisfy growing water demands in regions where the surface water and groundwater supplies have already been overexploited.

To support this system, the 20th century saw an explosion of water resource management infrastructure worldwide. Thousands of dams, reservoirs, and groundwater

wells were being built in conjunction with hundreds of miles of aqueducts to sustain both large cities in areas formerly considered too dry for habitation and cultivation of industrial-sized fields of crops in regions previously not known to receive enough precipitation to grow much food. Although dam and reservoir development has slowed in recent years, some notable exceptions exist in Africa and Asia, where countries typically gained access to this technology later on and have built several large-scale reservoirs. Likewise, many smaller hydropower dams are currently planned for construction in these regions (Wisser et al., 2013; Zarfl et al., 2014). The system of dams, reservoirs, aqueducts, and groundwater pumping is now global in scale.

The level and speed of dam or groundwater development did not occur without enormous benefits to humans, primarily related to food, energy, and water supplies. The augmentation of water supplies gained from reservoirs and groundwater pumping has, in part, enabled global food production to keep up with increases in population. Dams have generated copious amounts of carbon-free electricity, thereby lowering the production of greenhouse gases for every unit of energy produced. The clean water supplied by reservoirs has even served to decrease the incidence of diseases from waterborne pathogens (Gleick, 2000).

Unfortunately, largely due to the action-reaction based nature of society, a number of negative impacts have occurred due to these water management practices. The 'action' in this case is represented by the acceleration of dam, reservoir, aqueduct, and groundwater resource development once the technology became cheap enough and the benefits were fully realized. The lag time in the 'reaction' to the negative consequences stemming from these activities is proportionate to the exploitation of this resource often at

the expense of the environment. Had early developers or managers of water resource management infrastructure possessed the foresight to account for some of the potential problems and reacted sooner, some of the negative impacts that have now become more severe would have been avoided (Gleick, 2000).

The first such impacts to be widely recognized include losses in groundwater from overpumping of aquifers and changes in aquatic ecosystems due to dam development. Regional declines in the groundwater table have now been noted worldwide (Gleeson et al., 2012; Famiglietti et al., 2014; Richey et al., 2015). Ecosystem damage from reservoir and dam development including flow alterations and barriers to migration have threatened fish survival and even caused some species to go extinct (Richter and Postel, 2010; Liermann et al., 2012). In several instances, concern over these occurrences has caused politicians to implement new legislation, forced developers to seek alternative methods for dam construction, or even led water managers to request that some dams be removed (Bednarek, 2001; Villar and Ribeiro, 2011; Wild and Loucks, 2015). However, often spurred by economic interests in spite of the growing concern for ecosystems, the exploitation of this resource at the expense of the environment continues to be an ongoing problem.

Driven by the need to accurately represent how climate change will affect the planet through models, more recent interest in water cycle impacts from global water management systems has turned to how these affect both the water and closely linked energy cycles and thereby the climate system. For example, groundwater pumping for agriculture effectively increases the amount of “active” water in the terrestrial water cycle by exposing more water at the land surface. Heavily irrigated regions are thus prone to

higher rates of evaporation and water vapor transport, potentially leading to enhanced rates of precipitation and streamflow synoptically downwind (Gordon et al., 2005; Kustu et al., 2010; Pokhrel et al., 2012; Lo and Famiglietti, 2013). Similarly, reservoirs increase the amount of open water by 330-700% and intercept water from 40% of the terrestrial landscape (Wisser et al., 2013). The extent of this increase in surficial water area also results in locally elevated evaporation rates, as evaporative losses over reservoirs surpass 5% of the total global discharge (Lehner et al., 2011). Due to these higher levels of evaporation, enhanced rates of precipitation and water vapor transport have been statistically related to reservoir location (Hossain, 2010; Degu et al., 2011). When merely conducted at local or even regional scales, the collective impacts on the climate would be much smaller than suggested here. But, given the pace and scale of groundwater mining and reservoir management worldwide, this is a problem that must be dealt with through explicit representation of these processes in state-of-the-art climate models.

Despite these profound impacts on the water cycle emanating from water resource management, representations of irrigation, groundwater pumping, or reservoir management practices are not currently well integrated in or coupled to climate models. Such work is necessary for potential impacts to be properly represented in Earth System and Operational Hydrology models, which has been listed as one of the "grand challenges" by the World Climate Research Program's Global Energy and Water Exchanges project (WCRP-GEWEX) (Nazemi and Wheater, 2015). This would enable simulations of how these associated changes in evapotranspiration, water vapor formation, precipitation, and streamflow propagate through the water cycle in conjunction with the closely linked energy cycle to make better predictions of the weather and climate (Kumar et al., 2015).

In Earth System Science, researchers often attempt to first characterize a problem by direct observations. Models are then developed to test and validate the representation of these processes to the desired level of accuracy that is based on the end goal of the model. For reservoirs, the goal would be to represent both storage and outflow in a way that could adequately depict the changes in the timing and magnitude of flows, as well as how storage fluctuates over time, so these processes could be represented in climate models to evaluate the associated impacts on the climate system. Fortunately, plenty of observations of reservoir storage and outflow exist to develop these models. Unfortunately, given that reservoirs are human-managed systems, the storage and flow behavior of reservoirs is dependent on the function of the reservoir, which is highly variable in both space and time. As such, the development of a general set of equations to represent these processes for all reservoirs remains a difficult task.

Chapter two of this study details the development of a reservoir management model designed to link with a global Land Surface Model (LSM) to address this issue. For the reasons mentioned above and given the end goal of integrating the model in an LSM, the intent was to come up with the minimum complexity set of equations that could reasonably represent reservoir behavior. By 'minimum complexity', the aim was to use as few parameters as possible and minimize the number of terms that would not already be available to an LSM user. By 'reasonably represent reservoir behavior', the objective was to improve the representation of flows while still being able to simulate the annual and interannual variability of storage over long time periods. In addition, the way in which parameters were used and the link between model equations and air temperature allows reservoir operations simulated by the model to adapt to changes in hydrology that could be

induced by climate change, making it the first such model that explicitly accounts for climate change in the operation of reservoirs (Milly et al., 2008). In this way, the model could be linked to an LSM in a coupled or uncoupled context to simulate shifts in the reservoir management impacts on the climate system due to climate change up to several decades in the future.

Use of remote sensing data from the upcoming NASA Surface Water and Ocean Topography (SWOT) mission with an expected launch date in 2020 and 90% global coverage is ideal for use in the development of such a model. SWOT is anticipated to observe the surface area and elevation of water bodies down to a spatial resolution of 0.0625 km^2 and height accuracy of 10 cm (Biancamaria et al., 2015). Moreover, SWOT will allow for river discharge estimates down to 50 m in width (Pavelsky et al., 2014). For reservoirs, these observations will enable measurements of storage changes as well as discharge upstream and downstream, which are suitable for use in testing a reservoir operation scheme at the global scale. This is especially true for reservoir-river systems where data access is limited due to a lack of infrastructure or difficulty with international data sharing (Alsdorf et al., 2007).

Given these considerations, chapter three of this study shifted focus towards understanding how well NASA SWOT observations can be used to determine reservoir elevation and surface area changes, which will be employed during the mission to derive changes in reservoir storage. This work involved the use of simulated reservoir observations from the SWOTsim instrument simulator, which is a model created by researchers at the California Institute of Technology Jet Propulsion Laboratory in Pasadena. SWOTsim simulates SWOT data based on realistic SWOT orbit and instrument

error characteristics given a digital elevation model of water surface elevations. Because of the computational constraints of running this model globally, a number of theoretical reservoirs were designed to collectively account for spatial properties of global reservoirs. SWOTsim was then run over these reservoirs to assess the impacts of the respective spatial features on SWOT reservoir observations. The results were then verified by simulating SWOTsim over actual reservoirs. The impacts of the temporal resolution of SWOT were also assessed using in-situ records to evaluate how the return interval of SWOT observations will affect the ability to reproduce monthly records. Results were extrapolated to the global scale using expected satellite orbit trajectories and spatial properties of reservoirs, making it the first comprehensive study of anticipated SWOT observations of reservoirs and first where SWOTsim results in hydrology were applied globally.

In recognition of the shifting paradigm where water management systems must be developed to benefit humans while still accounting for ecological demands, chapter four of this study was designed to evaluate the effectiveness of these systems in representing the water needs of both environmental and human users. In this work, total water availability is derived from Gravity Recovery and Climate Experiment (GRACE) total water storage measurements and the resulting quantity is compared to consumptive water use (CWU) calculated from USGS water use records. Although necessarily resolved at a large spatial scale due to the coarse resolution of GRACE, the results provide an indication of where the managed system of groundwater and surface water supplies is falling short of accounting for both environmental and human demands. Moreover, given that previous water scarcity studies relied more heavily on output from different models that created a large disparity

in results (Wada et al., 2011), the established framework with a heavier dependence on remote sensing data should serve as a blueprint for future studies to improve consistency among findings.

Chapter 2

Development of a reservoir model for a global Land Surface Model (LSM)

As appears in: Solander, K., J.T. Reager, B.F. Thomas, C.H. David, and J.S. Famiglietti, 2016, Simulating human water regulation: the development of an optimal complexity, climate-adaptive reservoir management model for an LSM, Journal of Hydrometeorology, 17, 725-744.

2.1 Introduction

Reservoirs are an important aspect of water resources management worldwide. Although the pace of reservoir creation through dam construction in the United States has slowed (Graf, 1999), the number of global dams over 15 m tall has still grown substantially in recent years to over 50,000 (Lehner et al., 2011). The global cumulative reservoir storage capacity behind dams is 7,000-8,300 km^3, representing over 20% of the total annual discharge to oceans (Syed et al., 2010; Lehner et al., 2011). The proportion of discharge impounded behind reservoirs is even greater in the United States, as reservoir storage amounts to 75% of the annual discharge in this region (Biemans et al., 2011). Assuming an annual mean global river channel storage of 1200 to 2120 km^3 (Hanasaki et al., 2006), reservoirs increase the amount of standing, natural water by 330-700% and intercept water from lands covering an area of 53 million km^2, or 40% of the total terrestrial environment (Wisser et al., 2013).

The widespread occurrence of reservoirs is a testament to the associated many societal benefits, but impacts on regional hydrometeorology from these water bodies have also been noted. Evaporative losses from reservoirs exceed 5% of total discharge on a global scale, which surpasses the losses from both domestic and industrial water consumption combined (Lehner et al., 2011). Enhanced rates of regional water vapor transport and precipitation have been statistically related to reservoir location, which is strongest for larger reservoirs situated in warmer climates (Hossain, 2010; Degu et al., 2011). River fragmentation from dam construction has affected 60% of the world's largest rivers, accounting for approximately 90% of the discharge coming from these fluvial systems (Revenga et al., 2005).

Given the impacts of reservoir management on the water cycle and its close linkage to the energy cycle, these perturbations have an impact on the climate system as well. However, reservoirs have yet to be fully integrated into climate models to better understand the nature of these changes. Inclusion of reservoir behavior in large-scale land surface models (LSMs) that can be used to monitor the impacts on the water and energy cycles and how they interact dynamically is thus critical to better understand such behaviors and the relative impact on the climate system (Nazemi and Wheater, 2015a).

In this study, we develop general reservoir operation rule equations that can be used to simulate outflow and storage within an LSM to better represent reservoir management impacts and feedbacks on the climate system. Although the ultimate goal is to use these equations within an LSM, reservoir model coupling to an LSM and subsequent simulations and evaluations are beyond the scope of this paper. Rather, the intent of this study is to generate general reservoir operation rule equations, evaluate the performance

of equations in simulating reservoir outflow and storage, and demonstrate applicability of equations for use in an LSM. Furthermore, as other equations have already been developed towards this end, we describe the distinguishing features for the equations used in this study. In particular, we focus on describing the development of simpler, generalized reservoir equations, which is ideal for integration in an LSM, and exhibit how the equations are climate-adaptive through conducting and evaluating several experimental simulations. Unique equation properties that were used here as well as equations used in related efforts are discussed in more detail in the sections that follow.

2.2 Global and California Reservoir Modeling

Reservoir management is influenced by operation rule curves, which provide an indication of how the storage of water in a given reservoir changes throughout the year. The curves are a function of current and historic hydrologic conditions and the general purpose of the reservoir (Willis et al., 2011). Dam release restrictions and minimum environmental flow thresholds may impose further constraints on how a reservoir is managed. Given the typical high temporal variability in the hydrology and use of reservoirs (Nazemi and Wheater, 2015b), rule curves frequently serve as mere guidelines for operators rather than explicit storage thresholds that must be met year-round. Hence, operational criteria to direct modelers with simulations of releases often do not exist (Fekete et al., 2010). Given these considerations, attempting to develop a general system of equations that can accurately simulate outflow for multiple reservoirs remains a difficult task.

Further complicating generalized modeling of reservoir operations is the obsolescence of the assumption that past records in hydrology will hold true in the future due to ongoing environmental alterations caused by climate change (Milly et al., 2008). In the state of California for example, mean surface air temperatures are projected to increase by 2 to 6 °C by 2100 (Hayhoe et al., 2004), which is anticipated to exacerbate the already declining trend in annual snowpack and further shift the timing of peak runoff towards earlier in the season (Mote, 2006). Rising temperatures coupled with these hydrologic effects are expected to decrease available reservoir storage, promote additional deviations away from the natural flow regime in rivers, and enhance reservoir storage losses due to evaporation (Vanrheenen et al., 2004; Mote, 2006; Cayan et al., 2008; Barnett et al., 2008). These changes in the water cycle over both the land and atmosphere, combined with the rise in water demand from population growth, will lead to major water demand and supply shifts over the next century (Haddeland et al., 2014). It is thus essential that transformations such as these are accounted for in the long-term modeling of water management systems.

Despite the importance of including reservoir dynamics in large-scale hydrology models or LSMs, only a limited number of studies have been conducted towards this purpose and all have yet to be fully coupled to a climate model. Descriptions of a more comprehensive list of these studies can be found in Nazemi and Wheater (2015b), but some of the key studies are described in more detail here. The algorithms used to simulate reservoir releases in Hanasaki et al. (2006) to improve global discharge simulations provided the foundation for a number of subsequent studies. Initial releases for an operational year were based on the ratio of storage to total storage capacity so storage

could be recovered throughout the year when starting at a low volume. Successive releases were based on release targets, which changed depending on the downstream agricultural, industrial, and domestic water demands for that month relative to an inflow threshold. The targets were incorporated into actual releases, which were also a function of storage capacity to annual inflow ratios. Biemens et al. (2011) used a similar formulation but excluded industrial and domestic demands to determine releases based exclusively on crop water demands. Doll et al. (2012) used reservoir storage variations in the WaterGap Hydrology Model to help with differentiating between surface water and groundwater withdrawals in the agricultural, domestic, and industrial water use sectors. Wisser et al. (2010) simulated reservoir outflow solely from parameterized inflow, which was also used in Fekete et al. (2010) to assess reservoir and irrigation impacts on watershed nutrient exports. In addition, Haddeland et al. (2006) was the first to use a parameter optimization based scheme in conjunction with reservoir storage, inflow, evaporation, and dominant reservoir function within the Variable Infiltration Capacity (VIC) macroscale hydrologic model to simulate releases at the continental scale.

While these studies were developed to understand the impacts of reservoir management on streamflow and reservoir storage, not every study explicitly accounts for non-stationarity in the operator's response to changes in hydrology, which would alter model representations of reservoir outflow and storage. The water available to these managed systems is changing due to increasing stresses from population growth and climate change and the management of these systems will change accordingly. Models thus need to be made more adaptive to integrate these shifts, particularly when used for

forecasting future water resource management or climate systems (Wheater and Gober, 2013).

Another potential issue is that many of these studies were conducted for reservoirs at large or even global scales without the use of calibrated and validated generalized equations. Although useful for enhancing knowledge about the general Earth system and global water supplies, employment of general equations requiring minimal input is more advantageous for simulating reservoir behavior where no observations are available or for locations where insertion of a theoretical model is desired by a user. Moreover, employing generalized equations provides better justification for regional or global scale applications. Such a practice may also help to avoid eliminating localized reservoir management or climate characteristics from becoming part of the model structure.

For example, in the large-scale reservoir modeling studies mentioned above, any combination of storage, inflow, storage or inflow thresholds, storage capacity, dominant reservoir function, climate information such as evaporation and precipitation, and water demands were used as the basis to determine reservoir releases in the model. Given that the selection of which variables to use was dependent on the intended purpose of the model and the collective management characteristics of the reservoirs being modeled, which are in-turn heavily influenced by the spatial scale of the study, some of these variables are more important in determining releases in certain areas over others. Moreover, some of this information might not even be available over large portions of the globe, particularly in developing regions, meaning that large expanses of the land surface with reservoirs would not be simulated if these models were exclusively used. Modeled estimates of these variables could also be represented in the reservoir model, but this

introduces additional complexities by resulting in uncertainties that must be quantified. Hence, the better approach involves development of reservoir release algorithms using more general equations to maintain parsimony and ensure model inputs are appropriate to the data available.

With a high density of reservoirs and a diverse array of climate and spatial regimes, California serves as an ideal setting for generalized reservoir model development. Numerous statewide water management models have already been developed to determine optimum surface water and groundwater allocations given different management objectives. Model drivers included economic considerations (Jenkins et al., 2001), water supply allocation and storage priorities (Draper et al., 2004), human and environmental water demands (Yates et al., 2005), and historical surface water, land use, and water diversions (C2vSIM, DWR). These models typically require either a high number of inputs or parameters. Unfortunately, highly parameterized, multi-termed models make model calibration and validation more challenging (Kuczera and Mroczkowski, 2010) and thus computationally intensive to run in an LSM framework. Instead, a simpler model structure is required that minimizes the need for extra terms or parameters, while still adequately representing reservoir outflow and storage behavior.

The reservoir management model described herein was developed using California reservoirs as a test case with the intent of ultimately running within a large-scale LSM. As such, the model was designed so that LSM surface runoff at the upstream location of the targeted reservoir to be modeled will serve as reservoir inflow and the primary input. Outputs consist of reservoir outflow and storage, which were estimated through the optimization of parameter values. Optimal parameter values were generalized across

reservoir locations based on the inflow to storage capacity ratio to demonstrate applicability across larger spatial scales. Furthermore, the generalization based on these variables will allow an LSM user to 'synthesize' a reservoir at any model grid location given a desired storage capacity to achieve a realistic representation of reservoir management behavior. This will be useful to simulate climate impacts stemming from 'hypothetical' reservoirs, which would aid in the testing of potential climate effects from planned reservoir development on a global scale. Because seasonal changes in temperature are closely linked to the agricultural growing season (Nazemi and Wheater, 2015a), which in-turn heavily influences reservoir behavior in California, temperature was employed to distinguish between the equations used to simulate reservoir outflow and storage. Moreover, this feature was added to better allow for global-scale simulations and represent future reservoir storage and management shifts in response to a warming climate, which is one of the distinguishing characteristics of the model developed in this study relative to previous reservoir modeling schemes designed for global-scale simulations.

The materials and methods section that follows first describes the background for model development, including the study area, data sources, and criteria driving the selection of different components used in the model. Next, we discuss the different equations that were tested for use in the model and the measures employed to select the most appropriate set of equations for this study. This section also involves a detailed rationalization for incorporating temperature into the model. We then describe the optimization of model parameters for each reservoir and how the optimized parameter values were used to create generalized parameters. Finally, we explain the use of three

outside reservoirs for model validation and the statistics used for evaluation of model performance.

2.3 Materials and Methods

2.3.1 California Study Area

Reservoirs from California were selected for use in model development. California consists of 1,530 dams with a collective storage capacity that is approximately equivalent to the mean annual discharge from its rivers, resulting in a reservoir storage density of 239,000 m^3 per km^2 that is surpassed by only 2 of the 18 major water resource regions in the continental United States (Graf, 1999). Considering the extensive water resource management characteristics of this region and the access to a wide range of reservoir observations, California serves as an ideal test site for reservoir model development.

2.3.2 Data Sources

Data used in model development included temperature, as well as reservoir inflow, outflow, and storage. Temperature records were obtained from Parameter-elevation Regressions on Independent Slopes Model (PRISM) estimates at 2.5-arc-minute resolution (PRISM Climate Group, 2004). PRISM data was acquired by selecting the grid cells that encompassed the downstream-most location of the reservoir. PRISM was used over in-situ station temperature records, as the model is intended for use in an LSM, which also employs the use of grid-based temperature measurements to drive internal physical processes.

Reservoir inflow, storage, and outflow data was obtained from the California Data Exchange Center (www.cdec.water.ca.gov, May 20, 2014). This site is managed by the

California Department of Water Resources (DWR) and includes data collected by the United States Army Corps of Engineers (USACE), United States Bureau of Reclamation (USBR), and local county and municipal governments. Data from the 50 largest statewide reservoirs by maximum reservoir capacity with continuous monthly data from 1995-2013 simulation period were targeted for the study. A total of 14 reservoirs fit the criteria, which account for approximately 50% of the total statewide storage capacity and include the four largest by volume in the state. Summary hydrologic statistics and information for the reservoirs used in model development are included in Table 1. Reservoir locations are provided in Figure 1.

2.3.3 Model Criteria

Model development was driven by the need to maintain model parsimony and facilitate integration into a land surface model (LSM). Inputs to the model thus were kept to a minimum. Those already available to an LSM user consisted of inflow and temperature. Inflow will be derived from upgradient, surface runoff where a river-routing model will be used to transfer water between upstream and downstream reservoirs. Temperature will be used in the equation formulations as described in Section 2.3.4. Reservoir storage capacity and an initial storage condition are the only reservoir design variables required by the LSM user that are not currently available within the LSM modeling framework. Model outputs consist of dynamic estimates of reservoir outflow and storage calculated simultaneously at each timestep. Simulations in an LSM with river routing model included will allow reservoir outflow to be routed to downgradient locations, effectively mimicking flow in river channels, and reservoir storage will be linked to the LSM hydrology to allow for evaporation.

Although an initial storage condition was used for model development, once integrated into an LSM this could be achieved using reservoir water levels if the relationship between reservoir storage and elevation is known or could be reasonably estimated. Moreover, reservoir surface area and water level heights from the upcoming NASA Surface Water and Ocean Topography (SWOT) satellite mission could be used to derive change in storage to aid with these estimates. This mission is expected to observe reservoirs down to a surface area of 0.0625 km^2 with an expected launch date of 2020 (Biancamaria et al., 2010).

The reservoir model was run at a monthly timestep. Model behavior is thus best captured as broad seasonal variations in reservoir operations that are largely controlled by the timing of crop planting and harvest seasons relative to inputs such as snowmelt within the model development study area. Even still, the current reservoir model formulation permits operation at daily or sub-daily timesteps once coupled to an LSM to match the temporal scale of LSM output specified by the user. For example, the accumulation of daily LSM output over a given simulated month could be used as reservoir model input and to drive the decision behavior (mode switching, described in Section 2.3.4 below). Releases would then remain constant through time and only shift when reservoir behavior changes (i.e. monthly) according to the reservoir model. In this way, the reservoir management model would operate based on monthly inflow and temperature values, while still able to communicate with the LSM at sub-monthly intervals.

The justification for simulating reservoir behavior at a monthly timestep stems from the desire to ultimately represent long timescale reservoir impacts on the climate while running the model coupled to an LSM. Longer reservoir model timesteps are therefore

desired to decrease the sub-daily variability so the rules governing reservoir management become easier to generalize at these temporal scales, thereby making the associated impacts on the water cycle and climate system less challenging to estimate. Although this exempts management functions such as hydropower generation that occur at smaller timescales from being included, accounting for daily and sub-daily variations in reservoir behavior is beyond the scope of this study. More importantly, omitting explicit representations of these functions preserves a simpler model structure with minimal inputs, making it easier to achieve the goal of integration into an LSM

2.3.4 Model Development and Selection

The model was designed to simulate both reservoir outflow and storage simultaneously, as representing these characteristics are necessary to adequately capture reservoir behavior. Reservoir storage is updated using Equation 1:

$$S(t) = S(t - \Delta t) + [I(t) - Q(t)] \quad (1)$$

where S(t) is reservoir storage (m^3), I(t) is reservoir inflow (m^3/s), Q(t) is reservoir outflow (m^3/s), and t is time (s). This equation has been used to simulate reservoir storage in other studies (Hanasaki et al., 2006; Wisser et al., 2010; Fekete et al., 2010).

As highlighted previously, different formulations of reservoir storage and inflow provide the basis for simulating reservoir outflow in other studies (e.g. Hanasaki et al., 2006). Here, we test six different equation arrangements prior to application in this study (Table 2). Model #1 treats outflow as equal to inflow, which effectively ignores any influence of the reservoir on the outflow. For this reason, results from model #1 were

included to serve as a performance baseline. As long as the simulated outflow using the other reservoir models demonstrated superior performance over the results from model #1, the overall model performance was considered to be an improvement over the base case where the influence of reservoirs on outflow was ignored. The other models shown use either parameterized fractions of inflow and/or storage to simulate outflow. Model complexity was incrementally enhanced with each subsequent model that was tested by increasing the number of parameters.

As shown in Table 2, reservoir outflow equations were allowed to switch modes within the year to represent seasonal changes that typify California reservoir management behavior (Figure 2). During the initial stages of model development, the mode switching was achieved using the month of the simulated output. For instance, if the simulation was conducted within the summer months, the release equation was used. Otherwise, the recharge equation was used. However, given that the model was ultimately to be run on a global scale within an LSM, the use of months was less than ideal given the strong link between reservoir behavior and climate and locations across the globe that are not climatically similar during the same month. Ultimately, temperature was selected for this purpose, as many reservoirs exhibited a strong seasonal signal in outflow and storage behavior and this variable produced stronger results compared to other variables that were tested.

Temperature was used in the model by applying the recharge equation during the cooler months when the temperature of the simulated month fell below the baseline temperature, which is given as the mean temperature during the 5-year period immediately prior to the 1995 – 2013 model simulation period. During the cooler months,

reservoir inflow generally exceeds outflow due to increased runoff from snowmelt so a parameterized fraction of inflow is used to determine outflow and storage increases. Alternatively, the drawdown equation was applied during the warmer months when the temperature exceeded the baseline temperature. During this time, outflow tends to exceed inflow due to the heightened water demand from agriculture so a parameterized fraction of storage is used to determine outflow and the storage decreases. It is anticipated that the distribution of monthly temperatures above or below the baseline mean will be identical regardless of reservoir location in the upper or lower reaches of a given watershed. Also, it should be noted that seasonal-based equations have also been applied in other studies to determine reservoir releases (e.g. Hanasaki et al., 2006). The arrangement of temperature is shown in Equations 2 and 3:

$T(t) \leq T_b$: Recharge Equation (2)

$T(t) > T_b$: Drawdown Equation (3)

where T(t) is monthly temperature (°C) during the simulation period and T_b is the baseline temperature.

Variables other than temperature were tested for use in its place to implement the mode switching within the model. Of those variables, only temperature was found to produce as robust results as the use of months. Intuitively, this makes sense given that temperature is a natural proxy for seasons. Its use in this instance was also preferred given its functional connection with shifts in the length of the California growing season and given that the seasonal snowmelt pulse drives reservoir operations and this does not

always stay constant from one year to the next. Therefore, the way in which temperature is used enables easy adaptation of the model to other regions where agriculture and snowmelt drive reservoir operations, but at different times of the year. This could be critical for reservoirs located in farming areas around the Andes of South America, which is one of the few regions that have experienced substantial growth in reservoir development over recent years (Wisser et al., 2013). Selection of temperature over time to trigger mode switching is thus more in sync with the stronger link between reservoir operations, agriculture, and snowmelt globally, making it more ideal for use in global simulations within an LSM. Given that temperature is also reproduced with a higher degree of accuracy within this model framework relative to other variables makes it even more suitable for its current use in the model equations. There is also potential for explicitly relating temperature changes in the model to water demands, as it has already been used to help determine crop and livestock water demands in other studies (Nazemi and Wheater, 2015a).

Reservoir inflow, storage, and water demand thresholds have also been used to drive reservoir operation rules (Biemens et al., 2011; Wisser et al., 2010; Doll et al., 2009; Haddeland et al., 2006; Hanasaki et al., 2006). Monthly storage and inflow thresholds were tested for use in this study with marginal improvements in results and thus were omitted. Water demands were not used, as these would be difficult to reproduce directly within an LSM, which is the end goal for the model. Although not known to have been used to drive operation rules for large-scale reservoir modeling studies and not tested here, snow coverage, upper watershed rain-to-snow ratios, regional soil moisture, or reservoir water levels could have potentially been employed in a similar capacity. However, because

changes in temperature are more directly linked to climate change and the loss of stationarity in hydrologic models, the use of temperature as a proxy provides a stronger basis for the model adaptivity framework we applied. Moreover, the availability and reliability of temperature data exceeds that of the other variables, making it easier to implement within an LSM structure.

Additional model constraints were added to make the model more realistic by preventing storage from exceeding maximum capacity or falling below zero. In the event that simulated storage surpassed the user-defined storage capacity, outflow was simulated using Equation 4:

$$Q(t) = I(t) + \frac{S(t - \Delta t)}{\Delta t} \quad (4)$$

where S_{max} is the maximum storage capacity (m^3) for the given reservoir. An additional constraint was added to prevent reservoir storage from falling below 10% capacity, as this level rarely occurred in any of the observations used in model development and it follows the minimum accepted allowable storage level used by Hanasaki et al. (2006).

Performance of the different models that were tested was evaluated based on the outflow and storage best-fit statistics of the normalized root-mean-squared-error (nRMSE) where the RMSE is normalized to the mean of the observations, r^2 coefficient of determination (r^2), and Nash-Sutcliffe efficiency (NSE) during model optimization (Nash and Sutcliffe, 1970; Krause et al., 2005). Model complexity was increased incrementally until little improvement could be gained in model performance by applying more complex

formulations. This determination was achieved using the Akaike Information Criterion shown in Equation 5:

$$AIC = 2 * K + \ln(L) \quad (5)$$

where K is the number of parameters and L is the likelihood function (Akaike, 1974). Here, the likelihood function is assumed to be the difference between one and the nRMSE of observed and simulated reservoir outflow and storage, where the nRMSE has been normalized to the storage or outflow mean. The AIC method was chosen to acknowledge that model selection involves a trade-off between how well the model fits observations and the number of parameters used or model complexity. Thus, lower AIC values indicate a more ideal model in terms of both its best-fit statistics and number of parameters used.

2.3.5 Parameter Optimization

Parameter optimization was achieved for 11 reservoirs by changing parameter values to minimize the objective function for each reservoir individually. The objective function is defined as the Pareto front between observed and modeled reservoir outflow and storage nRMSE. Pareto optimization was necessary to implement here because the minimum objective function for outflow and storage are conflicting objectives. In other words, changing parameter values to find the minimum nRMSE for either storage or outflow will not necessarily result in the desired cumulative minimum nRMSE for both of these variables (Vrugt et al., 2003). Different initial values were tested to ensure the true optimum parameter values for each reservoir was obtained and avoid finding local objective function minima. The Nelder-Mead algorithm was used to minimize the objective

function (Nelder and Mead, 1965), which was solved by placing equal weight on reservoir outflow and storage so the Pareto optimum could be satisfied.

2.3.6 Parameter Generalization and Model Validation

Model parameters were generalized from the best-performing model to facilitate the automatic generation of reservoirs within an LSM and justify the utility of model equations for large-scale applications. Parameter generalization proceeded by regressing final parameter values to a quantitative reservoir characteristic, which included those already available to an LSM user, or those that could be easily input by a user. Final selection of the reservoir characteristic used in the parameter generalization was achieved by choosing the property with the highest r^2 coefficient of determination when regressed against the optimized parameter values obtained from each individual reservoir. Ultimately, the resulting generalized regression equation will be used to generate reservoirs within an LSM.

Reservoir characteristics that were tested empirically for use in parameter generalization consisted of both observed and modeled data. Observations were obtained from CDEC (www.cdec.water.ca.gov, May 20, 2014) and included reservoir storage capacity, elevation, latitude, longitude, coefficient of variation of monthly inflow, and inflow to reservoir storage capacity ratios (I:SC) calculated using Equation 6:

$$I:SC = \frac{I_{win}}{S_{\max}} \tag{6}$$

ere I_{win} is the mean total winter (October to May) inflow over the simulation period. It should be noted that annual inflow to storage capacity ratio was also tested here.

Moreover, the inverse of this ratio was used to dampen simulations of releases and avoid overflow for small reservoirs in Hanasaki et al. (2006). Modeled records that were tested for use in parameter generalization consisted of seasonal or annual precipitation and seasonal temperature obtained from 2.5-arc-minute resolution PRISM gridded data that encompassed the geographic coordinates of the reservoir. Note that although temperature was tested for use in parameter generalization, it does not necessarily have to be employed in the final model to maintain consistency with the use of temperature to select model equations, as these are two entirely different features of the model.

Following parameter generalization, additional model simulations were conducted for the same eleven reservoirs as well as three additional reservoirs to test the performance of the generalized parameters and for model validation. Model simulations for each of the calibration reservoirs were conducted using the generalized parameters so the results could be compared to the original parameter results optimized for each reservoir individually. Model validation was achieved using the generalized parameters to run the model for three additional reservoirs outside of those used in the development of the generalized parameters. Selection of validation reservoirs was based on availability of continuous records that matched the length of calibration reservoir records, as well as possession of diverse spatial and hydrological characteristics relative to the calibration reservoirs shown in Section 2.3.2.

2.4 Results

Average model performance statistics tested for the six models are shown in Table 3. Model #5 performed best in terms of the AIC, while model #4 and model #2 performed

only slightly worse with ΔAIC values of 0.05 and 0.07, respectively. Model #5 also had the highest mean outflow and storage r^2 of 0.56 and highest mean outflow NSE of 0.33. The next highest performing model for these statistics was model #4 with a mean outflow and storage r^2 of 0.54 and model #6 with an outflow NSE of 0.24. Model #4 also had the lowest mean outflow and storage nRMSE climatology of 0.23, while the value for model #5 was slightly higher at 0.25. Only the outflow performance from model #'s 5 and 6 universally exceeded the baseline performance from model #1 where outflow was treated as inflow.

Given its overall superior performance in the testing of the different models, model #5 was used for all subsequent analyses. Model calibration results for the individual reservoir parameter optimization are shown in Table 4. For the eleven calibration reservoirs, the overall mean outflow and storage nRMSE and climatology nRMSE ranged from 0.11 to 0.20 and 0.15 to 0.44, respectively. The mean outflow and storage r^2 ranged from 0.41 to 0.68, while the outflow NSE ranged from -0.97 to 0.76. The accompanying 1995-2013 modeled and observed outflow and storage time series for the three largest reservoirs are provided in Figure 3 with climatologies in Figure 4.

The optimized parameter response surfaces with respect to the objective function of both outflow and storage for the three largest reservoirs are shown in Figure 5. The response surface gradient was larger for that of outflow than storage, suggesting the minimum objective function was found more quickly for reservoir outflow. The absence of many heterogeneities and local minima in both the outflow and storage response surfaces suggests that the optimum parameter values could readily be obtained using the Nelder Mead algorithm as long as a few different combinations of initial parameter values were tested to adequately cover the parameter domain.

Figure 6 shows the Pareto fronts for the objective function of both outflow and storage for the three largest reservoirs. The results from this figure represent the objective functions using all combinations of parameter values covering the parameter domain that are divisible by 0.05. All three reservoirs display a similar shape where there is a greater spread of data at mid-range nRMSE storage values (~0.5-0.6), but smaller spread of data as the nRMSE falls outside this range. The results indicate that there were not as many combinations of parameter values that could reproduce the optimum outflow and storage simultaneously for the reservoirs.

Of all the reservoir characteristics that were tested empirically to determine the best-fit regression relationship with the individually optimized parameters for the generation of generalized parameter equations, the winter inflow to storage capacity ratios showed the strongest correlation. Further empirical testing showed a logarithmic fit best described the relationship between the winter inflow to storage capacity ratio and the optimized alpha parameter values, while a linear relationship best described the relationship between the winter inflow to storage capacity ratio and the optimized beta parameter values. The newly developed generalized parameter equations showing these relationships are provided in Equations 7 and 8:

$$\alpha = 0.2728 * \ln\frac{(I_{win})}{S_{\max}} + 0.5185 \quad (7)$$

$$\beta = 0.03127 * \ln\frac{(I_{win})}{S_{\max}} + 0.04781 \quad (8)$$

where and α and β are the model parameters. Final generalized parameter curves with accompanying 95% confidence intervals generated from these equations are shown in Figure 7.

Final parameter values and model performance statistics using the generalized parameter values from the outflow model #5 for each of the eleven calibration and three validation reservoirs are shown in Table 5. As evidenced by the nRMSE, r^2, and NSE values, the model performed better overall for the validation reservoirs than those used in the parameter generalization. The collective mean outflow and storage nRMSE and nRMSE climatology for both the calibration and validation reservoirs ranged from 0.11 to 0.23 and 0.17 to 1.01, respectively. The outflow and storage r^2 and outflow NSE ranged from 0.37 to 0.72 and -0.74 to 0.93, respectively. The accompanying 1995-2013 time series of modeled and observed outflow and storage for the three validation reservoirs are provided in Figure 8 with climatologies shown in Figure 9.

2.5. Discussion

2.5.*1 Model Selection*

Several of the outflow equations were under consideration for use in the study based on the similarities obtained during preliminary testing. Model #6 compared favorably to model #5 in terms of the nRMSE, r^2, and NSE, but due to the use of more parameters it did not perform as well with the AIC. Model #4 performed better in terms of the mean outflow and storage climatology nRMSE, but model #5 out-performed model #4 for all other statistics shown in Table 3. Based on its overall superior performance, model simulation and parameter generalization was achieved using model #5 where reservoir

outflow is simulated using a parameterized fraction of inflow during the cooler winter months and a parameterized fraction of storage during the warmer summer months.

2.5.2 Model Calibration and Generalization

The model performance for the eleven calibration reservoirs using the optimized parameters is similar to that of all reservoirs where the generalized parameters were used. The mean alpha and beta parameters were identical for the two reservoir groups, while the mean outflow and storage nRMSE values increased slightly and the mean outflow and storage r^2 and NSE decreased slightly for the reservoir group using the generalized parameters. The greatest difference in model performance statistics occurred with the mean outflow and storage nRMSE of the climatologies, which nearly doubled from 0.25 to 0.48 for the generalized parameter reservoir group. Use of generalized parameter values increased this statistic for each of the individual reservoirs by a minimum of 12% relative to the results where the parameter values were optimized for each reservoir individually. This decrease in model performance was expected, as the ability to reproduce the heterogeneities of reservoir management on an individual level becomes more difficult when parameters are used that better match collective over individual reservoir behavior. Similarly, the higher RMSE observed during low-storage periods in the Isabella and Pine Flat Reservoirs likely occurred from this phenomenon, as the reservoirs used to develop generalized parameters had lower levels of interannual variability in storage and the model performance is higher for these types of reservoirs.

The model did not perform as well for the New Melones, Trinity, Sonoma, and Camanche Reservoirs. As shown in Table 6, the generalized parameter performance statistics from these four reservoirs represent three out of the four highest mean outflow

and storage nRMSE values, three of the five highest mean outflow and storage climatology values, and the three lowest mean outflow and storage r^2 values when simulations are run using the generalized parameters. Furthermore, this group of reservoirs includes the only two with a negative NSE and the three lowest NSE values overall. To demonstrate the impacts that these reservoirs have on model performance, when they are excluded from the analysis, the mean performance statistics presented in Table 5 improves by 11% for nRMSE, 13% for the nRMSE climatologies, 6% for r^2, and 40% for NSE.

As these four reservoirs also had small storage coefficient of variation (S_{cv}) values and winter inflow to storage capacity ratios (I:SC) relative to the others in the study, the strength of model performance is closely related to the management intensity of the given reservoir. As shown in Table 6, the four reservoirs accounted for the four lowest S_{cv} values and three of the four lowest winter inflow to storage capacity ratios of the fourteen reservoirs that were tested. Lower S_{cv} values are indicative of smaller changes in monthly storage, which suggest more water must either be released or held back so outflow and inflow are closely aligned and storage remains closer to constant through time. Similarly, lower winter I:SC ratios are exemplified by reservoirs with larger storage capacities and thus higher storage-to-streamflow ratios and a greater degree of management intensity (Vorosmarty et al., 1997). Both scenarios suggest the degree of management intensity is enhanced for the four lower-performing reservoirs.

Given these considerations, although the model performs well for the majority of management reservoirs, those with higher management intensity are expected to be represented with lower accuracies. Based on the range of S_{cv} values and winter I:SC ratios for the four reservoirs relative to model performance, the accuracy of model simulations

improved for reservoirs with S_{cv} values greater than 0.22 and winter I:SC ratios above 2 x 10^{-7} s^{-1}. Despite these deficiencies in model performance, the results presented in Table 3 reveal the mean of performance statistics using model #5 far exceeded that when the baseline model #1 was applied, thereby indicating the simulation of discharge is still markedly improved overall when model #5 is used.

2.5.3 Model Caveats and Omissions

The omission of the Whiskeytown Reservoir from this analysis further provides support for the better model performance above a threshold S_{cv} value. Storage from this northern California reservoir is maintained at capacity during the summer months for recreational purposes, resulting in a storage S_{cv} value of 0.07, which is lower than all but one of the reservoirs listed in Table 5 and indicates a high degree of management intensity. Thus, despite meeting the targeted source data criteria in model development, observations from this reservoir were excluded, as attempting to account for the unique management characteristic of this reservoir while still capturing the more typical summer operation regime in California reservoirs was not possible given the model development criteria aim of maintaining parsimony. It is likely that similar or different management conditions exist for other global reservoirs that would make model application to those reservoirs less than ideal.

Constraints on releases from environmental flow requirements were not included due to the gross disparity in how these flows are managed worldwide and the lack of availability of this data. Although the model was developed in California where this might be feasible, it is ultimately intended for use at the global scale. In addition, due to the wide

variability of environmental flow requirements from one river system to the next, this would still be a difficult task even if only conducted within California.

Explicitly accounting for reservoir functions such as hydropower generation, flood control, and agricultural or domestic water supplies was avoided to maintain model parsimony and focus modeling efforts and representing reservoir behavior better over longer timescales, which was deemed necessary given the ultimate goal of integration into an LSM and evaluation of climate impacts. For the same reason, monthly rather than daily timesteps were used. Use of more complicated release equations or a finer temporal resolution to account for various reservoir functions might be ideal if the purpose of the study was to better represent reservoir outflow in a regional or global hydrology model. However, the purpose here was to find the minimal complexity equations that could be used to represent general reservoir behavior for use in an LSM so simulations of up to 100-years can be run to evaluate reservoir impacts on the climate. Considering these goals, shorter timesteps are not needed, but monthly rules can still be decimated into a daily timestep, as necessary, to match temporal scales if run within a coupled LSM framework.

The use of only California reservoirs for model calibration and validation when the model is ultimately intended for the global scale represents another shortcoming. However, given that similar practices were conducted in other studies (i.e. Hanasaki et al., 2006), and the focus of this research was to represent general reservoir behavior over longer timescales to analyze climate impacts, the use of regionally concentrated reservoirs for model development was viewed as justified. Moreover, reservoirs with a minimum of 19-years of continuous monthly data available were targeted for this study to better determine how model performance varies under different climate conditions and the

selected reservoirs fit these criteria. Use of reservoir records that have a higher degree of variability in climate is ideal in model development given the intended end use of the model to evaluate climate impacts in an LSM.

Other omissions from the model included storage losses due to evaporation, seepage, or sedimentation. An attempt was made to incorporate storage loss terms into the model for these variables with minimal improvement to model performance likely due to the strong spatial heterogeneity in how these processes behave that highlights the difficulty in incorporating them into a generalized model of reservoir behavior. Moreover, the contribution of these losses to the overall water budget of a reservoir is generally small meaning little can be gained in model performance by adding them. For example, evaporative losses generally only represent 5% of the total annual storage for large reservoirs, while seepage and sedimentation losses are typically at or below these levels (Gleick et al., 1992; Minear and Kondolf, 2009). Thus, the use of these loss estimates was avoided to maintain model simplicity. It should be noted that loss estimates from these variables were also not explicitly accounted for in simulations of reservoir releases in a number of other studies (e.g. Hanasaki et al., 2006; Wisser et al., 2010; Fekete et al., 2010; Biemans et al., 2011).

2.5.4 Climate-Adaptive Capability

The utilization of temperature as a proxy to select the model outflow equation, as shown in Equations 2 and 3, has important implications for incorporating climate change impacts into model simulations. Assuming a warmer future from climate change, holding the five-year baseline temperature constant in this equation means that as the model advances, the monthly mean temperature for a greater proportion of simulated months will

be above this baseline. Consequently, the summer drawdown equation would be favored over the winter recharge equation in model simulations. Ignoring the impacts on model simulations due to the changes in snowpack and surface runoff that would likely occur under such a warming scenario to only determine how reservoirs would change if reservoir management was held constant, one can anticipate simulated reservoir storage to diminish or even dry up.

To test this theory in the model, an experimental set of simulations were run for the Shasta Reservoir where the baseline temperature (T_b) was maintained as the 5-year 1990-1995 baseline and the monthly temperature input in the model from PRISM was artificially increased by increments of 0.5°C for each subsequent model run. As shown in Figure 10, the summer drawdown equation is increasingly favored with each incremental rise in temperature until the temperature increase reaches 11.5°C, which is when the summer drawdown equation is used exclusively to compute reservoir outflow. Ignoring any effects that warming might have on runoff, the shift in equation usage resulted in a corresponding mean annual storage decrease of approximately 55%.

In an attempt to incorporate the increased temperature effects on runoff as well, the model was re-run for the Shasta Reservoir under the same incrementally warming scenario while simultaneously decreasing reservoir inflow by 5% for each 0.5°C rise in temperature. The justification for the decrease in inflow is that the volume of water available to reservoirs is expected to decrease due to shifts in runoff towards earlier in the season (Mote, 2006) and slight decreases in projected California precipitation (Cayan et al., 2008). As a part of this experiment, the parameter values were allowed to change dynamically with the reductions in inflow, as the parameters are calculated based on the winter inflow

to storage capacity ratios. Hence, this feature effectively represents the implementation of a modification to operation procedures in response to climate-induced shifts in hydrology. An additional experiment was run where the parameter values were held constant to the initial values to better mimic no change in management operations to accommodate changes in inflow. As shown in Figure 10, only slight additional decreases in annual storage resulted from the experiment where dynamic parameters were used relative to the shift in equation usage. Alternatively, the results where constant parameter values were used show a substantial additional decrease in mean annual storage. Thus, when the parameter values are allowed to update with decreases in inflow, the losses in storage resulting from decreases in inflow are offset by reductions in outflow resulting from the decline in the magnitude of parameter values.

This experiment should not be used to imply that a 20% reduction in annual reservoir storage is imminent by 2100 due to the projected 4°C increase in temperature for California by the same year. Although an increase in the growing season and simultaneous rise in agricultural water demand is anticipated with additional warming, a more advanced analysis that examines these shifts on a per-crop or per-climate-regime basis is required to determine how the growing season will truly be altered to impact the relative lengths of the reservoir recharge and release seasons with each incremental rise in temperature. Furthermore, more robust estimates of projected climate data or hydrologic changes under different warming scenarios would be necessary to determine how the reservoir inflow used as input might shift. Fixed decreases in inflow were used for this analysis because the intent was merely to show how model simulations might change due to a decrease in runoff that is expected under a warming climate.

By allowing simulated operations to change with a shift in the temperature regime, the use of temperature in the model accounts for the obsolescence of the former assumption in hydrology that past records will hold true in the future because of climate change. As this change in stationarity is not expected to be temporary due to the long lifetimes of atmospheric CO_2 and thermal resistance of the Earth system (Milly et al., 2008), inclusion of potential affects from climate change in reservoir models as is done here is critical. Moreover, allowing the parameters to update to addresses changes stemming from non-stationarity has yet to be implemented in previous works (Nazemi and Wheater, 2015b). Assuming that operations are as strongly linked to temperature and the growing season as they are today, a modeling adaptation measure such as this allows for simulated operations to adapt with climate-change-induced shifts in hydrology, effectively simulating the human operator response and making these models more realistic. Failing to update this information would wrongly ignore the potential for excessive reservoir drawdown resulting from warming when the severity of such problems is expected to worsen due to climate change.

2.5.5 Expected Utility in a Land-Surface Scheme.

The ultimate goal of integrating the newly developed reservoir management model into an LSM is crucial to understanding how reservoirs interact with both the climate and the water cycle. Once coupled, the surface runoff routed downstream through a river routing model will serve as inflow to the reservoir model. Inflow will be partitioned between reservoir outflow (to be treated as existing surface runoff in the LSM), and reservoir storage (linked to the atmosphere component of the LSM through evaporation). The simple structure of the model equations combined with generalized parameters that

are numerically related to reservoir inflow and storage capacity means that the reservoir management model will support this capability, enabling reservoirs to be generated automatically based on the cumulative grid cell reservoir storage capacity defined by the user. The next phase of this work will involve coupling the two models and investigating the impacts that reservoirs have on the climate and hydrology.

Although the reservoir model parameters were optimized to produce generalized parameters that were validated regionally within California, the selected reservoirs matched the data availability criteria of having a long, continuous time series of variable climate conditions making them ideal for use in model development when the end goal is to integrate into a climate model. In addition, based on the way temperature is used in the equations, more robust model performance will occur in regions with distinct reservoir recharge and drawdown seasons. Similar to California, this could occur in areas with comparable climate patterns, management practices that are heavily influenced by agricultural water demands, or snowmelt-dominant runoff. Furthermore, the recharge and drawdown seasons for the targeted location to be modeled would not have to coincide exactly with the time of year as those in California. Rather, they need to merely be somehow related to temperature, as is shown in this study. For example, this could be accomplished by running the model in areas receiving increased recharge from elevated inflow during the cooler season due to elevated precipitation and/or runoff from snowmelt, and increased drawdown from higher agricultural demands during the warmer season. Potential examples of such areas throughout the globe include agricultural regions in the vicinity of the Andes in South America, the Murray-Darling agricultural region of Australia, and the continental United States where agriculture heavily influences reservoir

management and seasonal snowmelt plays a large role in inflows. The model performance thresholds identified for the reservoir storage coefficient of variation and winter I:SC will be used to provide additional guidance on which reservoirs within these regions are most appropriate for model simulations.

2.6 Conclusion

In summary, this study made several important contributions towards including reservoir management in an LSM. First, it tested a set of different equations that represent reservoir outflow and storage dynamics simultaneously. The group of equations yielding the highest overall model performance, as determined from the collective AIC, r^2, nRMSE, and NSE values, was selected for use in the reservoir model. Second, the model was designed to use temperature to better mimic the dual reservoir operation in California that is driven by the agricultural growing season and account for future climate change induced alterations in hydrology. As demonstrated through several experiments, the adaptation measure is capable of reproducing anticipated changes in storage from an increase in temperature and/or subsequent water demands, making it ideal for simulations of the future climate system. Third, the parameters were generalized to exhibit the utility of model applications at the global scales and for automatic generation of reservoirs within an LSM based on the specified storage capacity. Finally, although model performance caveats were highlighted for reservoirs with higher management intensities (e.g. $S_{cv} < 0.22$ or winter I:SC $< 2 \times 10^{-7}$ s^{-1}), strong model validation results (mean reservoir outflow and storage $r^2 = 0.67$) and simple model structure requiring minimal inputs show promise for intended application of the model within an LSM. The new, climate-adaptive reservoir

management model thus provides a great first step towards future use in conjunction with other rigorously calibrated and validated reservoir models within an LSM to evaluate human impacts on the terrestrial water cycle and climate system due to reservoir management.

Table 2.1 Summary of hydrology and spatial information for reservoirs used in model development.

Reservoir Name	River	Operator[a]	Use Code[b]	Latitude (°), Longitude (°)	Drainage Area (km^2)	Elevation (m)	Storage Capacity (km^3)
Shasta	Sacramento	USBR	IMPR	40.72, -122.42	17,262	378	5.61
Oroville	Feather	DWR	IMPR	39.54, -121.49	9,342	281	4.36
Trinity	Trinity	USBR	IMPR	40.80, -122.76	1,782	730	3.02
New Melones	Stanislaus	USBR	IMPR	37.95, -120.53	2,331	346	2.96
Pine Flat[c]	Kings	USACE	IR	36.83, -119.33	4,002	296	1.23
Folsom	American	USBR	IPR	38.68, -121.18	4,882	146	1.20
Isabella[c]	Kern	USACE	IR	35.65, -118.47	5,372	803	0.70
Millerton	San Joaquin	USBR	IR	37.00, -119.71	4,338	177	0.64
Camanche	Mokelumne	EB MUD	M	38.23, -121.02	1,603	80	0.51
Sonoma	Dry Creek	USACE	IR	38.72, -123.01	337	158	0.47
New Hogan	Calaveras	USACE	IMR	38.15, -120.81	940	221	0.39
Eastman	Chowchilla	USACE	IR	37.21, -119.97	609	187	0.18
Black Butte[c]	Stony	USACE	IR	39.81, -122.33	1,919	157	0.18
Kaweah	Kaweah	USACE	IR	36.42, -119.00	1,453	229	0.18

[a] USBR = US Bureau of Reclamation; DWR = California Department of Water Resources; USACE = US Army Corps of Engineers; EB MUD = East Bay Municipal Utilities District

[b] I = Irrigation; M = Municipal; P = Hydropower; R = Recreation

[c] Reservoirs used in validation, all others used in model calibration and parameter generalization

Source: CA DWR (www. http://www.water.ca.gov/damsafety/damlisting)

Table 2.2 Drawdown and recharge season reservoir outflow operating rules tested in model development stage arranged according to increasing model complexity.

Model Number: Name	Complexity Classification	Parameters Per Season	Recharge Season Operating Rule[a]	Drawdown Season Operating Rule[a]
1: Natural Flow	Zero	Zero	$I(t)$	[annual]
2: Annual Storage Release Targets	First	One	$\beta*S(t-\Delta t)$	[annual]
3: Annual Inflow Release Targets	First	One	$\alpha*I(t)$	[annual]
4: Seasonal Storage Release Targets	Second	One	$\alpha*S(t-\Delta t)$	$\beta*S(t-\Delta t)$
5: Winter Inflow, Summer Storage Release Targets	Second	One	$\alpha*I(t)$	$\beta*S(t-\Delta t)$
6: Winter Inflow and Storage, Summer Inflow and Storage Release Targets	Third	Two	$\alpha_w*I(t) + \beta_w*S(t-\Delta t)$	$\alpha_s*I(t) + \beta_s*S(t-\Delta t)$

[a] $I(t)$ = reservoir inflow; $S(t)$ = reservoir storage; α, β, α_w, β_w, α_s, β_s are parameters

Table 2.3 11-Reservoir mean (standard deviation) model performance statistics obtained during calibration.

Model No.	Optimized Parameter Values	ΔAIC[b]	Mean S + Q nRMSE[a]	Mean S + Q nRMSE clim.[a]	Mean S + Q r^2	Mean Q NSE
1	nc[c]	nc[c]	0.13 (0.06) [d]	0.41 (0.17) [d]	0.52 (0.22) [d]	0.24 (0.52)
2	β = 0.24 (0.03)	0.07	0.18 (0.07)	0.26 (0.06)	0.51 (0.14)	0.15 (0.22)
3	α = 0.31 (0.37)	0.54	0.35 (0.08)	0.85 (0.33)	0.26 (0.10)	-0.76 (0.88)
4	α = 0.19 (0.27) β = 0.21 (0.25)	0.05	0.17 (0.06)	0.23 (0.07)	0.54 (0.12)	0.20 (0.23)
5	α = 0.48 (0.22) β = 0.08 (0.04)	0	0.15 (0.03)	0.25 (0.09)	0.56 (0.10)	0.33 (0.51)
6	α_w = 0.15 (0.12) β_w = 0.08 (0.05) α_s = 0.17 (0.38) β_s = 0.13 (0.07)	2.05	0.17 (0.08)	0.23 (0.10)	0.51 (0.19)	0.24 (0.35)

[a] RMSE normalized to mean values
[b] AIC reported as the difference from the best-performing (lowest) value
[c] nc = not calculated because no storage simulations or parameters for baseline model
[d] Represents value obtained from outflow simulation only

Table 2.4 Model performance statistics obtained using optimized parameters for individual reservoirs.[a]

Reservoir	α	β	Mean S + Q nRMSE[b]	Mean S + Q nRMSE clim.[b]	Mean S + Q r^2	Q NSE
Shasta	0.58	0.08	0.12	0.18	0.63	0.51
Oroville	0.64	0.06	0.13	0.28	0.60	0.49
Trinity	0.24	0.06	0.16	0.18	0.57	-0.27
New Melones	0.02	0.05	0.18	0.44	0.47	-0.97
Folsom	0.75	0.09	0.12	0.26	0.58	0.76
Millerton	0.65	0.07	0.16	0.15	0.62	0.77
Camanche	0.60	0.04	0.16	0.36	0.41	0.52
Sonoma	0.46	0.06	0.19	0.32	0.45	0.41
New Hogan	0.45	0.09	0.11	0.17	0.67	0.63
Eastman	0.29	0.10	0.12	0.20	0.68	0.42
Kaweah	0.62	0.20	0.20	0.25	0.46	0.40
Mean	**0.48**	**0.08**	**0.15**	**0.25**	**0.56**	**0.33**
(Std Deviation)	**(0.22)**	**(0.04)**	**(0.03)**	**(0.09)**	**(0.10)**	**(0.51)**

[a] Outflow calculated using Model No. 5 from Table 2

[b] RMSE normalized to mean values

Table 2.5 Model performance statistics obtained using generalized parameters.[a]

Calibration Res.	**α**	**β**	**Mean S + Q nRMSE[b]**	**Mean S + Q nRMSE clim.[b]**	**Mean S + Q r^2**	**Q NSE**
Shasta	0.54	0.08	0.13	0.37	0.59	0.41
Oroville	0.51	0.08	0.15	0.46	0.57	0.36
Trinity	0.33	0.06	0.18	0.43	0.55	-0.04
New Melones	0.22	0.06	0.23	1.01	0.43	-0.74
Folsom	0.75	0.12	0.14	0.33	0.57	0.76
Millerton	0.71	0.11	0.23	0.28	0.51	0.73
Camanche	0.51	0.08	0.23	0.63	0.37	0.43
Sonoma	0.33	0.06	0.21	0.47	0.44	0.23
New Hogan	0.35	0.06	0.13	0.54	0.64	0.51
Eastman	0.32	0.06	0.15	0.44	0.69	0.40
Kaweah	0.74	0.12	0.21	0.28	0.42	0.42
Mean	**0.48**	**0.08**	**0.18**	**0.48**	**0.53**	**0.32**
(Std Deviation)	**(0.19)**	**(0.02)**	**(0.04)**	**(0.21)**	**(0.10)**	**(0.41)**
Validation Res.	**α**	**β**	**Mean S + Q nRMSE[b]**	**Mean S + Q nRMSE clim.[b]**	**Mean S + Q r^2**	**Q NSE**
Pine Flat	0.53	0.08	0.17	0.22	0.64	0.59
Isabella	0.47	0.07	0.18	0.51	0.64	0.47
Black Butte	0.82	0.14	0.11	0.17	0.72	0.93
Mean	**0.60**	**0.10**	**0.15**	**0.30**	**0.67**	**0.66**
(Std Deviation)	**(0.19)**	**(0.04)**	**(0.04)**	**(0.18)**	**(0.04)**	**(0.24)**

[a] Outflow calculated using Model No. 5 from Table 2

[b] RMSE normalized to difference between maximum and minimum values

Table 2.6 Storage coefficient of variation and winter inflow to storage capacity ratios and rank relative to model performance for the 14 calibration and validation reservoirs using generalized parameters.

Reservoir Name	S_{cv} [Rank][a]	Winter I:SC [Rank][a]	S + Q nRMSE [Rank][a]	S + Q nRMSE climatol. [Rank][a]	S + Q r^2 [Rank][a]
Shasta	0.24 [10]	1.08 [5]	[13]	[9]	[6]
Oroville	0.28 [9]	0.98 [7]	[11]	[7]	[7]
Trinity	0.20 [12]	0.50 [12]	[8]	[8]	[9]
New Melones	0.22 [11]	0.34 [14]	[5]	[1]	[13]
Folsom	0.32 [6]	2.29 [2]	[10]	[10]	[8]
Millerton	0.31 [7]	2.05 [4]	[3]	[12]	[10]
Camanche	0.19 [13]	0.96 [8]	[2]	[2]	[14]
Sonoma	0.10 [14]	0.50 [11]	[1]	[3]	[12]
New Hogan	0.30 [8]	0.54 [10]	[12]	[4]	[3]
Eastman	0.62 [2]	0.47 [13]	[9]	[6]	[2]
Kaweah	0.98 [1]	2.26 [3]	[4]	[11]	[11]
Pine Flat[b]	0.46 [5]	3.98 [6]	[7]	[13]	[5]
Isabella[b]	0.51 [3]	3.14 [9]	[6]	[5]	[4]
Black Butte[b]	0.50 [4]	10.13 [1]	[14]	[14]	[1]

[a] Ranking from highest to lowest value
[b] Validation reservoirs

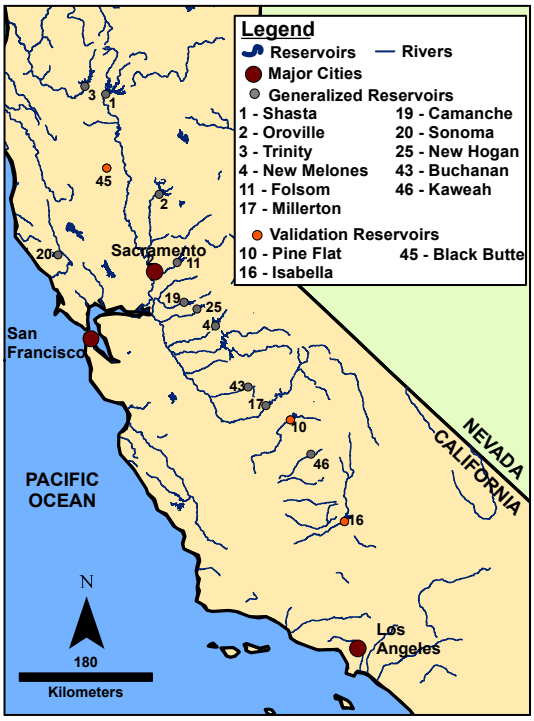

Figure 2.1: Locations of reservoirs used in model development. Numbers denote respective statewide storage capacity rank.

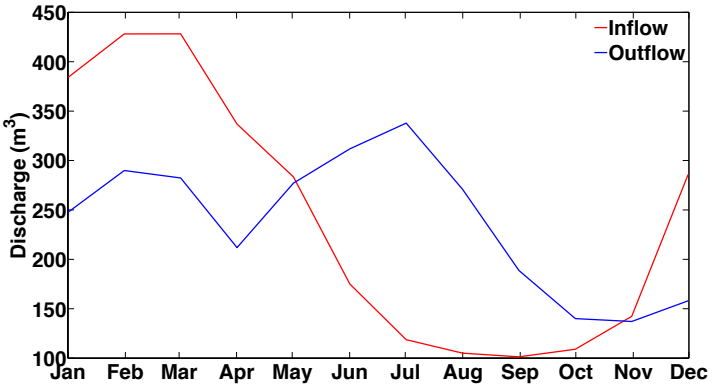

Figure 2.2: 1995-2013 Shasta Reservoir observed inflow and outflow climatology demonstrating typical California seasonal reservoir behavior where inflow exceeds outflow during wet season and outflow exceeds inflow during dry season.

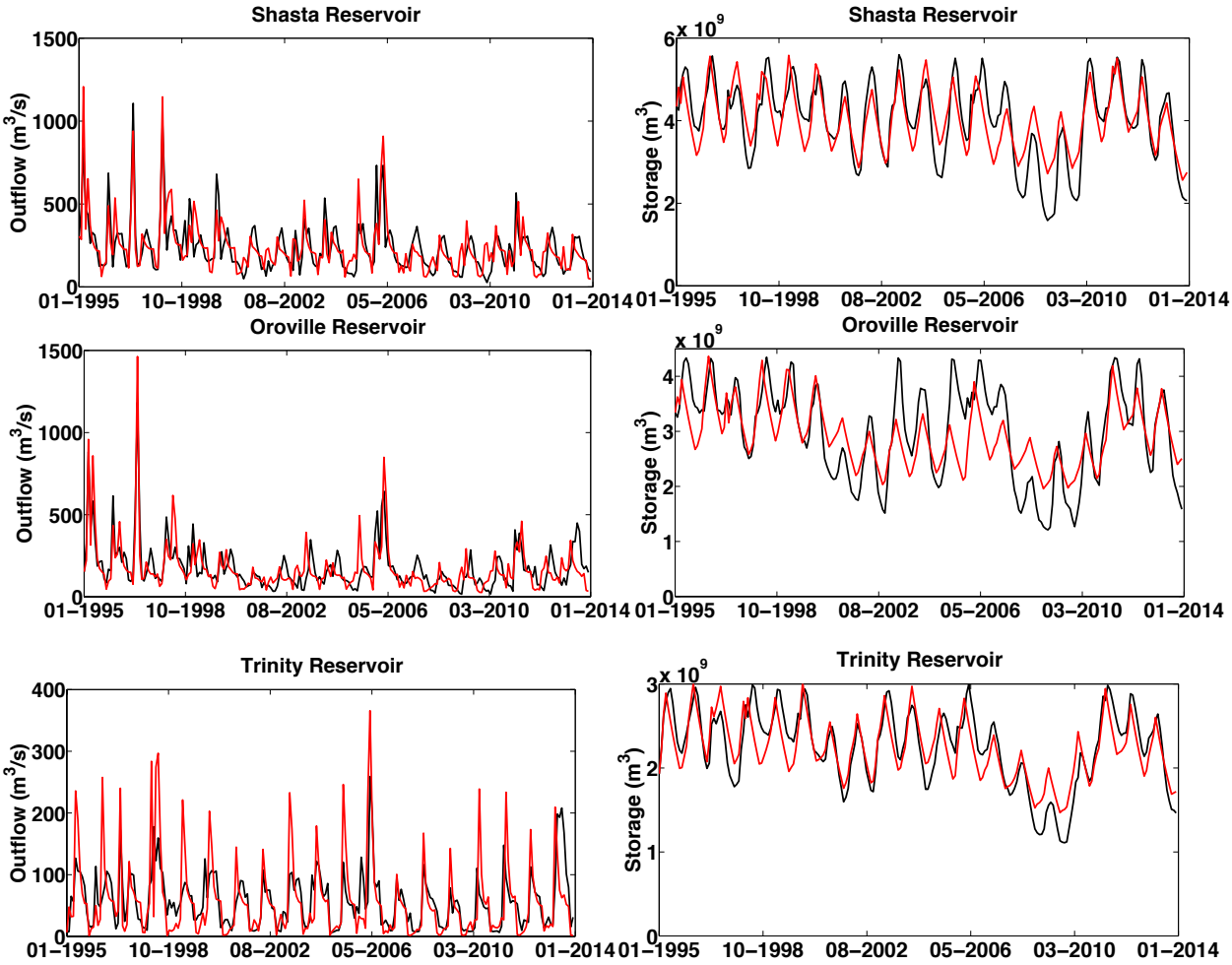

Figure 2.3: 1995-2013 observed and simulated reservoir outflow (left) and storage (right) time series for the three largest calibration reservoirs: Shasta (top), Oroville (middle), and Trinity Reservoirs (bottom). Simulations performed using individually optimized parameters for each reservoir.

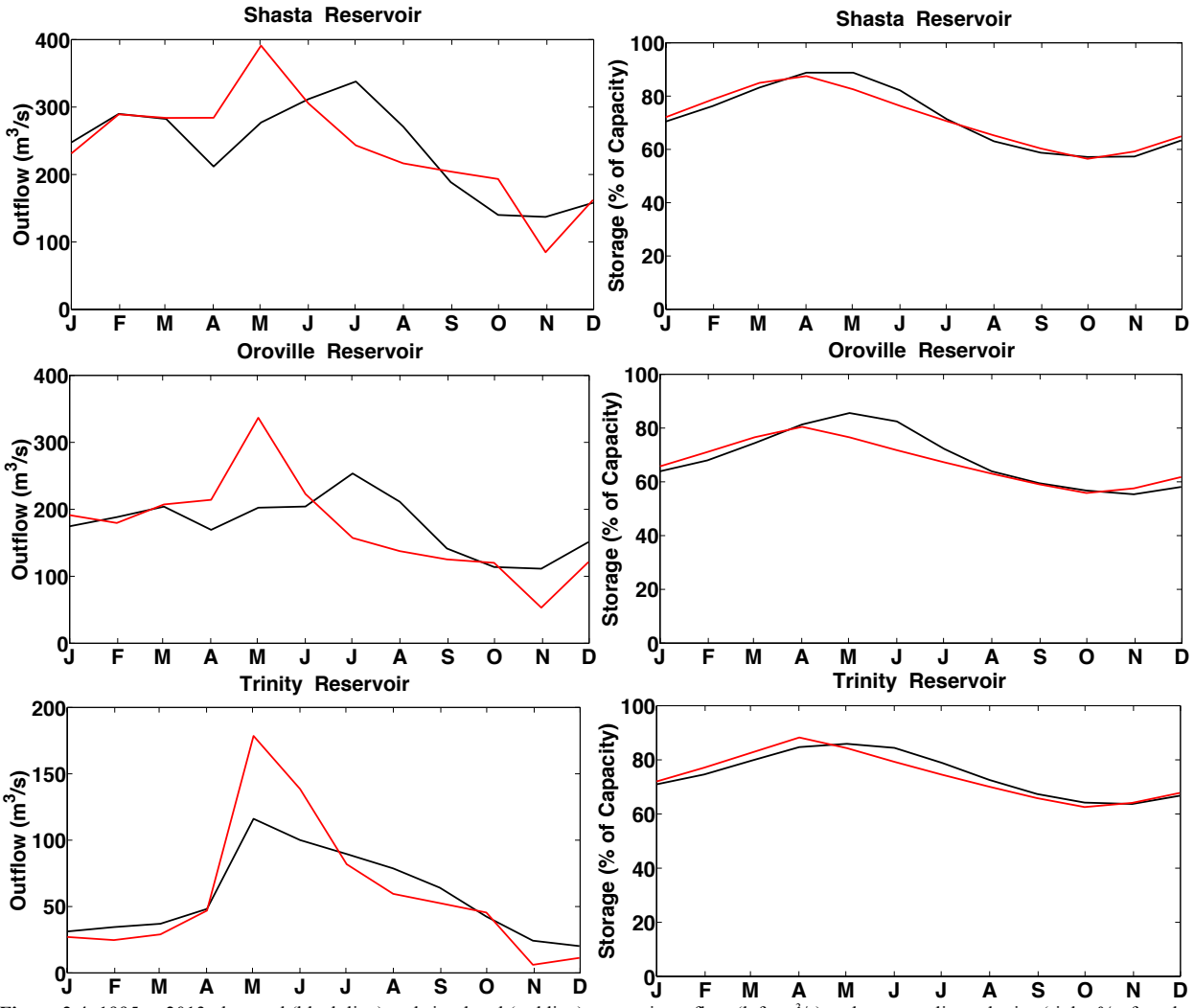

Figure 2.4: 1995 to 2013 observed (black line) and simulated (red line) reservoir outflow (left, m^3/s) and storage climatologies (right, % of total capacity) for the three largest calibration reservoirs: Shasta (top), Oroville (middle), and Trinity (bottom). Simulations performed using individually optimized parameters.

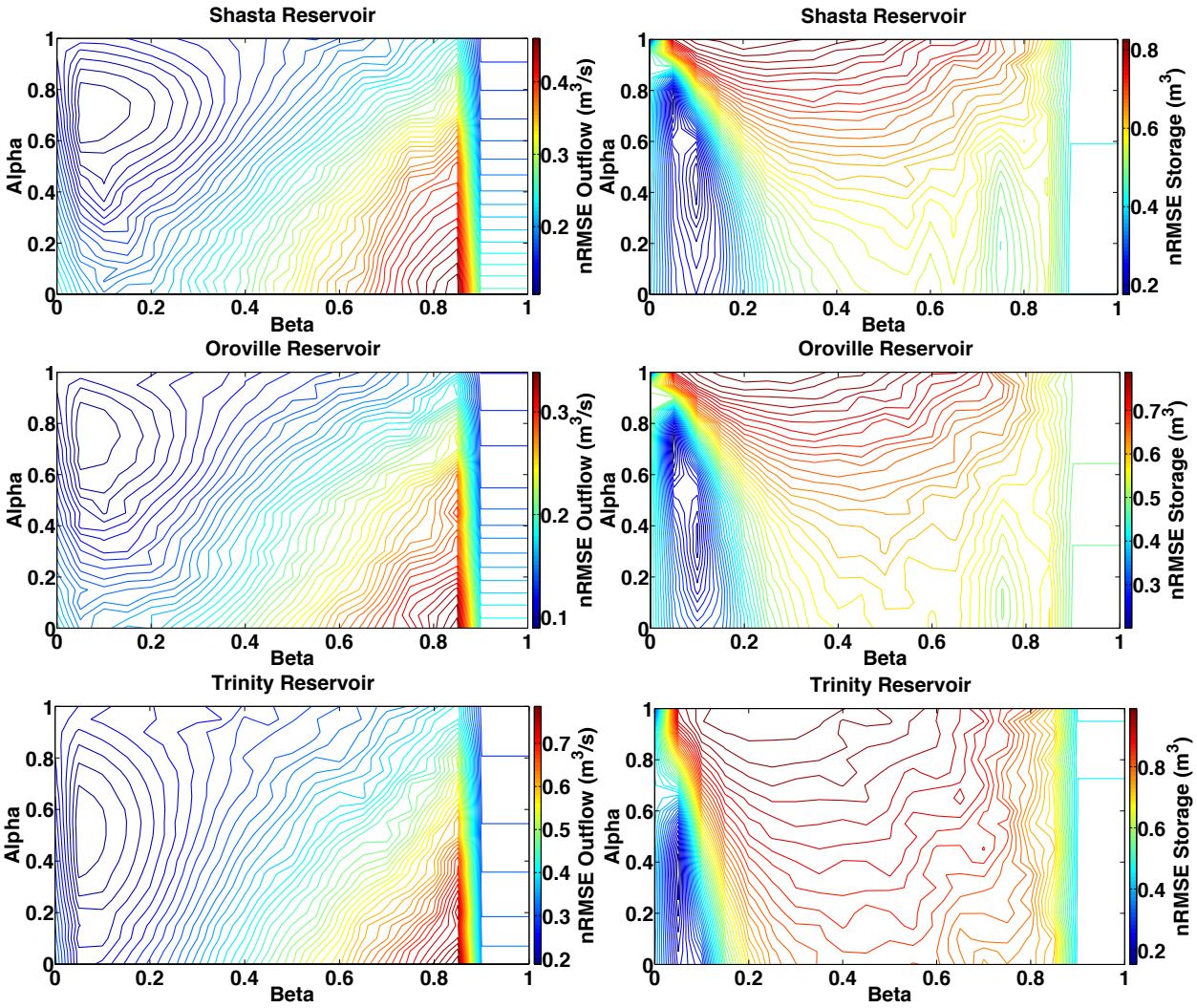

Figure 2.5: Reservoir outflow (left) and storage (right) parameter domain plots with respect to RMSE for the three largest reservoirs: Shasta (top), Oroville (middle), and Trinity (bottom).

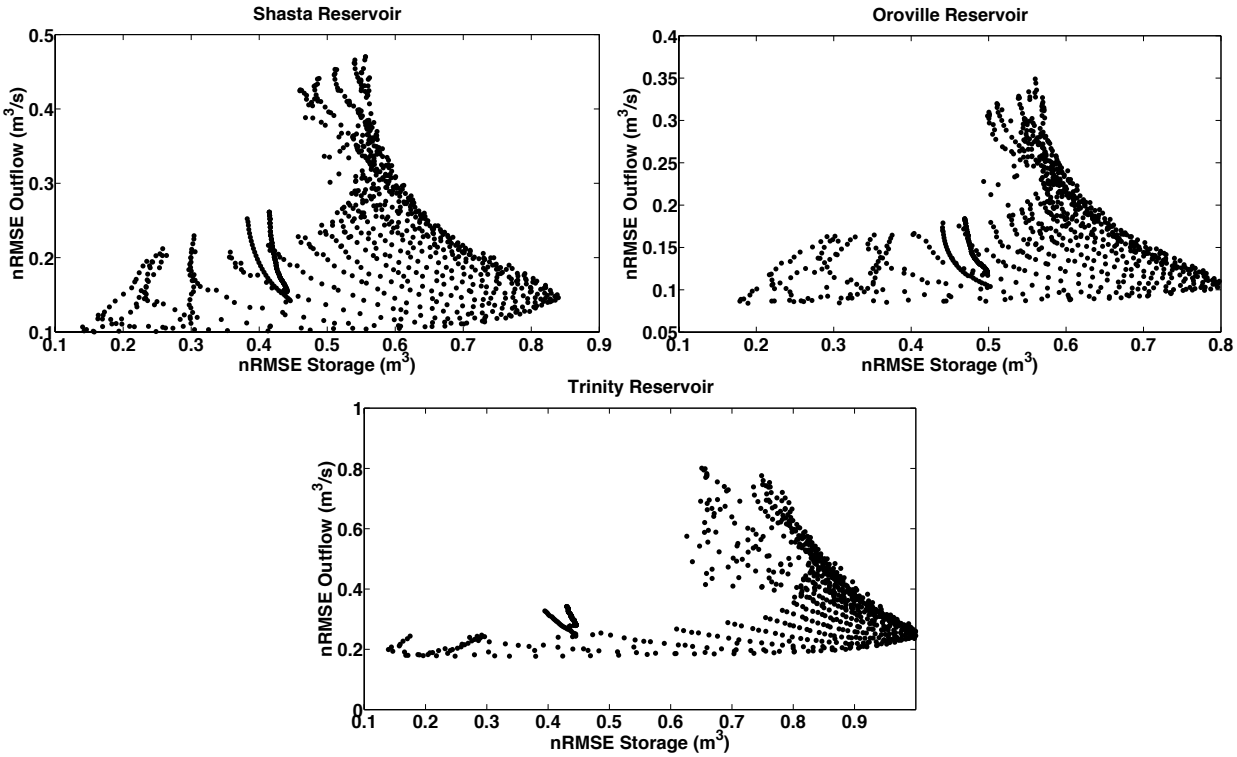

Figure 2.6: Pareto fronts for combinations of parameter values between zero and one showing RMSE outflow and storage for Shasta (top left) Oroville (top right), and Trinity (bottom left).

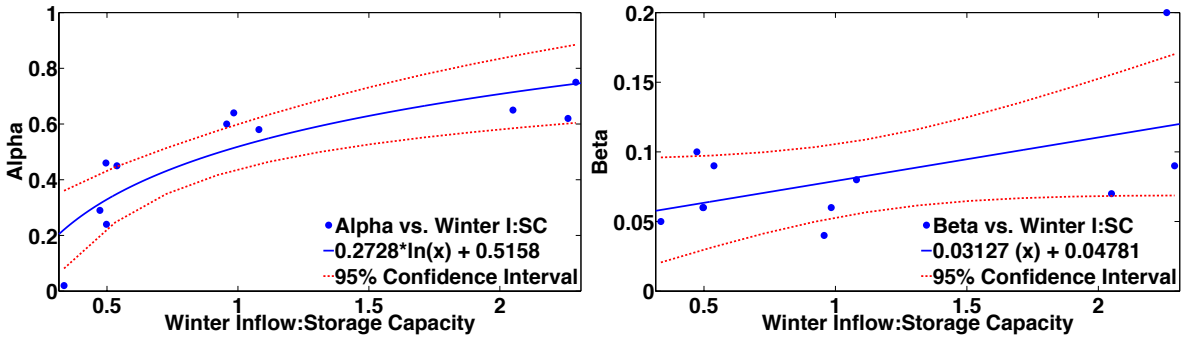

Figure 2.7: Generalized parameter curves showing results of regression between final alpha (left) and beta (right) parameter values optimized for each reservoir individually against the October to May winter I:SC for the eleven calibration reservoirs.

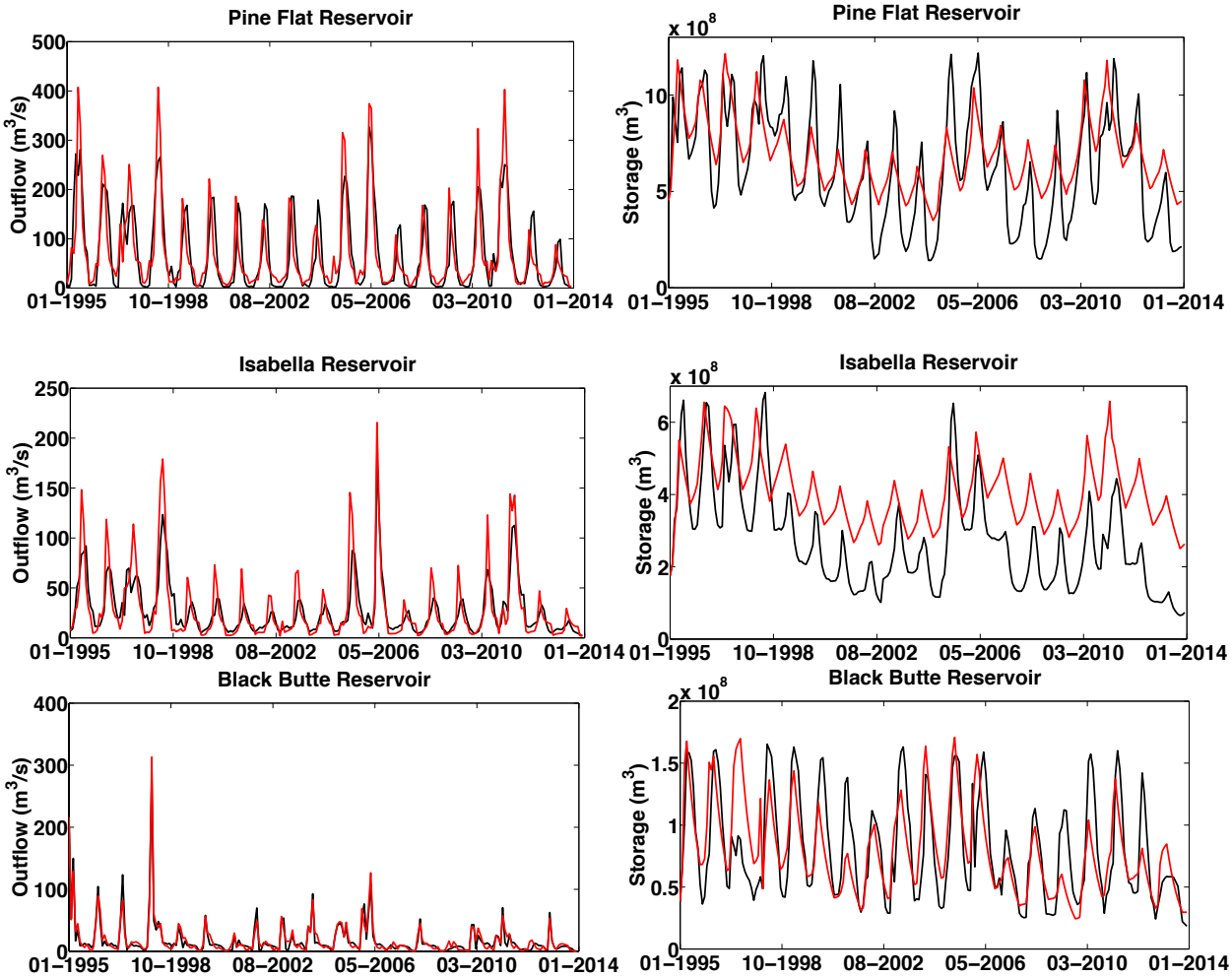

Figure 2.8: 1995 to 2013 observed and simulated reservoir outflow (left) and storage (right) time series for the three validation reservoirs Pine Flat (top), Isabella (middle), and Black Butte Reservoirs (bottom). Simulations performed using generalized parameters.

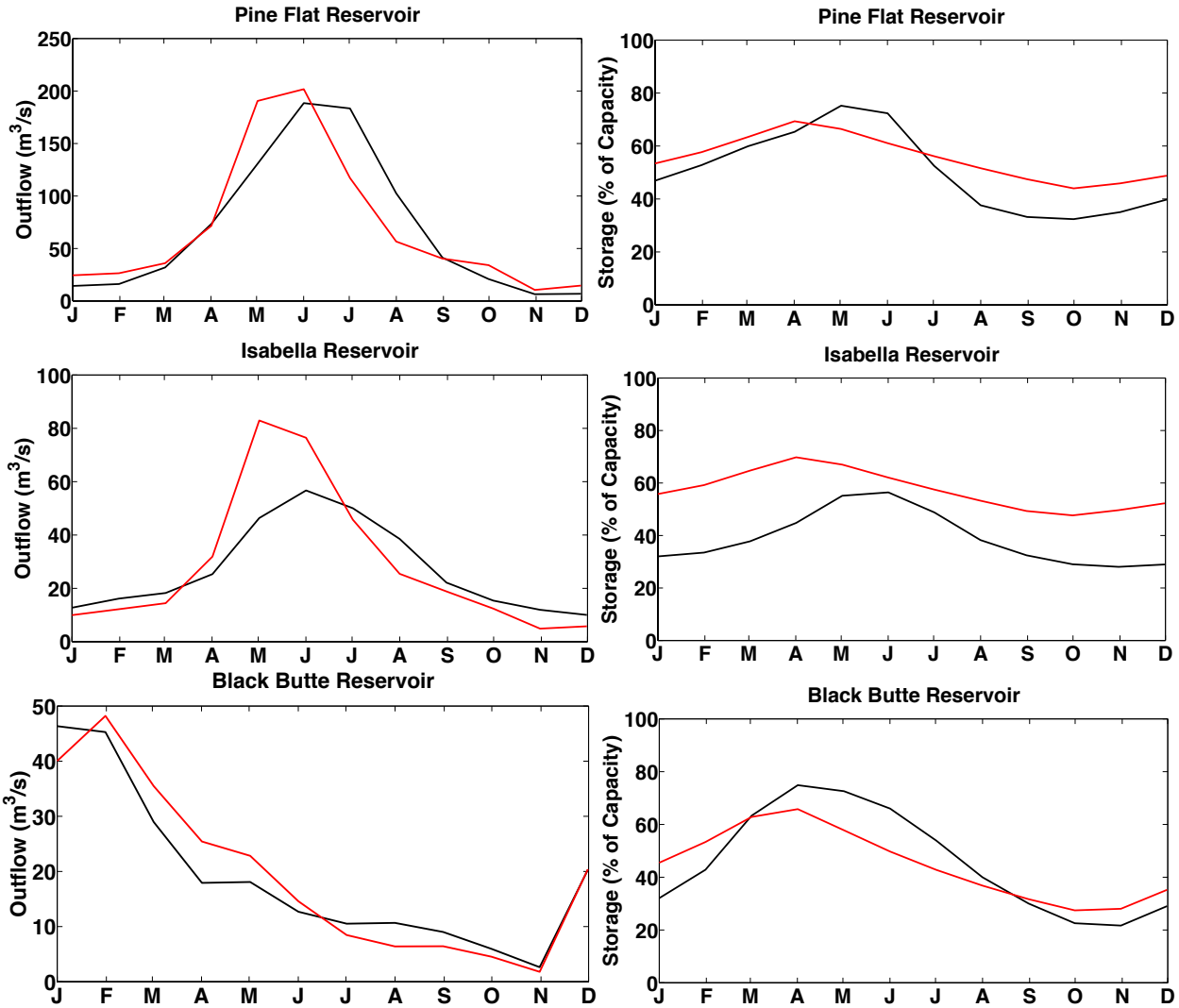

Figure 2.9: 1995 to 2013 observed and simulated reservoir outflow (left) and storage climatologies (right) for the validation reservoirs Pine Flat (top), Isabella (middle), Black Butte (bottom). Simulations performed using generalized parameters.

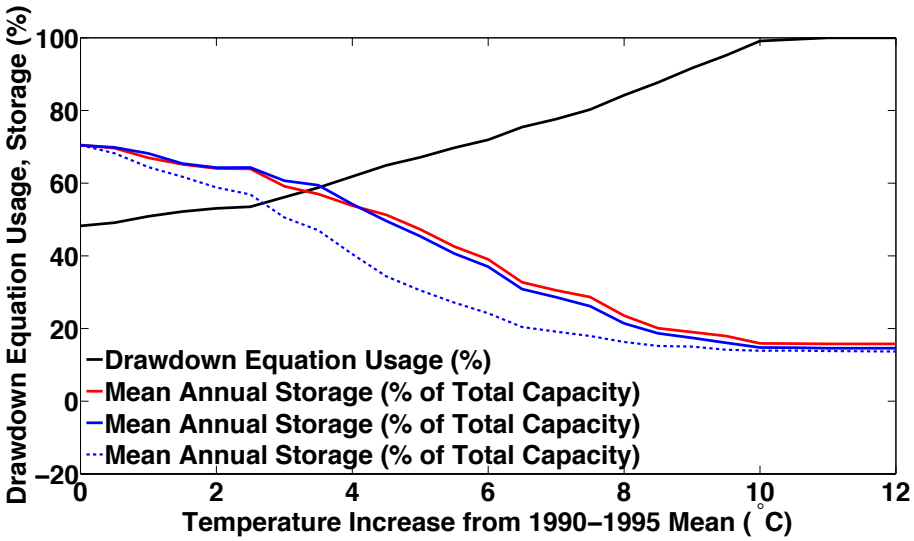

Figure 2.10: Effects of temperature increase on model simulations in terms of drawdown equation usage (black line) and on mean annual reservoir storage due to operation impacts (red line), and combined inflow and reservoir operation with dynamic parameters (solid blue line) and without dynamic parameters (dotted blue line). Analysis based on 1995 to 2013 simulations for Shasta Reservoir.

Chapter 3

How well will SWOT observe global reservoirs?

As appears in:

Solander, K., J.T. Reager, and J.S. Famiglietti, 2016, How well will the Surface Water and Ocean Topography (SWOT) mission observe global reservoirs?, Water Resources Research (in press).

3.1 Introduction and Background

The widespread occurrence of reservoirs globally serves as a testament to the critical importance of reservoirs to water resources management. Over 50,000 global dams exist with a cumulative reservoir storage capacity totaling 7,000-8,300 km^3, or one-fifth of the total annual discharge to oceans (Hanasaki et al., 2006; Syed et al., 2010). Water from reservoirs accounts for 30-40% of global irrigation and supports 12-16% of the world's food production (World Commission on Dams, 2000; Lehner et al., 2011). Recently, reservoirs have also received increased attention for their relevance to pressing environmental issues such as sea level rise (Chao et al., 2008), climate change, (Schneider and Hook, 2010), greenhouse gas emissions (Baros et al., 2011) and evaporative water losses during drought (Castle et al., 2015). Due to the large number of significant studies involving reservoirs that have alerted people to global environmental change issues,

reservoirs along with lakes have been termed the hydrologic 'canaries in the coalmine' (Williamson et al., 2009).

Given the importance of these water bodies to observations of water supplies, energy resources, and global environmental change, understanding total reservoir storage and how it varies through time is essential. Historically, reservoir observations were conducted in-situ and largely confined to industrialized nations, which have more of the infrastructure in place to make such measurements. More recently, monitoring gauges worldwide have been in decline and most developing countries still don't have the financial resources or institutional mechanisms in place to make consistent and reliable measurements (Alsdorf et al., 2007). Even for those countries with the appropriate infrastructure and funds, the international sharing of reservoir operations information for research use is often not a national priority (Famiglietti et al., 2015).

Within the past four decades, alternative methods of observing reservoirs have been developed through advancements in remote sensing, which has expanded the reservoir observation network to the global scale (Yoon and Beighley, 2014). Remote sensing technology most relevant to direct observations of reservoirs includes satellite altimeters, optical sensors onboard orbital platforms such as the Moderate Resolution Imaging Spectroradiometer (MODIS) and Landsat satellites, as well as SAR imagery such as RADARSAT, JERS-1, and ERS. Collectively, these instruments have been used to observe changes in reservoir surface areas and height at various temporal and spatial frequencies depending on the specifications of the instrument being used (Alsdorf et al., 2007). Combining these two measurements has allowed for remote estimates of reservoir storage

change in a number of studies (Zhang et al., 2006; Smith and Pavelskly, 2009; Gao et al., 2012; Yoon and Beighley, 2014; Cretaux et al., 2015).

Unfortunately, the poor spatial and temporal frequency of measurements and interference from the land surface or weather prevents the application of these techniques over a wide range of spatial and temporal scales. In addition, use of one instrument over another often involves tradeoffs. For instance, the Landsat satellite offers a high spatial resolution of 30m for inundation area measurements, but at a low repeat orbit pass of over two weeks; whereas MODIS offers daily temporal coverage, but at a much more coarse spatial resolution of 250 – 500 m (Gao et al., 2012). Both instruments have difficulty penetrating through clouds or smoke from forest fires (Eilander et al., 2014), which is particularly problematic in the low latitudes due to the persistence of the Inter-tropical Convergence Zone (ITCZ) and the common practice of biomass burning in these regions. Layover from topography or vegetation also interferes with signal trajectories leading to higher noise in signal returns. Moreover, the narrow swath widths of most altimeters leads to gaps in the spatial coverage and high wind speeds lead to larger errors in measurements by SAR imaging (Alsdorf et al., 2007). Even if such issues did not exist, a lack of consistency in the timing of repeat pass cycles from satellites offering altimetry and surface area measurements hampers the ability to make regular or consistent reservoir storage change estimates. As a result, calculating storage from these techniques is typically only conducted for larger reservoirs (storage capacity > 1 km^3) because the spatial and temporal sampling and atmospheric interference issues are less of an issue for this size class (Gao et al., 2012).

Information obtained from the NASA Surface Water and Ocean Topography (SWOT) satellite mission (expected 2020 launch) is anticipated to considerably improve upon

existing satellite estimates of reservoirs. The SWOT payload consists of the Ka-band Radar Inferometer (KaRIn) synthetic aperture radar (SAR) on both sides of the satellite, conventional nadir altimeter, water vapor radiometer, and precise orbit determination suite. The central frequency of the SAR system is 35.75 GHz with a 200-MHz bandwidth. Incidence angles of 0.6° to 3.9° will result in azimuth and range pixel sizes of 60 m and 10 m, respectively. The SAR will operate in bistatic mode meaning the electromagnetic signal will be generated by one antenna closest to the swath and both this antenna and the other located 10-m apart are designed to receive the backscattered signal (Fjørtoft et al., 2014).

SWOT will produce higher spatial resolution observations of both water surface height and inundated area, allowing for more accurate estimates of changes in reservoir storage. The 78-degree orbit inclination allows for a maximum 21-day repeat orbit pass with an 11-day mean repeat orbit at low latitudes. The satellite will be equipped with a Ka-band swath radar interferometer capable of producing two wide swaths covering 50-km each on either side with a 20-km gap at nadir for the Ku-band altimeter. The aggregate 100-km swath width is expected to capture all lakes and reservoirs greater than 0.0625 km^2. Although offering global coverage, actual coverage is expected to be approximately 90% due to gaps in adjacent satellite tracks and spacing between nadir altimeter measurements (Biancamaria et al., 2015).

Based on the large quantity and distribution of reservoirs that will be monitored by SWOT and the short three-year mission lifetime, it is essential to characterize the associated measurement error prior to launch to facilitate effective processing and use of data during the mission. Anticipated major sources of error include those related to the instrument, satellite orbit, signal delay caused by the atmosphere, spatial or temporal

sampling patterns, vegetation interference, layover from heterogeneities in the land surface, and supplemental data processing (Durand et al., 2008; Biancamaria et al., 2010). Another issue is the effects of backscatter at low incidence angles over darker water surfaces where the land-water contrast is low, causing such surfaces to be incorrectly classified as terrain. More details about this problem including calibration of the backscatter coefficient can be found in Fjørtoft et al. (2014). SWOT reservoir height measurements are projected to be accurate to within 10 cm for reservoirs greater than 1 km^2 and 25 cm for those greater than 0.0625 km^2 but below 1 km^2 (Biancamaria et al., 2015). The expected error of reservoir surface area measurements is less than 15% of the total area (Rodriguez, 2015). Even still, it is necessary to further refine these reservoir height and area error properties specifically for reservoirs, as this estimate applies to both lakes and reservoirs and is based on the properties of the instrument on-board SWOT rather than actual tests conducted exclusively for reservoirs.

Several studies have analyzed different aspects of expected river, reservoir, and lake observations or applications using SWOT. Some of these studies invoked the use of the SWOTsim instrument simulator, which was developed to simulate expected SWOT measurements over the land surface based on realistic satellite error and orbit characteristics (Rodriguez and Moller, 2004). For instance, data assimilation techniques in conjunction with simulated SWOT data produced from SWOTsim and a hydrodynamics model were used to evaluate the feasibility of estimating SWOT discharge and its expected accuracy characteristics in the Ohio River Basin (Andreadis et al., 2007; Durand et al., 2010; Moller et al., 2010). Data assimilation methods were also used to compile virtual SWOT observations of reservoir elevation into a model to improve optimal releases for the

Selingue Dam in the Niger River Basin (Munier et al., 2015). Pavelsky et al. (2014) estimated how much SWOT will improve global discharge observations by determining the number of SWOT-observable river basins from an inventory of river widths developed from the Hydro1K dataset. This number was then compared to in-situ-observable river basins based on Global Runoff Data Centre (GRDC) and United States Geological Survey (USGS) gauge information. Lee et al. (2010) generated virtual SWOT measurements of lake storage changes for three large regions in the northern high latitudes using realistic SWOT spatiotemporal sampling of water surface heights from lake gauges and ENVISAT altimeter measurements, and inundated areas obtained from Landsat satellite imagery. Storage change errors of less than 5% were found for large lakes (>1 km^2) and less than 20% for small lakes (<0.01 km^2). Moreover, elongated shaped lakes were determined to have higher errors than those exhibiting a more circular geometry.

Although these studies serve as excellent prototypes for the expected accuracy of future SWOT observations in land surface hydrology and the lake error estimate studies likely have many similarities with those for reservoirs, a number of key differences between reservoirs and lakes indicate a more detailed analysis of SWOT error properties for reservoirs is still warranted. For example, reservoir shapes tend to display a more dendritic topology and are thus more elongated with mean surface areas typically an order of magnitude higher than that of lakes, as lakes typically exhibit more rounded, symmetrical shapes. Because reservoirs are often created to augment water supplies, provide for flood control, or generate electricity, the variability in reservoir surface area and height is often much higher than that of lakes to accommodate abrupt changes in human water demands. Alternatively, lakes are defined as natural systems with generally

lower water surface area and height variability linked to variations in precipitation, evaporation, and discharge. Moreover, the close linkage of reservoirs to people lends them the distinction of more likely to be located in regions with elevated human populations, such as in the low- to mid-latitudes, whereas lakes are much more concentrated in the higher latitudes (Cooke et al., 2005). Combined, these topologic, hydrologic, and spatial factors will likely lead to unique error characteristics in SWOT reservoir measurements relative to lakes, thereby providing the motivation for a more detailed assessment of SWOT observations of reservoirs.

Despite the distinction between lakes and reservoirs noted above, in reality, few water bodies commonly classified as lakes that are located in developed areas at lower latitudes hold true to this definition. Dams often exist at the head of outflows to manage flows for different uses and/or diversions exist to augment water supplies. With few exceptions, lakes predominantly exist in an unaltered, natural condition at high latitudes or alpine environments where human development is often minimal.

In this study, we evaluate the ability of SWOT to observe reservoirs using both in-situ reservoir storage records and virtual SWOT data generated from SWOTsim. First, aliasing due to the temporal resolution of SWOT is assessed by comparing "true" monthly reservoir storage computed from daily in-situ storage observations to "SWOT-based" monthly reservoir storage estimates computed from subsampled in-situ daily storage measurements at the expected range of SWOT repeat orbit cycles. Although we only use California reservoirs for this portion of the study, the use of the repeat orbits allows us to extrapolate the implications of the temporal results to all parts of the world covered by SWOT. Second, we use SWOTsim measurements of water surface height and area to

evaluate how different spatial characteristics of reservoirs will impact the reservoir observation performance of SWOT. This information will be useful in determining the likely error characteristics for a reservoir based on its morphology or environmental settings prior to launch. Finally, we simulate SWOT measurements of water surface area and height for six California reservoirs covering three size classes using SWOTsim to provide a more realistic assessment of SWOT reservoir measurement accuracies and validate some of the results obtained from the first two components of the study.

3.2 Methods

3.2.1 Data Sources

In-situ data were obtained from the California Data Exchange Center (CDEC, www.cdec.water.ca.gov, August 18, 2014). CDEC serves as a repository for statewide hydrology data from the United States Army Corps of Engineers (USACE), United States Bureau of Reclamation (USBR), and local county and municipal governments. Only data from 2008 to 2012 was used because it included both wet and dry years relative to historic statewide annual precipitation levels; thus a high proportion of the variability in climate information was captured in these datasets (NOAA, 2014). In addition, the use of more modern records increased the likelihood that continuous in-situ data were available, thereby decreasing the need to address gaps in the record.

3.2.2 Temporal Analysis

For the temporal analysis portion of the study, we generate monthly 'virtual SWOT' data from daily observations of reservoir storage to compare to monthly records of storage. Daily reservoir storage was obtained from 63 California reservoirs (Figure 1), which were

selected based on the availability of continuous data during the targeted study period. Daily storage data from these reservoirs were subsampled at 3-, 5-, 10-, and 20-day regular intervals to approximately match the expected SWOT repeat orbit passes over one cycle (Biancamaria et al., 2010). The resulting sub-monthly storage data were then converted to monthly values by computing the mean out of the number of observations that fell over a given month. The computed 'virtual SWOT' monthly data were compared to in-situ monthly data calculated from continuous daily data using the mean percent error (ε) of storage (%) shown in Equation 1:

$$\varepsilon = \frac{\sum_{i=1}^{n}\left[S_o(t) - S_s(t)\right]}{n * \sum_{i=1}^{n} S_o(t)} * 100 \qquad (1)$$

where n is the number of monthly observations, S_o is the in-situ monthly storage (m^3) and S_s is the monthly storage (m^3) computed from sub-sampled daily records.

It is acknowledged that the actual SWOT repeat orbit will occur at irregular intervals. For instance, a 5-day repeat orbit indicates SWOT will observe a location approximately four times over a 20-day period, but not necessarily every 5th day. Regular sampling frequencies are used here because we were not attempting to exactly replicate the sampling frequency of SWOT observations over the limited number of California reservoirs that were tested. Rather, we aimed to capture the range of variability in error resulting from the array of expected global temporal sampling frequencies, thereby better mimicking the sample frequency error for global reservoirs and not just those in California.

3.2.3 Spatial Analysis: Theoretical Reservoir Experiments

The second phase of the study involved the use of SWOTsim (v2, downloaded 1 October 2014) to determine how reservoir size, shape, orientation, neighboring topography, and partial swath coverage will impact the performance of SWOT. SWOTsim involves running a series of modules to process a set of realistic SWOT orbit files, as well as digital elevation maps and water elevation files supplied by the user. Elevation and orbit information is interpolated to the sensor cross-track and along-track geometry according to the specified ground spacing input into SWOTsim. This information is then used to create the ground-coordinate digital elevation map, which in turn, is used in conjunction with realistic radar parameters to generate the interferogram by running several additional modules (Peral et al., 2012). The resulting interferogram is an image of water surface elevation swaths based on instrument errors, orbit, and spatial resolution of the satellite (Andreadis et al., 2007). This provides the basis of which all simulated water surface area and elevation estimates were made using SWOTsim. More information regarding user-defined SWOTsim parameters and settings are contained in the Appendix (Table A1).

SWOT reservoir surface area and height data was generated for theoretical reservoirs using SWOTsim, which includes a comprehensive set of expected global orbit swath paths over one 21-day SWOT cycle. The coordinates of the theoretical reservoirs were adjusted to ensure that the entire reservoir was completely within the boundaries of the orbit paths, as the theoretical experiments were designed to determine the minimum expected error in SWOT observations for different spatial characteristics.

The accuracy in reservoir surface area and height was calculated directly from SWOTsim by comparing the simulated to "truth" estimates. Errors in reservoir surface area were evaluated using the percent bias, which is shown in Equation 2:

$$\theta_A = \frac{A_t - \sum_{i=1}^{k}(g_i * a_i)}{A_t} * 100 \quad (2)$$

where theta-A is the surface area bias (%), A_t is the true inundated surface area (m^2), g is the satellite ground resolution (m), a is the azimuth spacing (m) determined from SWOTsim, and k is the number of pixels associated with the observed reservoir. The product of the ground resolution and azimuth spacing is equal to the pixel area, the sum of which equals the simulated area of the given reservoir. Errors in reservoir height were calculated using the mean height bias, shown in Equation 3:

$$\theta_H = \frac{\sum_{i=1}^{k}(H_t,i - H_s,i)}{n} * 100 \quad (3)$$

where theta-H is the height mean bias (%), H_t is the true and H_s is the simulated water surface height (m) given n observations. The accuracy in height observations (sigma-h) was also estimated using the root-mean-square-error (RMSE), which is shown in Equation 4:

$$\sigma_H = \left[\frac{\sum_{i=1}^{k}(H_t,i - H_s,i)}{n} \right]^{\frac{1}{2}} \quad (4)$$

where H_t is the mean theoretical reservoir water surface height (m) and H_s is the simulated water surface height (m) given n observations.

Each theoretical test involved the creation of artificial reservoirs through construction of distinct water depth and digital elevation model (DEM) files, which served as the domain inputs for SWOTsim. The water depth and DEM files were developed to test only the influence of a single spatial characteristic (size, shape and orientation, topography, or partial reservoir coverage) on the performance of SWOT during each series of tests. This was achieved by holding the other spatial characteristics not actively being examined constant and using static water levels and heights to isolate the impact on observation error to only the targeted variable being tested. The number of different simulations conducted to adequately characterize the effect of a given spatial property on the error depended on the expected range of that variable likely to be observed in the real world. More details about the simulations for the different spatial tests are presented in Table 1 and in the paragraphs that follow.

The reservoir size tests proceeded by simulating SWOTsim over reservoir sizes up to 10^4 km^2, which spans the global range of reservoir surface areas (Figure 2). Only circular reservoir shapes and flat surrounding topography with static water levels were used to isolate the influence on errors to reservoir size.

The experiment for the influence of reservoir shape on SWOT observations worked similarly. For this set of simulations, only the shape of the reservoir was altered between each test. Shapes that were tested included ellipses with varying axis ratios ranging from 24:1 (more elliptical) to 1:1 (circle). This sequence was selected based on the tendency of reservoirs to form dendritic patterns comprised entirely of elongated ovals or those that

more closely resemble a lake with symmetrical surface areas. For each series of aspect ratios that were tested, three different sizes were evaluated including 10^0, 10^1 and 10^2 km^2, which represent the more common reservoir sizes found globally (Figure 2). Ellipses were oriented either parallel (along-track) or perpendicular (cross-track) to the orbit pass in SWOTsim to capture the full range of reservoir shape and orientation effects on SWOT observations. Flat topography and static water levels were used.

The experiment for reservoir topography was conducted by changing the topographic slopes adjacent to the reservoir while holding all other spatial factors constant for each test. Different slopes that were used ranged from 0 to 1.7 m/m at 0.17 m/m increments. The slopes were kept uniform to a finite distance away from the reservoir to effectively form a topographic bowl on all sides of the reservoir. Only circular shapes were tested with a uniform size of 10^1 km^2 and static water levels.

The theoretical reservoir experiment involved examining the impact of partial reservoir coverage by the swath path on SWOT reservoir height observations. Note that the impact of partial reservoir coverage on inundation area measurements was not explored. This aspect was avoided because presumably when only part of the reservoir is covered by the swath, ancillary SWOT data will be used to estimate the total inundation area of the given reservoir. Partial reservoir coverages that were assessed ranged from approximately 1 to 50%, as differences in height observations did not vary by as much once the reservoir was covered by at least half of the swath. Tests were conducted separately for partial coverages in the near-range and far-range portions of the swath, as errors are not expected to be uniform throughout the swath due to larger and more variable pixel sizes in the near-range section (Fjørtoft et al., 2014). Both 1:1 and 24:1 aspect ratios

oriented parallel and perpendicular to SWOT orbit were tested to capture the full range of influence from different reservoir configurations. Only flat surrounding topography with a size of 10^1 km^2 and static water levels were used for this series of experiments.

3.2.4 Spatial Analysis: Actual Reservoir Experiments

The final phase of this study involved the use of SWOTsim to evaluate the expected performance of SWOT for actual reservoirs. Six California reservoirs were selected based on the coverage of three size classes (<10 km^2, 10-100 km^2, and >100 km^2), as well as different spatial and climate regimes (Figure 1, Table 2). The use of California reservoirs was ideal because like California, reservoirs at the global scale tend to be located in low- to mid-latitude regions where expected SWOT orbit pass frequencies and trajectories would be similar. Only static water surface height and inundation area were investigated, as the impacts on aliasing due to the temporal resolution of SWOT were already investigated in the first part of this study. Surrounding reservoir topography was taken from the NASA ASTER GDEM v2 at 30 m resolution (http://gdex.cr.usgs.gov/gdex/) due to the large increase in computation time for minimal gains in improved results at a higher spatial resolution. Reservoir inundated area bias and reservoir height mean bias were again calculated using Equations 2 and 3, respectively. Multiple simulations were conducted for each reservoir where the domain was manually shifted by 0.02-degree longitude increments prior to each simulation until the entire width of the swath was covered to account for the differences in error properties throughout the swath. The number of simulations conducted for each of the six reservoirs is: 3, 19, 20, 15, 23, and 17 (ordered from largest to smallest by surface area).

3.3 Results

3.3.1 Temporal Analysis

The results for the portion of the study that evaluated the error due to expected SWOT observation frequencies show that smaller reservoir sizes with lower observation frequencies yield higher errors in SWOT reservoir observations. The mean monthly storage percent error (equation 1) generally fell between 0.1-1% for the highest sampling frequency of one observation per every three days and 1-5% for the lowest sampling frequency of one observation per every 20-days. Errors between these ranges were obtained for the more moderate sampling frequencies of one measurement per every 5- and 10-days. Comparisons of monthly storage time series computed from daily (truth) and sub-sampled daily storage records (synthetic) at different sampling frequencies for the small (<10 km^2), medium (10 – 100 km^2), and large (>100 km^2) size classes are shown in Figure 3. The difference between the two records for any given observation did not vary by more than 1% at the highest sampling frequency and 10% at the lowest sampling frequency.

Comparable patterns were observed in the nRMSE, Nash-Sutcliffe efficiency (NSE), and 95% confidence interval results. As displayed in Figure 4, the storage nRMSE generally fell below 10^{-1} for the smaller sampling frequency and was an order of magnitude lower for the higher sampling frequency. Similarly, the NSE increased for larger reservoirs with higher sample return intervals. The NSE between true and synthetic storage records was also only observed to be consistently above 0.8 for the higher sampling frequencies of one observation per every three-, five-, and ten-days. As shown in Figure 5, the thickness of the 95% mean confidence interval in synthetic storage estimates decreased exponentially with

an increase in reservoir storage capacity. The highest value of approximately 23% of maximum storage capacity was observed for the smallest reservoir at the lowest sampling frequencies. Furthermore, the 95% confidence interval width was approximately six times greater for the lowest sampling frequency relative to the highest. Mean confidence intervals approached an asymptote in reservoirs above 10 km^2 for all sampling frequencies.

3.3.2 Spatial Analysis: Theoretical Reservoir Experiments

Performance statistics in the theoretical reservoir size spatial experiments were also indicative of lower accuracies for smaller reservoir surface areas. As portrayed in Figure 6, the positive bias in reservoir surface area (equation 2) decreased exponentially from a high of 21% to a low of less than 0.1% for the smallest 10^{-1} km^2 and largest 10^4 km^2 reservoir size classes, respectively. Correspondingly, the mean negative bias of reservoir height observations (equation 3) ranged from approximately -20 cm for the smallest reservoir size to less than 1 cm for all reservoirs larger than 10^1 km^2.

In general, the theoretical reservoir shape and orientation experiments showed greater bias in water surface area and heights at higher aspect ratios (Figure 7). This scenario typically held true for each of the three size classes that were tested where the greatest bias was again observed in the smallest size class. The bias in surface area ranged between approximately 10-30% for the smallest reservoir size class of 10^0 km^2, but was less than 10% for all aspect ratios of the two larger size classes that were tested. Mean bias in reservoir height exhibited greater overall variability than the surface area results, but as shown in Table 3 and similar to the surface area results, the bias was higher for smaller reservoirs oriented parallel rather than perpendicular to SWOT orbit. Moreover, the

percent bias in surface area increased by a factor of over two and the mean bias in height increased by a factor of more than 1.5 when the reservoir size decreased by an order of magnitude.

The test on surrounding reservoir topography revealed an increase in the magnitude of the surface area and height biases with enhancements in topographic slopes. This magnitude increase was most pronounced between slopes of approximately 0.1 m/m and 0.2 m/m for the surface area bias, while changes in the accuracy were more gradual at higher slopes (Figure 8). The mean biases in reservoir height ranged from a minimum of +/-1 cm to a maximum of -15 cm. Shifts in the accuracy of height measurements with increases in topographic slope were more variable than with the surface area results. Overall, height measurements were still less accurate at higher slopes, as the mean RMSE (equation 4) for slopes above 0.8 m/m was 6.0 cm compared to 4.9 cm (20% decrease) below this slope threshold.

For the partial reservoir coverage tests, as expected the higher mean biases in reservoir height were associated with lower reservoir coverages for all experiments (Figure 9). The discrepancy in bias between the near and far range tests was much higher for the series of parallel to orbit trials, while this difference in magnitude was much smaller for the perpendicular to orbit and circular reservoir tests. The maximum height bias of 35 cm was observed in the near range experiments oriented parallel to orbit, while the maximum bias was less than 6 cm for all other reservoir configurations and reservoir coverages that were tested. Once the swath coverage of the reservoir exceeded 30% for all experiments, the bias in reservoir height converged towards 0 cm.

3.3.3 Spatial Analysis: Actual Reservoir Experiments

Results from the actual reservoir simulations are presented in Figure 10. The median, 25th and 75th percentile area bias values are generally clustered close to zero for all reservoirs. The results from the smallest reservoir type represent an exception to this rule, as the median bias approached 20% with a 15-30% range for the 25th and 75th percentile values. Other 25th and 75th percentile values were close to the respective median values for the reservoir except for the fourth-largest reservoir, which had values that ranged from approximately -50-0%. Similar to the area bias results, low variability was observed in the mean height bias results, as the median, 25th and 75th percentile values were less than 15 cm for all but the fourth largest reservoir, which had a much higher 25th to 75th percentile range and median of approximately 25 cm. Area and height outliers outside the 25th and 75th percentiles were observed for all but the largest and fourth largest reservoirs, as well as the smallest reservoir only for the mean height bias results.

3.4. Discussion

3.4.1 Temporal Analysis

The temporal analysis portion of the study aimed to determine how well the sampling frequency of SWOT could be used to reconstruct monthly reservoir storage records. Such information will be useful for integrating into hydrologic models at similar timesteps, or for local or regional water supply monitoring systems. Moreover, this information indicates how well SWOT will be able to reproduce observations over time, as the rest of the study only evaluated error characteristics from instantaneous measurements. Based on the results, the potential for aliasing the true hydrologic signal due to the SWOT repeat orbit pass is minimal except for in the case where the smallest

reservoir sizes expected to be visible by SWOT (<3 km^2) are being sampled at the lowest frequency of one observation every 20-days. Errors in individual observations for these reservoirs at this sample return interval approached 10%, which could be problematic when trying to integrate into a hydrologic model or to provide accurate information about local or regional water supplies. Based on Figure 2, approximately 40% of global reservoirs fall within this size class. Of these, only approximately one-third (13% of total) are expected to be sampled at the lowest sampling frequency where aliasing may be an issue given the global repeat orbit passes for different reservoir sizes shown in Figure 11. Nevertheless, Figure 5 indicates that above a reservoir size threshold of approximately 10 km^2 the difference in temporal sampling error associated with reservoir size is negligible and large shifts are only related to changes in the sampling frequency. Such a finding reiterates the importance of reservoir surface area on the expected accuracy of observations.

The ability to reproduce daily or sub-daily records from observations made at the range of expected SWOT sampling frequencies was not conducted as a part of this study. This information would be more beneficial for incorporating into models that use smaller timesteps or to provide useful information for reservoir functions that are more reliant on operational changes that occur over shorter timescales, such as hydroelectricity generation or flood control. Had such an analysis been performed, higher levels of aliasing would have been expected due to the large shifts in storage often associated with a single storm or abrupt snowmelt-inducing weather event that would be difficult to reproduce for all reservoir sizes at even the highest sampling frequency expected by SWOT. This was

beyond the scope of this study, however, as here the interest was to evaluate the potential for aliasing at timescales that are more scalable to the temporal resolution of SWOT.

3.4.2 Spatial Analysis: Theoretical Reservoir Experiments

Many of the errors in SWOT surface water observations related to size are linked to edge effects of the given water body, meaning that higher perimeter to surface area ratios of smaller water bodies result in a lower degree of accuracy (Lee et al., 2010). Indeed, results from the theoretical experiment for reservoir size impacts on SWOT observations support this argument. Mean reservoir surface area biases of 10% were observed in reservoirs with areas that were approximately double the size threshold of 0.0625 km^2, which is listed as the minimum inundated area expected to be visible by SWOT (Rodriguez, 2015). For the next highest size class of 1 km^2, the surface area bias dropped by one-half to less than 5% and continued to decrease asymptotically towards 0% for all reservoir sizes above this size. Similar trends were noted in the height bias results, as the magnitude in bias decreased exponentially from a maximum of 20 cm for the smallest 0.1 km^2 reservoir to less than 5 cm for all reservoirs above 1 km^2. Even still, given that 80% of reservoirs found worldwide are greater than 1 km^2, surface area and height error stemming from size alone should not contribute greatly to the total error for observations made by SWOT.

The SWOTsim results from the reservoir shape and orientation experiments revealed that reservoirs oriented parallel to orbit at higher degrees of ellipticity have a stronger influence on the accuracy in observations. For the perpendicular to SWOT orbit experiments, the area and height biases for all three reservoir sizes in Figure 7 more closely resemble the results for the same reservoir sizes shown in Figure 6, indicating the errors are predominantly due to the size of the reservoir. Alternatively, when the aspect

ratio was oriented parallel to orbit, the area bias increased and mean height bias was more variable and reached maximum values for all three size classes at higher aspect ratios (>20:1), suggesting reservoir shape and orientation can have a much higher impact on the accuracy than size at extreme aspect ratios for the parallel to orbit case. For example, the surface area bias for the 1 km^2 reservoir size in Figure 7 is more than 350% higher than in Figure 6. In addition, as shown in Table 3, the mean height bias increased by an average of over 150%, 200%, and 400% for the 1, 10 and 100 km^2 reservoirs oriented parallel relative to those configured perpendicular to orbit. Analogous to the effects noted in the reservoir size experiments, the reduction in accuracy for large aspect ratios stems from the greater perimeter to surface area ratio and thus stronger edge effects resulting in a higher rate of landtype misidentification by the satellite.

The irregularities in the curves shown in Figure 7 can be explained by the nature of the SWOT instrumentation. For instance, the sensitivity of measurements to error is primarily a function of the mixed pixels, which are more prevalent in water bodies oriented parallel to satellite orbit because of the side-scanning arms of the interferometric Synthetic Aperture Radar on-board SWOT, which leads to an increased surface area and height bias for reservoirs with aspect ratios oriented parallel rather than perpendicular to SWOT orbit. In addition, changes in accuracy are expected when swath coverage of the reservoir switches from dominance in the far-range to the near-range portion of the swath, as projected pixel range sizes are larger and more variable in the near-range due to stronger layover from higher signal-to-noise ratios (SNR) (Fjørtoft et al., 2014). The higher variability in the mean height bias and area bias above an aspect ratio of twenty is likely the result of this phenomenon. Changing the aspect ratio of the reservoir means it will

either capture more or less of the near-range portion of the swath, leading to shifts in the accuracy relative to adjacent aspect ratios.

During the actual mission, it is expected that utilizing results from multiple orbit passes over a single reservoir will help to minimize the area error emanating from dominant coverage in the near-range portion of the swath. This is an iterative process – the greater the number of observations, the better the accuracy. Given this, the error will improve much sooner for reservoirs located at higher altitudes where SWOT repeat passes will be more frequent. However, the shape, size, and orientation of the reservoir will also play a role in the number of repeat observations by different swaths, thereby compounding this problem. For this reason, although potentially achievable using multiple simulations from SWOTsim, we felt it was necessary to instead focus our efforts in determining observation accuracy of reservoirs on cases where the reservoir is largely intersected by a single swath. Analysis of improving reservoir area observations with the use of multiple swaths is too complicated and different of a problem, making it better suited for another study.

According to the topographic results for the theoretical reservoirs, increases in surrounding topography enhanced the bias for both reservoir surface area and height. This phenomenon is largely the result of topographic layover, which is expected to be an issue when the slope of the local terrain exceeds the incidence angle of 0.6-3.9° (Fjørtoft et al., 2014). Similar to the shape and orientation test results, the bias in height measurements was more variable with changes in slope making it difficult to ascertain the influence of layover. However, the height RMSE was found to be 23% higher for larger slopes above 0.8 m/m, thereby still indicating the presence of stronger layover at higher slopes.

The same phenomenon involved with the irregularities observed in the theoretical reservoir results for shape and orientation was explored further with the experiments involving the effects of partial reservoir coverage. With the exception of the parallel to orbit series of tests, the magnitude in height bias for the near and far range experiments was similar given the same percent reservoir area coverage. The larger discrepancies observed in parallel to orbit tests is likely due to higher layover in the near range from larger SNR, as observed in the shape and orientation experiments. The reduction in bias to near-zero for all simulations above 30% reservoir coverage represents an important finding for the reliability of reservoir height estimates that are not completely covered by the swath, as partial swath coverage observations of water bodies are expected to be common occurrences during the actual mission.

3.4.3 Spatial Analysis: Actual Reservoir Experiments

Results from the SWOTsim simulations involving actual reservoirs in California corroborated the findings from the theoretical reservoir experiments. The smallest reservoir again had the largest median in area bias values. The median height bias results were not as strongly linked to reservoir size, which was due to the higher variability in height accuracies stemming from reservoir shape and orientation or topographic layover effects that were demonstrated in the theoretical experiments. The median height bias values were still within the range of anticipated values shown in the theoretical experiments, as all were less than 15 cm with the exception of the fourth largest reservoir (18.45 km^2). As expected from the reservoir shape and orientation experiments, a much larger range in the 25th to 75th percentile biases and median height bias occurred for the fourth largest reservoir due to its strong parallel-to-orbit orientation. Also as anticipated

from previous results, outliers and higher biases for the fourth largest reservoir occurred when swath coverage of the reservoir was predominantly in the near-range, which led to higher layover from increased SNR. In spite of these high biases observed in individual results, the large number of simulations conducted for each reservoir largely canceled out the effects of the outliers on the median, and the 25th to 75th percentile range for most of the reservoirs.

Testing the influence of reservoir shape on observation accuracy with the true reservoir simulations was avoided because in reality reservoirs come in too many different shapes to adequately quantify this when only six reservoirs were used. The impact of reservoir shapes on observation error was still tested with the theoretical reservoirs because within this more experimental setting, the expected error range could be captured by testing reservoirs with extreme shapes, such as very high aspect ratios oriented both parallel and perpendicular to orbit. In doing so, the maximum amount of error resulting from the shape of the reservoir was effectively constrained, which was our intent. The number of real reservoirs that could be tested was restricted due to the computational limitations of SWOTsim, so much of the discussion of the true reservoir simulation results focuses on verification of the theoretical reservoir simulation results.

Ideally, SWOTsim would have been run over every reservoir across the globe. However, running SWOTsim over a global DEM (or even California) at the necessary spatial scale is too computationally intensive to generate results in a reasonable amount of time. As such, the theoretical reservoir experiments were devised to represent the expected range of global error stemming from each spatial error source more simply and verified these results with the six California reservoir simulations. In this way, one can still get a

general quantitative sense of how much spatial error will occur for any given global reservoir by matching its spatial characteristics to the spatial error properties we find here. We go through this procedure with one of the reservoirs that was tested in Figure 12.

Results from the analysis in Figure 12 show a total error of 0.88-1.40 km^2, representing 2.35-3.74% of the aggregate total area of the eight ellipses used to make this calculation. The total percent bias is reasonably close to the median error value of 0.72% presented in Figure 10 for the Black Butte Reservoir, thereby verifying that this method can be used to estimate area errors for any global reservoir. Only eight ellipses were used here as a means of demonstrating this method, but we acknowledge disaggregating the reservoir shape into different numbers of ellipses may be used, depending on the desired level of accuracy when applying this technique. Furthermore, we point out that errors due to reservoir topography were not accounted for in this calculation, as topography biases were shown to contribute less than 0.3% for a reservoir of approximately the same size as Black Butte (Figure 8). Although small, we note here that these errors might increase for smaller reservoirs where the error due to topographic interference would represent a greater portion of the total reservoir surface area.

3.4.4 Study Limitations and Caveats

We chose not to go through a similar procedure to determine height errors for the Black Butte Reservoir due to the much higher variability in height biases from the changes in shape and orientation shown in Figure 7. These errors are potentially further compounded by the large height biases associated with layover from surrounding topography, which would also apply had we taken this additional step. Instead, we point out here that with the exception of reservoirs displaying more extreme spatial

configurations and/or those situated adjacent to highly variable topography, the height bias results we present here are largely in agreement with the specifications reported in Rodriguez (2015). As such, when attempting to apply the results from this study to estimate reservoir height biases for SWOT observations, we encourage the use of +/- 10 cm as the maximum water surface height bias for reservoirs above 1 km^2 and +/- 25 cm bias for those between 0.0625 km^2 and 1 km^2 except when the reservoir exists in more extreme geospatial conditions, such as is the case for the fourth smallest actual reservoir that was tested in this study.

SWOTsim was used to evaluate the observation accuracy of exclusively reservoir surface area and elevation. It is noted that other types information will be gathered from observations of these two fields that we did not explore here. For example, reservoir area-elevation relationships can be used to better understand the bathymetry to improve estimates of storage. Furthermore, the product of these two terms can be used to determine changes in storage, which can also be used to estimate storage if the initial volume is known. However, we chose to focus the evaluation from this study on the accuracy of primary observations of water surface area and elevation that will be made by SWOT, as well as any error resulting from the expected frequency of observations. Although important, exploration of how well SWOT will be able to reproduce area-elevation relationships and storage changes is outside the scope of the work in this study.

It is further acknowledged that the six reservoirs used in the actual reservoir test cases fall short of the total number of reservoirs found worldwide. Using a small subset of reservoirs for this study component was conducted for two reasons. First, running the simulator for every reservoir was impractical due to the intense computation time required

to complete such an endeavor. Second, SWOTsim is constantly being updated and improved. Later SWOTsim releases are expected to be more representative of actual SWOT measurements and may facilitate application over much larger areas as alogrithms used to process the data evolve and computation times decrease. Newer versions of the simulator are expected to have additional modules to improve the water surface location and land classification errors relative to the version that was used in this study. Furthermore, as SWOTsim is only a model, results should be considered as mere representations of reality based on the current state-of-the-art physical understanding of what the satellite will observe. True accuracy in observations will only be realized during the actual mission. The results shown in this study, although improving upon the understanding of expected error characteristics of reservoirs from SWOT, should thus be used as a benchmark to guide future work with SWOT reservoir observations rather than accepted as the absolute truth.

It is also important to note that the largest surface area of the six reservoirs that were tested was less than 120 km^2 even though the largest reservoir surface area found worldwide exceeds 66,000 km^2 (Lehner et al., 2011). Excluding this size class from the study was justified, however, because the bias in reservoir surface area diminished to less than 1% of the total surface area and mean bias in height was representative of others in both the reservoir test cases and theoretical experiments. Moreover, as demonstrated in the theoretical experiments, the area and height biases were smallest for the largest theoretical reservoir that was tested of 10,000 km^2, which is much closer to the high end of the range of global surface areas. Thus, omitting the larger size classes from the analysis was not believed to result in the loss of much additional information.

3.5 Conclusions

This study characterized the temporal and spatial errors of SWOT reservoir observations using a combination of in-situ reservoir records and model results. It represents the first study known to the authors to investigate the SWOT observation accuracy exclusively for reservoirs and not just natural lakes. In addition, we accomplished this using SWOTsim, which integrates error properties of the instrument and satellite orbit, thereby making the results more comparable to what is expected from the actual mission than what has previously been accomplished for lakes or reservoirs at this level of spatial and temporal resolution.

Despite the previously noted limitations, several important temporal and spatial performance thresholds were highlighted throughout the course of the study. The temporal analysis showed that converting SWOT observations to monthly values does not result in severe aliasing except for with the smaller reservoir sizes (<3 km^2) at the lowest expected satellite orbit return interval where errors of up to 10% were observed for a single observation. Based on the cumulative distribution function (CDF) for reservoir surface areas shown in Figure 2, less than 13% of reservoirs worldwide considered to be observable by SWOT are expected to fall under this size class as well as sampled at low enough frequencies to where temporal aliasing might pose an issue.

The theoretical and test case reservoir simulations revealed that reservoir size has the largest influence on the accuracy of SWOT surface area and height measurements. Reservoirs larger than 1 km^2, which account for approximately 80% of those observed globally, are expected to have surface area and height biases of less than 5% and -5 cm, respectively. Errors for reservoir sizes below the 1-km^2 threshold increased exponentially

up to an area bias of 21% and height bias of -20 cm. In certain situations, specific geospatial characteristics of the reservoir played a larger role in SWOT water surface area and height observation errors. For instance, higher elliptical aspect ratios and orientation of the reservoir parallel to orbit were observed to increase errors by up to factors of three and six for surface area and height estimates, respectively, in the three more common reservoir sizes that were tested. Increases in surface area errors due to rises in topographic slope were most dramatic around a slope of 0.17 m/m and the height RMSE was 23% higher for slopes above 0.8 m/m relative to slopes below this magnitude. The partial reservoir coverage tests revealed that above 30% coverage of the reservoir for all spatial configurations and orientations, height estimates were reliable and showed a near-zero bias. Swath coverage that was dominated in the near range also resulted in much higher error estimates for both area and height measurements. Evidence from the actual reservoir simulations agrees with these findings, as larger reservoirs (>2 km^2) result in smaller area and height biases, except in the instance where the reservoir had a more extreme elliptical geometry oriented parallel to orbit or swath coverage is concentrated in the near-range.

The findings presented herein provide more in-depth insight into future SWOT reservoir observations. As the development of SWOTsim improves, additional simulations of reservoirs and other surface water features will only continue to be more representative of expected SWOT global surface water observations. Even still, the results presented here represent the first, more realistic attempt at reproducing global reservoir behavior as seen by SWOT. This information will be useful for determining SWOT error characteristics of a given specific reservoir a priori to mission launch and should serve as a blueprint for

subsequent studies that incorporate SWOT reservoir observations into global monitoring systems or hydrologic models.

Table 3.1 Summary geospatial statistics for theoretical reservoir experiments.

Spatial Test	No. Simulations	Area (km^2)	Aspect Ratio	Orientation Relative to Orbit (°)	Slope (m/m)	Swath Coverage[1] (%)
Size	6	$10^{-1} – 10^{4}$	1:1	--	0	100
Shape/Orientation	18	$10^{0} – 10^{2}$	-24:1 to 1:1	0 & 90	0	100
Topography	6	10^{2}	1:1	--	0 – 1.667	100
Swath Coverage	8	10^{1}	1:1	--	0	N: 2 – >50
Swath Coverage	7	10^{1}	1:1	--	0	F: 4 – >50
Swath Coverage	7	10^{1}	-24:1	90	0	N: 4 – >50
Swath Coverage	7	10^{1}	-24:1	90	0	F: 6 – >50
Swath Coverage	5	10^{1}	24:1	0	0	N: 1 – >50
Swath Coverage	7	10^{1}	24:1	0	0	F: 1 – >50

[1] N = near-range coverage, F = far-range coverage

Table 3.2 Summary hydrology and spatial information for reservoirs used to evaluate SWOT performance.

Reservoir Name	River	Use Code[a]	Latitude (°), Longitude (°)	Drainage Area (km^2)	Elevation (m)	Storage Capacity (km^3)	Surface Area (km^2)
Shasta	Sacramento	IMPR	40.72, -122.42	17,262	378	5.61	120.35
Pine Flat	Kings	IR	36.83, -119.33	4,002	296	1.23	24.16
Isabella	Kern	IR	35.65, -118.47	5,372	803	0.70	46.13
Black Butte	Stony	IR	39.81, -122.33	1,919	157	0.18	18.45
Natoma	American	RP	38.65, -121.19	4,916	40	0.11	2.19
Loon	Gerle	P	39.00, -120.31	21	1,944	0.09	5.86

[a] I = Irrigation; M = Municipal; P = Hydropower; R = Recreation

Table 3.3 Reservoir shape and orientation test area and mean height bias

Size (km2)	Orientation	Mean Area Bias (%)	Mean Height Bias (cm)
10^2	Both	1.4	0.2
10^1	Both	4.3	1.0
10^0	Both	13.4	3.9
10^2	Parallel	1.8	0.4
10^2	Perpendicular	0.8	0.1
10^1	Parallel	5.9	1.3
10^1	Perpendicular	2.4	0.6
10^0	Parallel	17.7	4.7
10^0	Perpendicular	7.8	3.0

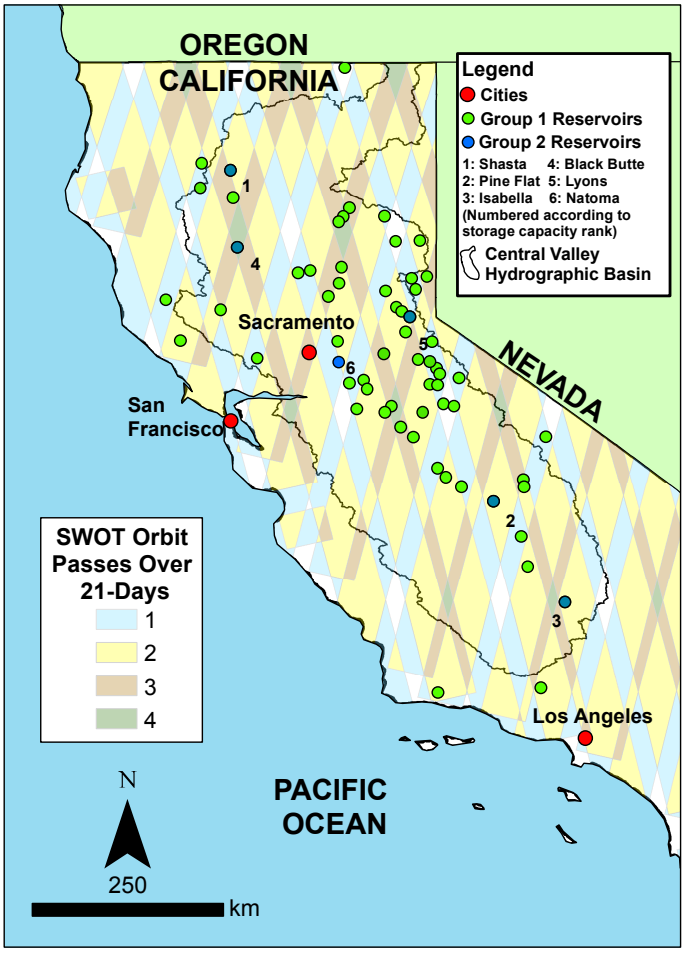

Figure 3.1: Location of reservoirs used in temporal analysis portion of study (Groups 1 and 2, blue and green circles) and actual reservoir test cases (Group 2, blue circles). Projected SWOT flight paths overlain for California where given swath is color-coded according to 21-day cycle repeat orbit pass (Repeat orbit pass data obtained from the Centre national d'etudes spatiales [CNES]).

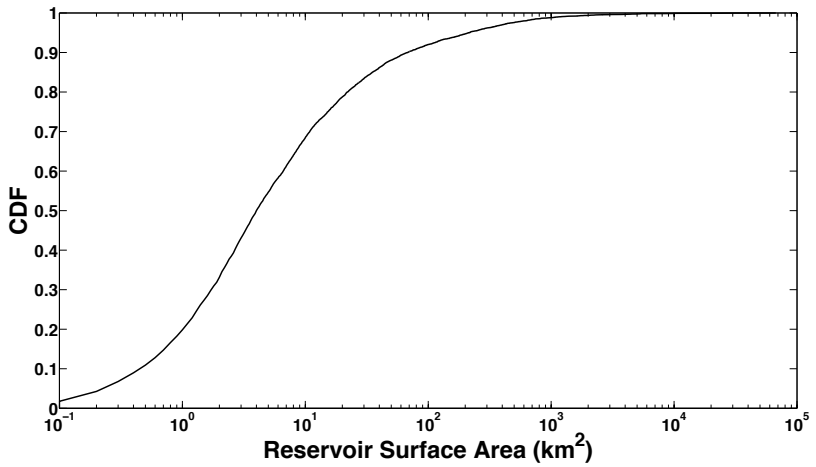

Figure 3.2: Global reservoir surface area Cumulative Distribution Function (CDF). Analysis incorporates data obtained from over 6,000 global reservoirs (Lehner et al., 2011).

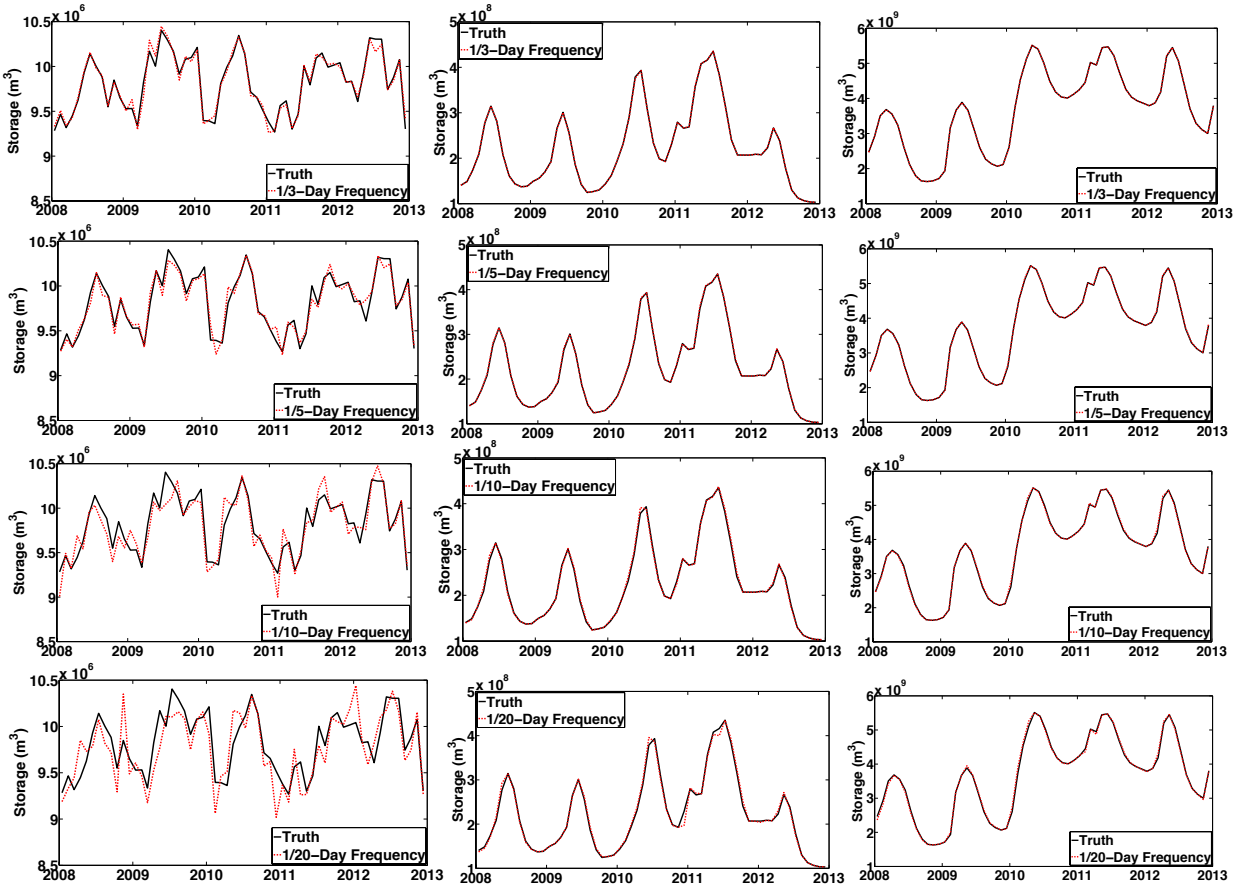

Figure 3.3: 2008-2012 in-situ truth (black) and synthetic (red) monthly reservoir storage for the three different size classes: Natoma < 10 km^2 (left), Isabella 10 to 100 km^2 (middle), and Shasta > 100 km^2 (right). Analyses shown for 3-day (top), 5-day (2nd from top), 10-day (2nd from bottom), and 20-day (bottom) repeat satellite pass.

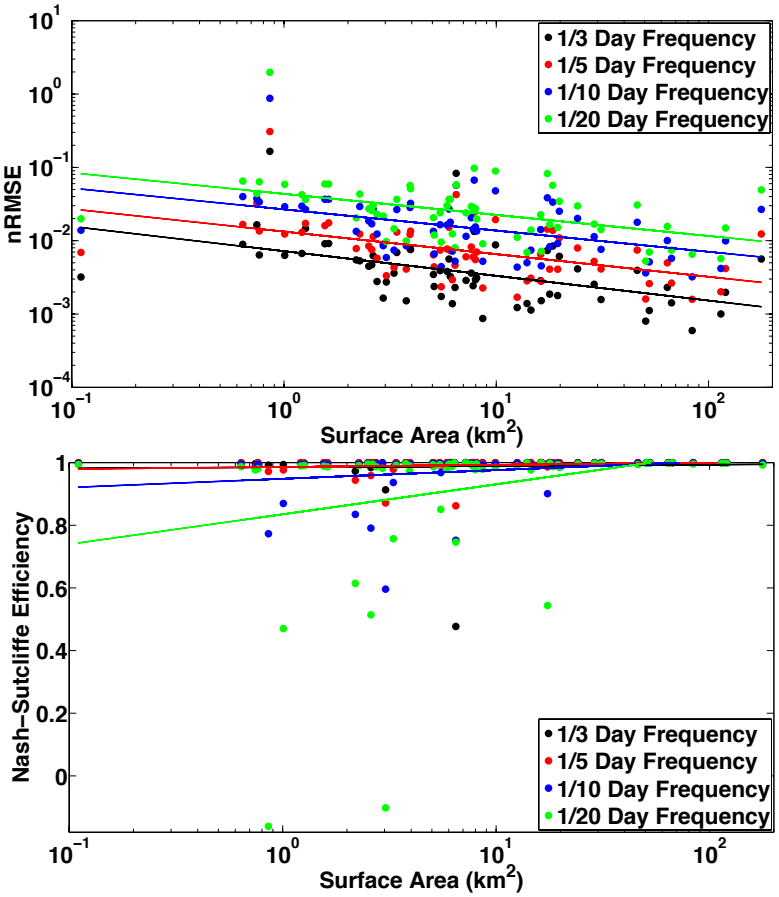

Figure 3.4: Normalized root-mean-squared-error (top) and Nash-Sutcliffe efficiency (btm) by reservoir storage capacity for 3-day (black), 5-day (red), 10-day (blue), and 20-day (green) sampling frequencies shown for the 63 reservoirs used in temporal analysis. Slopes of regression lines through points for different sampling frequencies are also shown. Mann-Kendall trend test with Sen's slope estimator indicate all nRMSE trends are statistically decreasing and NSE trends are statistically increasing with reservoir storage capacity ($p<0.05$). Root mean square error normalized to the mean.

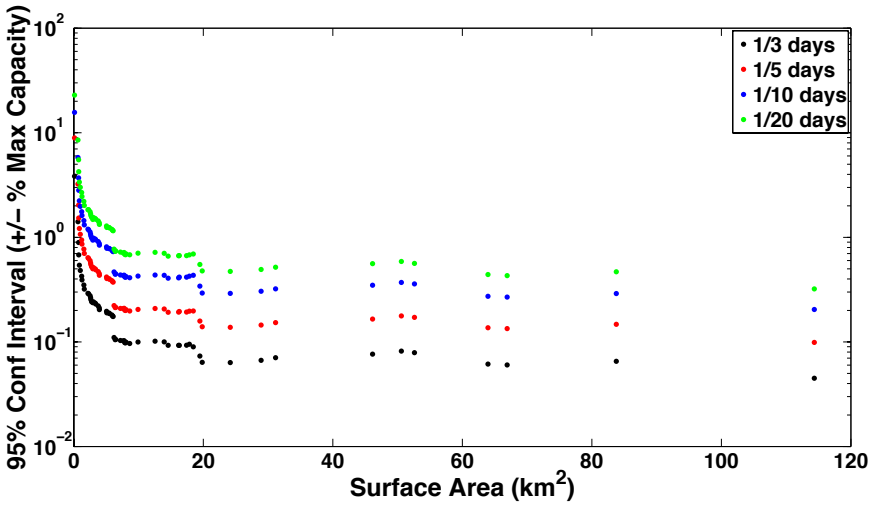

Figure 3.5: 95% confidence interval thicknesses for synthetic storage estimates expressed as the percent maximum capacity of the given reservoir and arranged by maximum storage capacity for 3-day (black), 5-day (red), 10-day (blue), and 20-day (green) sampling frequencies shown for the 63 reservoirs used in temporal analysis.

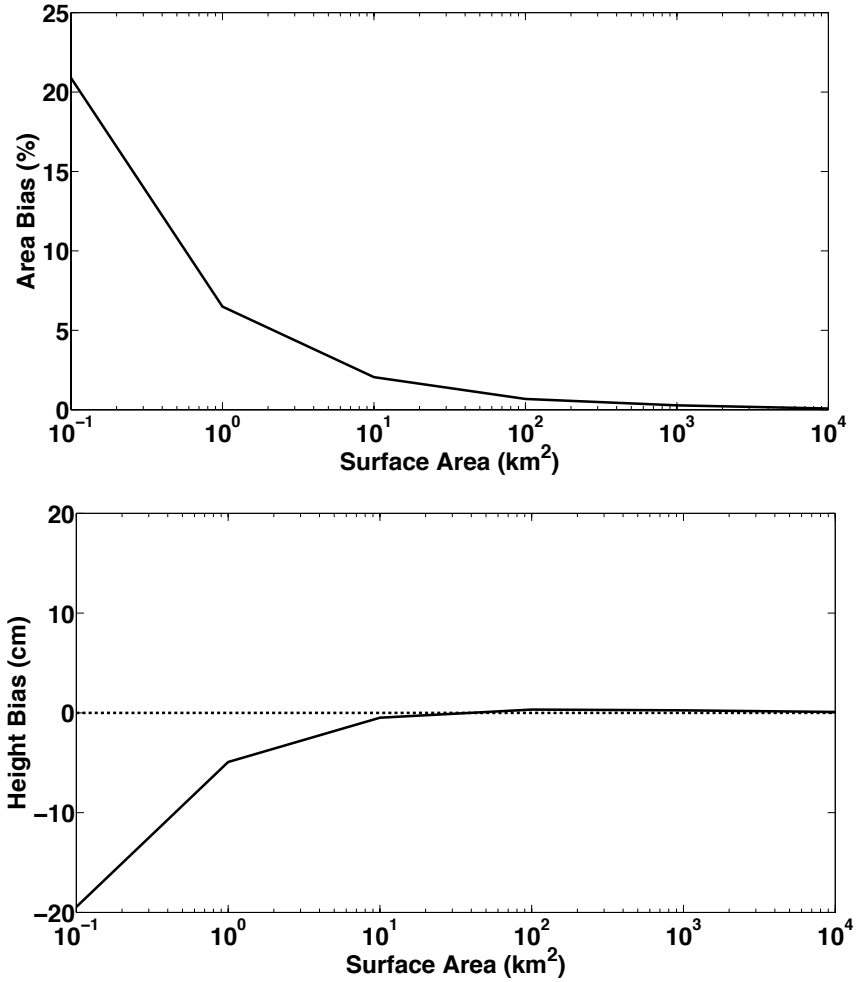

Figure 3.6: SWOTsim bias in reservoir surface area (top) and mean bias in water surface height (btm) for different reservoir sizes. More information regarding this series of tests is listed in Table 3.1.

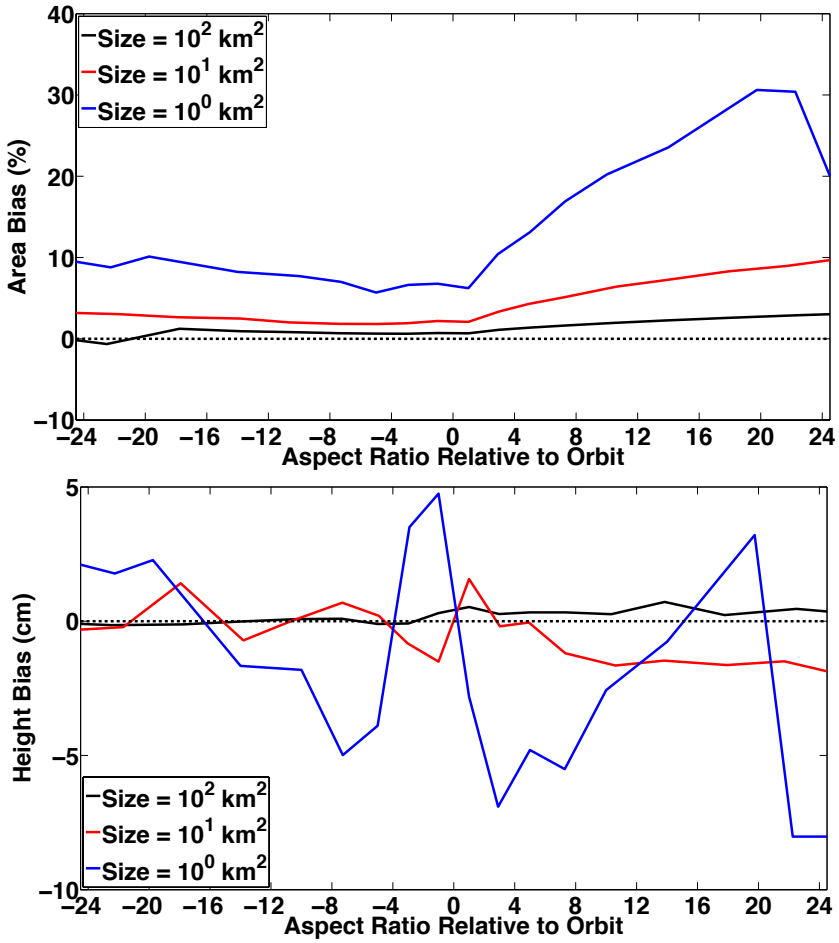

Figure 3.7: SWOTsim bias in reservoir surface area (top) and mean bias in water surface height (btm) for different reservoir aspect ratios. Negative aspect ratios indicate reservoirs oriented perpendicular to orbit, while positive values denote parallel to orbit. Analyses conducted for reservoirs of size 10^2 km^2 (black), 10^1 km^2 (red), and 10^0 km^2 (blue). More information regarding this series of tests is listed in Table 3.1.

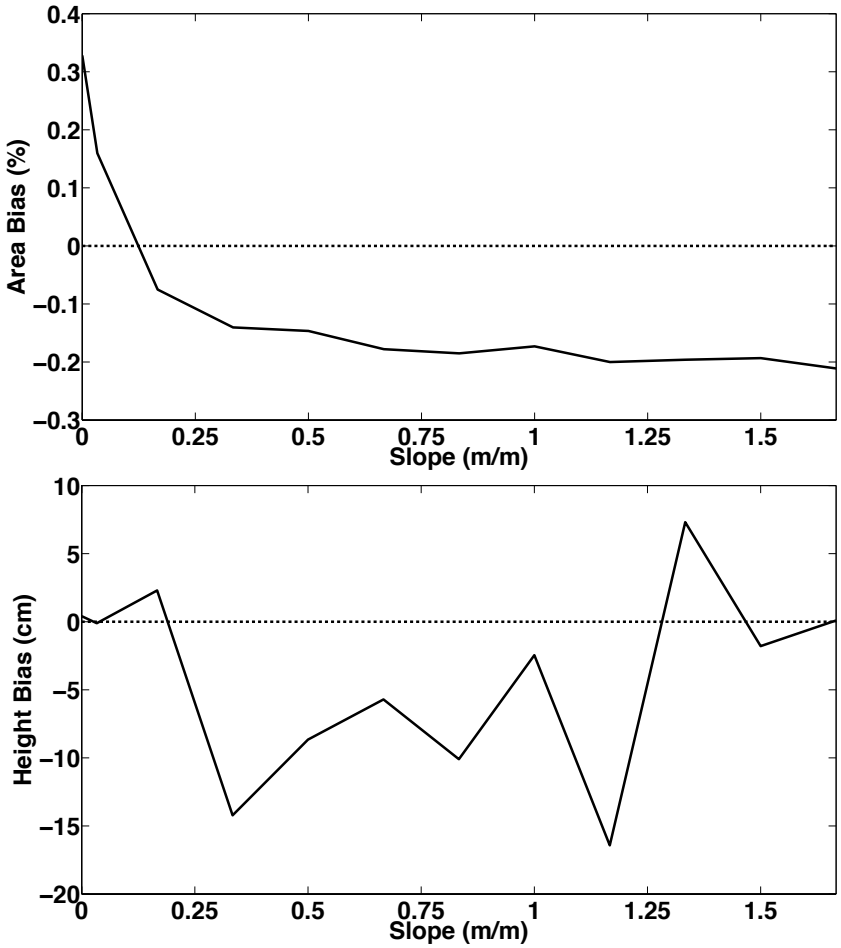

Figure 3.8: SWOTsim bias in reservoir surface area (top) and mean bias in water surface height (btm) for different adjacent topographic slopes. Reservoir size held constant at 10^1 km^2 for each test. More information regarding this series of tests is listed in Table 3.1.

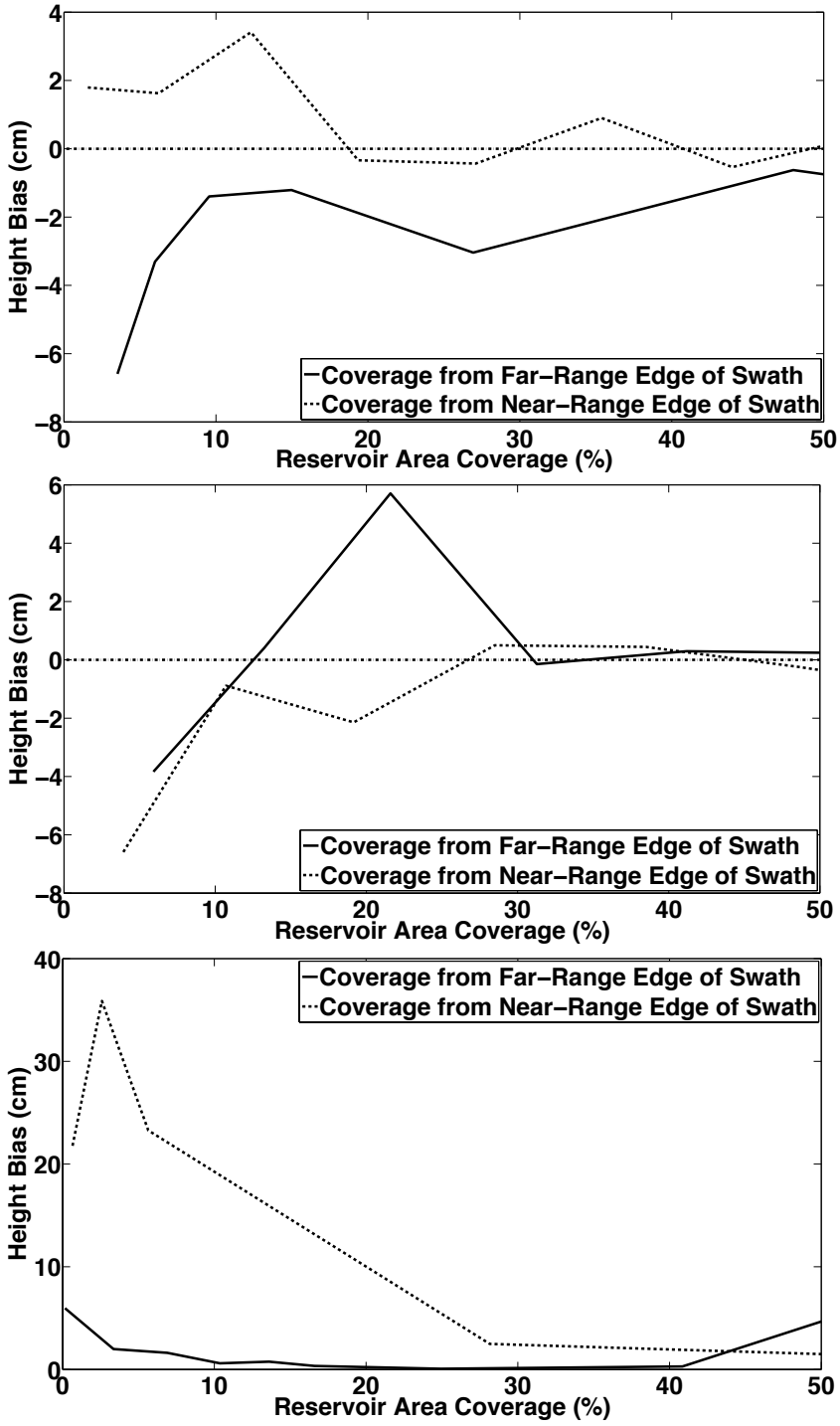

Figure 3.9: Mean bias in water surface height for partial swath coverage of reservoirs with 1:1 aspect ratio (top) and 24:1 aspect ratios oriented perpendicular to orbit (mid) and parallel to orbit (btm), as determined by SWOTsim. Analyses conducted for reservoir sizes of approximately 10^1 km^2. More information regarding this series of tests is listed in Table 3.1.

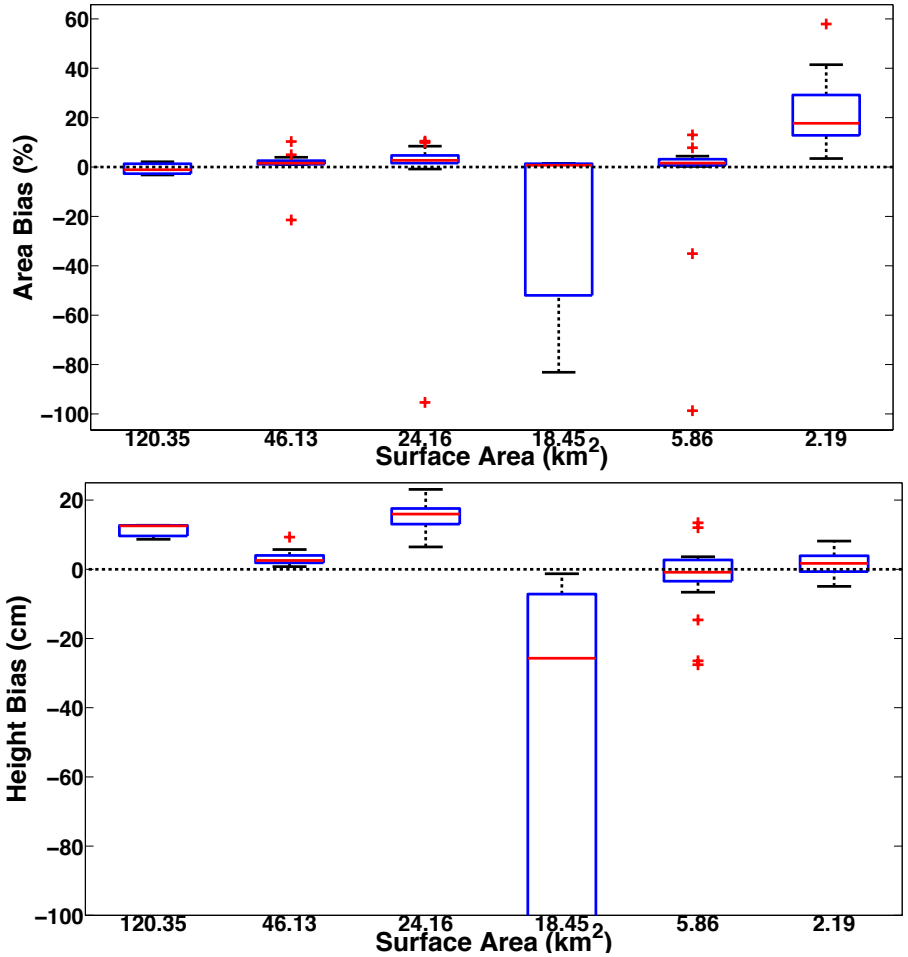

Figure 3.10: Box plots of area (top) and height bias (btm) for six California reservoirs. Multiple simulations represented by each plot. Median represented by red line and boxes indicate the 25th and 75th percentiles. Outliers denoted by red crosses and whiskers extend to range of values not considered a statistical outlier. Lower range of 25th to 75th (-900 cm) and whisker (-2300 cm) not shown to focus on distribution of median values relative to 0 cm.

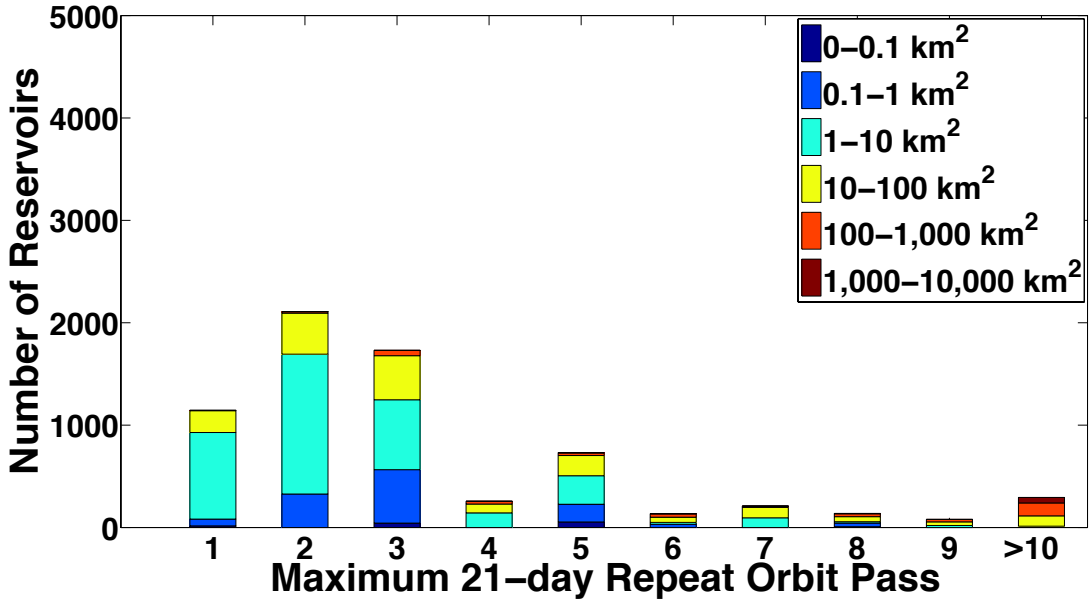

Figure 3.11: Expected SWOT repeat orbit pass frequencies for global reservoirs colored according to reservoir size: 0-0.1 km^2 (dark blue), 0.1-1 km^2 (blue), 1-10 km^2 (light blue), 10-100 km^2 (yellow), 100-1,000 km^2 (orange), 1,000-10,000 km^2 (dark red). Estimates derived from the number of repeat orbit passes intersecting a reservoir over a given SWOT cycle, which includes only partial swath coverage based on the expected ability to use ancillary data to reproduce accurate inundated areas and derivation of accurate height measurements demonstrated in this study (Data used to make plots obtained from the Centre National d'Études Spatiales [CNES] and global reservoir dataset from Lehner et al., 2011).

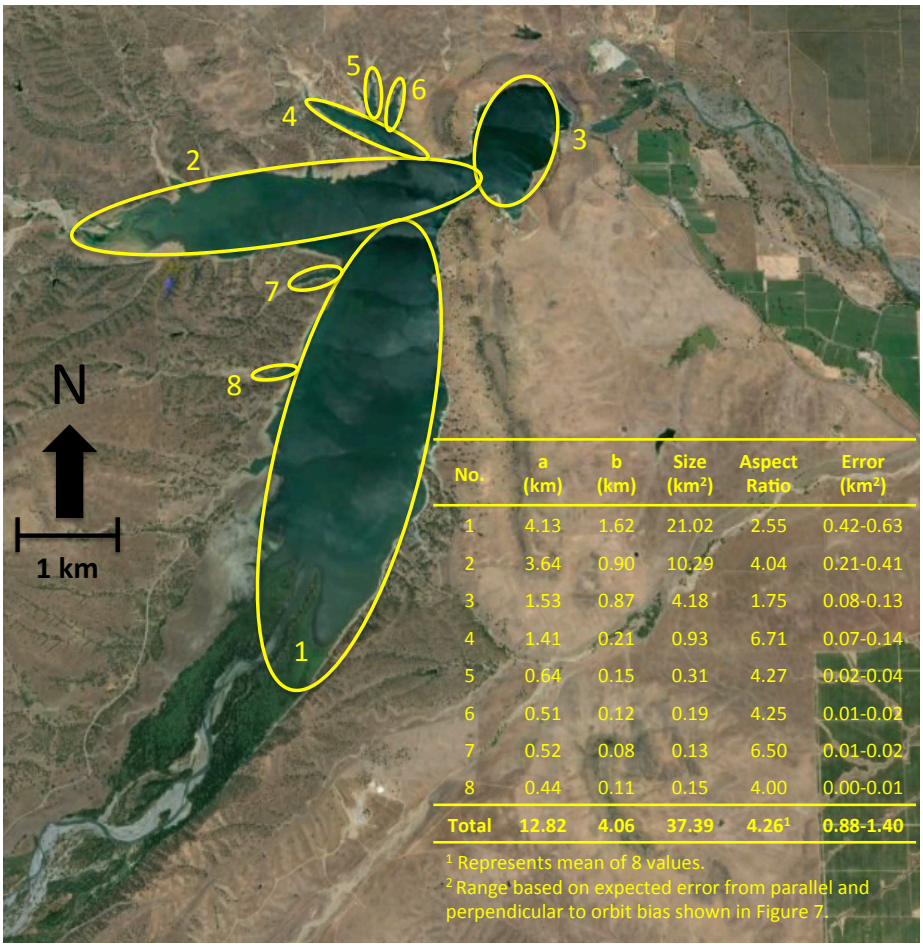

No.	a (km)	b (km)	Size (km²)	Aspect Ratio	Error (km²)
1	4.13	1.62	21.02	2.55	0.42-0.63
2	3.64	0.90	10.29	4.04	0.21-0.41
3	1.53	0.87	4.18	1.75	0.08-0.13
4	1.41	0.21	0.93	6.71	0.07-0.14
5	0.64	0.15	0.31	4.27	0.02-0.04
6	0.51	0.12	0.19	4.25	0.01-0.02
7	0.52	0.08	0.13	6.50	0.01-0.02
8	0.44	0.11	0.15	4.00	0.00-0.01
Total	**12.82**	**4.06**	**37.39**	**4.26[1]**	**0.88-1.40**

[1] Represents mean of 8 values.
[2] Range based on expected error from parallel and perpendicular to orbit bias shown in Figure 7.

Figure 3.12: Estimation of area error for Black Butte Reservoir using results from theoretical reservoir experiments presented in Figure 7. Elliptical areas calculated using formula: a*b*π where a is the major axis and b is the minor axis. Image from Google Earth (2013).

Chapter 4

Examining sustainable water use using observations from GRACE over the continental United States

4.1 Introduction

The ability to manage water resources more sustainably is of increasing importance due to the numerous alarming observations of diminishing global water supplies. Approximately 80% of the population worldwide resides in an area with present threats to water security (Vörösmarty et al., 2010). Over 50% of the world's largest aquifers show declining trends in groundwater storage change (Richey et al., 2015) and 1.7 billion people inhabit areas where groundwater resources are considered in danger (Gleeson et al., 2012). Many of these water shortages and groundwater declines affect transboundary regions, which are transparency and international cooperation is lacking (Rodell et al., 2009; Biancamaria et al., 2011; Voss et al., 2014). Within the United States, of greatest concern is the southwest, which includes the transboundary Colorado River basin that shares a border with Mexico. Near decadal groundwater and surface water declines were reported in this region due to the high intensity of water resource management being practiced (Christensen and Lettenmaier, 2007; Famiglietti et al., 2011; Castle et al., 2013). Increasing demands from a growing population coupled with shifts in availability of supplies under a warming climate are only expected to exacerbate many of these disturbing trends (Vörösmarty et al., 2000; Oki and Kanae, 2006; Alcamo et al., 2007; Schewe et al., 2014).

Heightened concerns over unsustainable water management practices, in part, gave rise to methods that quantify the ecological importance of water so environmental uses are more appropriately valued in water management systems. Two such developments include the concepts of ecosystem services and environmental flow thresholds (EFTs). Ecosystem services were established in recognition of the vast number of inherent assets offered by the environment that provide a direct benefit to people. Those pertaining to water resources include, among others, water regulation and supply, nutrient cycling, heat regulation, habitat support, food production, and recreation (Costanza et al., 1997). The prevailing thought behind this concept with respect to water is that because human water use comes at a cost to these services, these losses must be considered whenever water is extracted from a region. This has been achieved through assigning monetary value to each service to assess policy options within the free market economy. Unfortunately, most of these attempts have proven to be too difficult due to the complexity in attaining international or inter-organizational consensus in the appropriate financial worth of a given service (Costanza et al., 2011).

Similarly, the concept of EFTs arose out of recognition that maintenance of the natural flow regime in rivers is vital to the survival of freshwater animals and plants to avoid the collapse of aquatic ecosystems (Richter et al., 1996). As is the case with ecosystem services, information required to properly characterize EFTs for all river basins is lacking and there is currently no universally accepted method used to calculate EFTs (Hanasaki et al., 2008). Because the magnitude and duration of the different flows that must be upheld varies according to the species targeted for protection and many river

reaches are inhabited by multiple species, delegation of the appropriate EFT is frequently too complicated and hence official EFT designations are missing from most river basins.

Recognizing this problem, Richter et al. (2011) devised a "presumptive standard" to use in basins where EFTs do not currently exist. This standard was based on several case studies mostly within the contiguous United States where necessary flow characteristics to maintain healthy ecosystems were quantified. Based on their assessment, the authors determined that flow modifications above 20% of the natural daily flows result in moderate to severe ecosystem damage and thus used this value as the standard with intended application to basins where EFTs are absent. This represents the most restrictive standard relative to others applied in previous works, which collectively ranged from 20-80% of mean annual runoff and/or groundwater recharge considered at either daily, monthly, or annual timescales (Tennant, 1976; Cullen, 2001; Smakhtin et al., 2004; Hanasaki et al., 2008).

Simultaneous to the development of EFTs, the magnitude and extent of global water scarcity was concurrently being examined. The seminal work by Falkenmark (1989) established the Water Crowding Index (WCI), where chronic water shortage and severe water scarcity was classified as <1,700 m^3 yr^{-1} and <500 m^3 yr^{-1} total water availability (TWA) per capita, respectively. Nearly one-quarter of global river basins were observed to be under severe water stress by comparing water demand to availability in a global hydrology model (Alcamo et al., 2003). Projected global blue (renewable surface and groundwater) and green water (precipitation that naturally infiltrates) shortages of 36% and 50%, respectively, were estimated using a hydrology and vegetation model that distinguishes between consumptive (water lost to evapotranspiration) and non-

consumptive use (return flows to rivers and groundwater), while accounting for EFTs (Rockström eta al., 2009). Similarly, monthly modeled and observed data were used while accounting for EFTs to identify nearly 40% of the global population inhabits river basins with blue water shortages (Hoekstra et al., 2012). Many of these concepts were synthesized using a global hydrology model to estimate the blue water sustainability index, which is the ratio of combined nonrenewable groundwater use and EFT volume exceeded by surface water use to the consumptive blue water use (Wada and Bierkens, 2014).

Collectively, these studies have provided great insights into the global sustainability of water management systems, but several issues exist with the formulation and calculation of these indices. First, these studies heavily rely on modeled output, raising questions about the validity of the results. The use of different models to generate water scarcity estimates is responsible for the gross inconsistencies found among existing studies, as the number of people reported as inhabiting regions with severe water stress differs by up to a factor of almost eight (Wada et al., 2011). Furthermore, in some cases the estimations of water availability do not account for the total amount of water (surface water and groundwater) that is available to a given area. Given the large exchange of water taking place between groundwater and surface water in the hyporheic zone (Findlay, 1995), failing to integrate both into these assessments potentially results in underestimation of total water availability and thus overestimation of water stress.

In this study, we address these deficiencies by developing a new method to calculate water stress while relying more on observations from in-situ water use data and satellite-based total water storage (TWS) obtained from GRACE. Total water availability (TWA) is estimated from the monthly accumulation of surface water and groundwater above the

annual minimum and the fraction available to humans is determined by accounting for ecosystem requirements. The resulting volumes are compared to actual consumptive water use data at the same spatial scale. Finally, necessary water use reductions to achieve sustainability over the study period are calculated. By decreasing the need for models in favor of satellite and ground observations to evaluate water stress, the consistency in results among future studies will be enhanced.

4.2 Methods

Data used to calculate TWS came from the Gravity Recovery and Climate Experiment (GRACE) satellite mission (Tapley et al., 2004). GRACE is used to examine global monthly changes in the gravity field over large areas (>200,000 km^2), which are directly related to the TWS changes at the same space and time scales. In this study, 2003-2015 Release 05 GRACE data was used, which were generated from the Center for Space Research, University of Texas at Austin and are available from the NASA Jet Propulsion Laboratory Physical Oceanography Distributed Active Archive Center (http://podaac.jpl.nasa.gov). Grid scaling factors available from the same website were applied to remove effects from sampling and post-processing of GRACE observations. Soil moisture data over the same period was derived using a multi-model mean from the VIC, Noah, and Mosaic land surface models running within the North American Land Data Assimilation System (NLDAS) (Mitchell et al., 2004).

Water use data came from the United States Geological Survey (USGS) National Water-Use Information Program, which collects comprehensive, county-level surface water and groundwater use statistics across all sectors every five-years. The data is available for

download directly from the USGS website (http://water.usgs.gov/watuse/). Here, we use the 2005 and 2010 data to coincide with the GRACE observation period (Kenny et al., 2005; Maupin et al., 2010). Because only two-years of data were available, we use a benchmark average to represent water use over the entire study period. Although irrigation accounts for 80-90% of consumptive water use overall (Döll and Siebert, 2002; Rost et al., 2008; Hoekstra et al., 2012; Döll et al., 2014), industrial and domestic water use contributes a much greater proportion in more urbanized areas so these quantities were also included in the total water use estimates.

The GRACE, NLDAS, and USGS data were scaled to the two-digit Hydrologic Unit Code (HUC) USGS watershed boundaries (Table 4.1) due to the coarse spatial resolution of GRACE. Moreover, as watersheds represent the characteristic spatial unit most commonly associated with water resource management, distributing the data at this scale provides a more practical approach to presenting water use with respect to availability across the landscape. County-level data from the USGS and grid-based data from GRACE that were intersected by a HUC basin divide were dealt with by weighting the data in direct proportion to the area that fell on either side of the boundary. Only data from the continental United States was used, as comprehensive in-situ water use statistics at the sub-national scale is not available from outside the United States.

Annual TWA for the 18 two-digit HUC basins was calculated using Equation 1:

$$TWA\left(t_{yr}\right) = \sum_{t=0}^{12}\left[\left(TWS\left(t_{mo}\right) - TWS\left(t_{mo}+1\right)\right) - \left(SM\left(t_{mo}\right) - SM\left(t_{mo}+1\right)\right)\right] * EC \qquad (1)$$

$$TWS\left(t_{mo}\right) > TWS\left(t_{mo}+1\right)$$
$$SM\left(t_{mo}\right) > SM\left(t_{mo}+1\right)$$

where TWA is the annual total water availability (m^3 yr^{-1}), TWS is the monthly total water storage from GRACE (m^3 mo^{-1}), SM is the monthly soil moisture storage from NLDAS (m^3 mo^{-1}), and EC is the environmental coefficient (Figure 4.1), which was added to account for environmental demands. Here, we use the two-digit HUC basin EC values estimated by Smakhtin et al. (2004a), which were also based on groundwater recharge and changes in surface water storage, as estimated from a global hydrology model. Note that in Equation 1, the difference in the cumulative month-to-month TWS and SM for each year starting on December of the previous year only for consecutive months where the TWS and SM of the lead month exceeds those of the trailing month. The volume represented by SM is necessarily subtracted from TWS, as this amount is not considered to be available for use. Both the GRACE and NLDAS data are presented in the form of anomalies relative to the 2004-2009 period.

The general principle behind Equation 1 is that within each year, the TWS reaches a maximum in a given basin largely due to seasonally elevated precipitation that exceeds ET, leading to an accumulation of water within the system. Correspondingly, TWS falls to an annual minimum when the levels of ET exceed precipitation, resulting in more water leaving the basin through the atmosphere. Thus, the accumulation of water losses within the basin can be taken as the total "active" amount of available water for use from the system within a given year. This volume is calculated by summing the difference in month-to-month TWS and SM decreases over a calendar year. The presumptive standard is applied to account for the portion of the resulting volume that must remain in the environment to minimize damage to the ecosystem. Hence, it is assumed the residual

water must stay in the environment in the form of stored surface water and groundwater to be available for environmental use.

Annual consumptive water use was calculated using Equation 2:

$$CWU(t_{yr}) = U_{irr} * CF + U_{dom} * 0.20 + U_{ind} * 0.15 \quad (2)$$

where U_{irr} is the irrigation (m^3), U_{dom} is the domestic (m^3), and U_{ind} is the industrial annual water use (m^3). CF is the consumptive water use fraction of the irrigation water use, otherwise known as the irrigation efficiency and is assumed to be 60% (Döll and Siebert, 2002; Rost et al., 2008; Hoekstra et al., 2012; FAO, 2012; Döll et al., 2014). Note that we assume the consumptive water use fraction of domestic and industrial water use to be 20% and 15%, respectively. Annual consumptive use from Equation 2 was compared to TWA from Equation 1 for each HUC basin using Equation 3:

$$CWU : TWA_{an} = 100 - \frac{[TWA(t_{yr}) - CWU(t_{yr})]}{TWA(t_{yr})} * 100 \quad (3)$$

where CWU: TWA_{an} is the annual consumptive water use to total water availability ratio (%) and is identical to the Water Stress Indicator (WSI) established by Smakhtin et al. (2004b).

Given the known uncertainty in the environmental coefficient and irrigation efficiency parameter values, a parameter sensitivity analysis in supplementary Table 4.2 was used to present the mean annual consumptive water use to availability ratios

calculated using Equation 3. Both parameters were allowed to vary by +/-0.15 to assume a standard sigma range. Parameter sensitivity results were shown only for the six western HUC basins due to preliminary tests that revealed the ratios to be highest in this region.

Finally, the maximum percent reductions in water use that are necessary to achieve sustainability were calculated for those basins with large consumptive water use to availability ratios. This was achieved by determining the water use that would result in no net shortage or excess in use relative to availability over the long-term when the least conservative parameter values were used.

4.3 Results

The results indicate that within the United States, the highest degree of water scarcity occurred in the southwest (Figure 4.2). Use of the median parameter values indicate consumptive water use exceeded 150% annual TWA twice in the Lower Colorado, which is made up almost exclusively of Arizona. In addition, the 100% threshold was also surpassed twice in California and the Rio Grande reached a high mark of 99% in 2013. Overall mean consumptive water use (2003-2015) to availability ratios in the west ranged from a low of 27% in the Great Basin to a high of 79% in the Lower Colorado. Figure 4.3 shows the entire range of use to availability ratios over the study period for the six western basins resulting from the different parameter value combinations. Five of the six basins revealed an increasing trend, which ranged from –0.1% yr^{-1} in the Rio Grande to 3.5% yr^{-1} in the Lower Colorado. None of the trends were significant at the 95%-level. 2012 represented the single worst year in terms of sustainable water resource management, as

consumptive water use in each of the five southwestern two-digit HUC regions exceeded 60% TWA during this year.

The national annual water balance statistics for the TWA and benchmark consumptive water use data based on the range of parameter values that were used are shown in Table 4.3. The annual water use to availability ratios were calculated by weighting the fractions according to HUC basin size. Therefore, the first column of information provides an indication of the overall spatial coverage of this fraction on an annual basis, rather than the actual balance of use to availability, which is presented in the final column. Water use to availability ratios over the continental United States ranged from a low of 13% in 2004 to a high of 29% in 2012. Extreme values for the balance of TWA and water use ranged from a low of approximately 300 billion m^3 in 2006 to a high of 730 billion m^3 in 2004. The mean, maximum, minimum, and standard deviation shown in this table are based on the within-HUC-region values obtained over the study period and are therefore much higher or lower than implied by the 2003-2015 annual data.

Figure 4.4 shows the 2003-2015 mean, maximum, minimum, and standard deviation of benchmark consumptive water use to availability fractions resulting from the median set of parameter values. Focusing on the west, consumptive water use exceeded 12-29% water availability when the minimum TWA was used and 48-191% when the maximum TWA was used. The plot displaying the maximum TWA is strikingly analogous to the 2012 plot from Figure 4.2, as the 100% consumption to availability ratio also occurred in the two southwestern HUC regions during this time. Overall, the standard deviation was much higher in the southwestern basins, pointing to the larger degree of water resource variability in this region relative to elsewhere in the United States.

The maximum reductions in water use required for balancing long-term consumptive water use with availability for the five southwestern basins are shown in Table 4.4. These values were obtained using the least conservative parameter values and indicate a minimum water use curtailment of 8% in the Great Basin (16) to a maximum of 64% in the Rio Grande (13) is necessary to achieve long-term water resource sustainability in the region.

4.4 Discussion

This study represents the first attempt known to these authors at using observations from GRACE and in-situ records to evaluate sustainable water use management while accounting for environmental water needs over a large region. Moreover, by using GRACE, both surface water and groundwater are being represented, thereby providing a more holistic depiction of spatially distributed sustainable water use in the United States. Below, we clarify the key results, highlight some levels of agreement with our work to those of other studies, explain some caveats with the methods used, and mention some important ecological implications that may already be underway due to ongoing problems with water stressed regions.

4.4.1 Results Highlights and Comparisons

According to the results, water scarcity in the United States is only a perpetual problem in the west. When median parameter values were used, consumptive water use in the six western basins consistently exceeded 15% TWA and 40% long-term mean in four of the six basins. Consumptive water use was even found to surpass 100% TWA in both the Lower Colorado (15) and California (18) basins and the long-term mean was greater than

50% and 75%, respectively, in these areas. Given the prognosis of warmer conditions resulting in runoff decreases of up to 10-20% over this region (Milly et al., 2008) that will likely cause a corresponding reduction in TWA, water scarcity is only expected to worsen. Such a forecast suggests that shifts in current water use practices are urgent to achieve sustainability and water shortages for humans or the environment are avoided.

Further confirming the severity of water scarcity in these regions are the ubiquitous increasing trends in water use to availability over the study period. It should be noted that because a benchmark water use volume was used, the positive trends actually signify losses in TWA rather than true declines in sustainable water use over time. Many of these affects are attributed, in part, to the presence of severe regional droughts, which were particularly bad in both Texas and California towards the end of the study period (Long et al., 2013; Swain et al., 2014; Thomas et al., 2014).

The results presented herein bare some similarities to other studies that analyzed sustainable water use over the same region. Vörösmarty et al. (2000) determined much of the population inhabiting the southwestern United States lived in areas where water use exceeded 40% of the availability. Alcamo et al. (2003) calculated 1995 total withdrawals in the southwest to represent greater than 80% of availability. Wada et al. (2011) also found water use represents over 80% availability, a level so severe that the authors listed it as being economically limiting. Moreover, they determined this region to have the highest dynamic water stress index values, which is a measure of the frequency and duration of water scarcity combined with the magnitude of stress. Further corroborating these studies, Hoekstra et al. (2012) discovered blue water use to exceed availability in much of the southwest during the majority of months in a given year.

Annual ratios of consumptive water use to renewable water supplies at the two-digit HUC basin scale were also determined by USGS (1983). These results compare favorably to the median parameter results of consumptive water use to availability ratios obtained in this study. The ratios for the Upper Colorado (14), Pacific Northwest (17), and California (18) were higher in this study – 41%, 29%, and 54% relative to 29%, 5%, and 34% respectively. Rio Grande (13) and Great Basin (16) ratios were slightly lower in the current study – 54% and 27% relative to 59% and 41%, respectively. The ratio obtained for the Lower Colorado (15) was calculated for the entire Colorado Basin, as the individual terms that comprised renewable water supplies could not be accurately estimated for the Lower Colorado basin alone at the time of that study. Nevertheless, the results were similar – 79% (now) relative to 105% (previous).

The discrepancies in the results are related to a number of factors. First, the USGS study used much earlier records to estimate renewable water supplies and consumptive water use, which likely differ from contemporary datasets. In addition, basin-distributed renewable water supplies were estimated much differently by the USGS than how TWA is calculated in this study. The method involved subtracting groundwater depletion from the sum of cumulative basin discharge and consumptive water use. Such a practice assumes all water in a given basin is available for human use as long as groundwater depletion is not present, thereby omitting environmental water use requirements, which are accounted for in the current study. This omission alone effectively overestimates renewable supplies resulting in an underestimation of the resulting consumptive water use to renewable water supply ratios.

4.4.2 Shortcomings and Limitations

Several other water supply features that could alter the results in basin-scale water use sustainability were also not estimated. For example, there was no attempt to incorporate water quality into the calculations of water availability, making the estimates from this study more conservative based solely on this omission. Second, inter-basin water transfers were not addressed. This is problematic for locations on both the import- and export-side of the transfer. For instance, when water is removed from a basin, the minimum annual TWS might be biased low, thereby resulting in an artificially inflated calculation of TWA. Alternatively, basins on the receiving end of this water might have a high bias in minimum annual TWS and thus a lower TWA will be calculated. We anticipate this to only be a major issue in regions such as the California and the Colorado basins where inter-basin water exchanges are high.

Area-proportionate weighting methods were used to distribute the county-level water use and GRACE-grid-cell-derived availability data across two-digit HUC boundaries. More sophisticated scaling procedures were not employed because given the large size of the two-digit HUC regions, the simpler method we used was deemed sufficient. Future work will ideally involve statistical downscaling of the data where more complex weighting techniques might be necessary to avoid introducing larger errors.

Although the surface area represented by three of the two-digit HUC basins is below the 200,000 km^2 threshold listed as the ideal minimum spatial resolution for GRACE data (Rodell and Famiglietti, 2001; Yeh et al., 2006), the scaling factors applied improve the spatial resolution to one-degree, which is well above the area of the three smallest basins. In addition, because the calculated consumptive water use to availability ratios were relatively low in the small basins compared to elsewhere, additional work such as

combining basins to improve accuracy was avoided so basin-to-basin comparisons of results could be achieved.

The use of a benchmark annual water use value for the different HUC regions represents a major shortcoming of this study. Ideally, temporally continuous, annually resolved water use data for the continental United States that coincided with the GRACE observation record would have been available, but data within the targeted period was limited to 2005 and 2010. In spite of this deficiency, the consumptive water use from these two-years differed by only 2-14% in the southwestern United States HUC basins where water use practices were found to be the least sustainable, thereby minimizing any appreciable bias in the results from this limitation. Furthermore, Wada et al. (2011) also employed a benchmark water use from 2000 for comparison to simulated blue water availability so global water stress could be evaluated in a similar study. They found good agreement with reported values of water stress, indicating climate variability has a much greater influence on changes in water stress than annual variations in water use, hence providing justification for a benchmark water use value.

The application of uniform environmental coefficient and irrigation efficiency parameter values represents another major study limitation. Although the environmental coefficient parameter was spatially distributed, use of a single value for an entire HUC 2 basin over the study period implies environmental water requirements are constant in space and time when in reality they are much more variable depending on the number and type of species present (Pahl-Wostl et al., 2013). Likewise, the actual irrigation efficiency is nonlinear in space and time. Despite these uncertainties, we note here that when the median irrigation efficiency of 60% is used, the 2003-2015 mean annual net irrigation

water use differed from the 1995 values computed by Döll and Siebert (2002) and 2007 numbers reported in FAO (2012) by only 16% and 13%, respectively. Even still, further work is needed to better spatially and temporally characterize the presumptive standard and irrigation efficiency values to attain more robust results.

The coarse spatial and temporal scaling employed in the analysis represents another major study caveat. More severe water scarcities or surpluses exist at finer spatial or temporal scales, as has been shown in similar studies (Meigh et al, 2009; Wada et al., 2011). However, the larger spatiotemporal resolution associated with the GRACE TWS observations and USGS water use records necessitated the annual timescale and spatial resolution at the two-digit HUC basin scale. Employment of statistical downscaling methods and/or modeled output to achieve higher resolutions was avoided to prevent introducing greater uncertainty into the results. Given that calculations conducted at smaller spatial resolutions could reasonably account for more local water management practices (e.g. desalination, rainfall capture and reuse, and water treatment and recycling) that impact water use sustainability but are not accounted for in this study, future efforts should attempt conducting evaluations at these scales.

4.4.3 Ecological Implications

Unsustainable water use practices have dire consequences for aquatic ecosystems and evidence exists that some of these impacts might already be underway. For instance, Richter et al. (2011) acknowledge that a presumptive standard of 10% is necessary to provide the fullest ecological protection, but adhering to this standard in this study would cause mean consumptive water use to exceed water availability in all five southwestern HUC regions except when the most conservative irrigation efficiency is applied. Indeed,

several major ecological impairments due to changes in river flow regimes have been reported. In their review of global studies surveying ecological damage from flow alterations, Poff and Zimmerman (2010) found ecological modifications reported in 92% of the studies with consistently negative changes occurring in fish species abundance, diversity, and demographic parameters. During the two-decades following 1979, the number of vulnerable, threatened, endangered, and extinct North American freshwater species steadilyy rose (Jelks et al., 2008). Within the southwest region of the United States alone, even slight flow alterations were observed to favor the establishment of invasive vegetation in riparian areas over native species (Merrit and Poff, 2010). Furthermore, in California, freshwater fish species that are extinct or at-risk of extinction rose from 62% in 1989 to 83% in 2011. Major flow augmentations were listed as one of the main causes of this decline (Moyle et al., 2011).

4.5 Conclusions

For the first time, regional basin-scale sustainable water use was evaluated using observations from space and ground measurements. Results indicate the least sustainable water management practices exist in the southwest, where consumptive water use averaged over almost 50% of the annual water availability in three southwestern two-digit HUC basins when median parameter values were applied. Reductions in water use of up to 67% were found to be required for consumptive use to meet availability so sustainability could be achieved. Aquatic ecosystems will likely be severely impacted due to current unsustainable water management practices and evidence exists that many of these changes might already be occurring.

Based on the uncertainties in the parameters used to generate the results, greater emphasis should be given to the framework developed here for future studies of sustainable water use derived from remote sensing until parameter and scaling issues are better resolved. Future efforts in this area should primarily focus on better constraining the presumptive standard and irrigation efficiency parameters both spatially and temporally. Second, results should be downscaled to increase their utility for water resource managers. Finally, more continuous water use data from new observations or models should be used. Such actions would be beneficial towards producing more robust spatially and temporally distributed consumptive use to availability ratios that could be employed to better pinpoint areas where immediate changes to water management practices are necessary to mitigate water stress and avoid major ecological damage.

In spite of the parameter uncertainties, given that understanding how available supply varies with demand is arguably more important for sustainability than accurately determining how much water we have, the established framework provides an excellent opportunity to explore where water resource management systems are adequate and where they are falling short. Moreover, the study offers a foundation for further investigations of sustainable water use from remote sensing at different spatial and temporal scales. Reducing the reliance on models in favor of remote sensing and in-situ observations will increase the consistency in results among future studies, thereby making for a more robust analysis.

Table 4.1. Two-digit HUC Basin Areas over the continental United States

No. and Name	Area (km^2)
01 – New England	165,992
02 – Mid-Atlantic	288,421
03 – South Atlantic-Gulf	721,778
04 – Great Lakes	431,959
05 – Ohio	417,636
06 – Tennessee	105,335
07 – Upper Mississippi	464,981
08 – Lower Mississippi	269,437
09 – Souris-Red-Rainy	156,306
10 – Missouri	1,311,720
11 – Arkansas-White-Red	610,720
12 – Texas-Gulf	474,331
13 – Rio Grande	339,936
14 – Upper Colorado	290,364
15 – Lower Colorado	360,345
16 – Great Basin	362,883
17 – Pacific Northwest	719,137
18 - California	413,492

Table 4.2. Sensitivity analysis of irrigation efficiency and environmental coefficient to estimate consumptive water use to availability fractions for the western US.

13 – Rio Grande	**Irrigation Efficiency (%)**						
Environmental Coefficient	**45**	**50**	**55**	**60**	**65**	**70**	**75**
0.57	52	57	63	68	74	79	85
0.62	48	53	58	63	68	73	78
0.67	44	49	53	58	63	67	72
0.72	41	45	50	54	58	63	67
0.77	38	42	46	50	55	59	63
0.82	36	40	44	47	51	55	59
0.87	34	37	41	45	48	52	55
14 – Up Colorado	**Irrigation Efficiency (%)**						
Environmental Coefficient	**45**	**50**	**55**	**60**	**65**	**70**	**75**
0.48	40	45	49	54	58	63	67
0.53	37	41	45	49	53	57	61
0.58	34	37	41	45	48	52	56
0.63	31	34	38	41	44	48	51
0.68	29	32	35	38	41	44	47
0.73	27	30	32	35	38	41	44
0.78	25	28	30	33	36	39	41
15 – Low Colorado	**Irrigation Efficiency (%)**						
Environmental Coefficient	**45**	**50**	**55**	**60**	**65**	**70**	**75**
0.48	80	88	96	103	111	119	127
0.53	72	79	87	94	101	108	115
0.58	66	73	79	86	92	98	105
0.63	61	67	73	79	85	91	97
0.68	56	62	67	73	78	84	89
0.73	53	58	63	68	73	78	83
0.78	49	54	59	64	68	73	78
16 – Great Basin	**Irrigation Efficiency (%)**						
Environmental Coefficient	**45**	**50**	**55**	**60**	**65**	**70**	**75**
0.58	25	28	31	34	36	39	42
0.63	23	26	28	31	33	36	38
0.68	22	24	26	29	31	33	36
0.73	20	22	25	27	29	31	33
0.78	19	21	23	25	27	29	31
0.83	18	20	22	23	25	27	29
0.88	17	19	20	22	24	26	28
17 – Pac Northwest	**Irrigation Efficiency (%)**						
Environmental Coefficient	**45**	**50**	**55**	**60**	**65**	**70**	**75**
0.52	29	32	35	38	41	44	47
0.57	26	29	32	34	37	40	43
0.62	24	27	29	32	34	37	39
0.67	22	24	27	29	32	34	36
0.72	21	23	25	27	29	32	34
0.77	19	21	23	25	28	29	32
0.82	18	20	22	24	26	28	30

18 - California	Irrigation Efficiency (%)						
Environmental Coefficient	**45**	**50**	**55**	**60**	**65**	**70**	**75**
0.62	51	56	61	67	72	77	83
0.67	47	52	57	62	67	72	76
0.72	44	48	53	57	62	67	72
0.77	41	45	49	54	58	62	67
0.82	38	42	46	50	54	58	62
0.87	36	40	44	48	51	55	59
0.92	34	38	41	45	49	52	56

Table 4.3. Summary water balance statistics over the continental United States [a].

Year	Consumptive Water Use: TWA Ratio (%)[b]	TWA - Consumptive Water Use (m^3)
2003	17 [13 - 23]	4.1E+11 [3.3E+11 - 4.9E+11]
2004	13 [9 - 17]	7.3E+11 [6.1E+11 - 8.4E+11]
2005	16 [12 - 21]	5.2E+11 [4.3E+11 - 6.2E+11]
2006	23 [17 - 31]	3.0E+11 [2.4E+11 - 3.6E+11]
2007	27 [20 - 36]	3.3E+11 [2.6E+11 - 4.0E+11]
2008	19 [14 - 26]	4.4E+11 [3.6E+11 - 5.2E+11]
2009	26 [19 - 35]	4.9E+11 [4.0E+11 - 5.8E+11]
2010	21 [16 - 29]	3.4E+11 [2.7E+11 - 4.0E+11]
2011	24 [18 - 32]	4.2E+11 [3.4E+11 - 5.0E+11]
2012	29 [22 - 39]	4.9E+11 [4.0E+11 - 5.8E+11]
2013	22 [17 - 30]	4.0E+11 [3.2E+11 - 4.7E+11]
2014	16 [12 - 21]	5.3E+11 [4.3E+11 - 6.2E+11]
2015	17 [13 - 23]	4.5E+11 [3.7E+11 - 5.3E+11]
MEAN[c]	21 [15 - 28]	4.5E+11 [3.7E+11 - 5.3E+11]
MAX[c]	38 [29 - 51]	8.6E+11 [7.2E+11 - 9.9E+11]
MIN[c]	10 [8 - 14]	1.8E+11 [1.4E+11 - 2.3E+11]
STD[c]	8 [6 - 11]	1.1E+10 [9.7E+09 - 1.3E+10]

[a] results based on median parameter values, while range in brackets calculated using least and most conservative parameter values

[b] weighted by two-digit HUC areas

[c] based on within-HUC-region results over study period

Table 4.4. Maximum water use reductions needed to achieve sustainability

Two-digit HUC Region	Water Use Reduction (%)[a]
13 – Rio Grande	25 [0]
15 – Lower Colorado	61 [5]
18 – California	30 [0]

[a] Reduction necessary to achieve sustainability for maximum annual use to availability and mean over the study period (brackets) based on least conservative parameter estimates

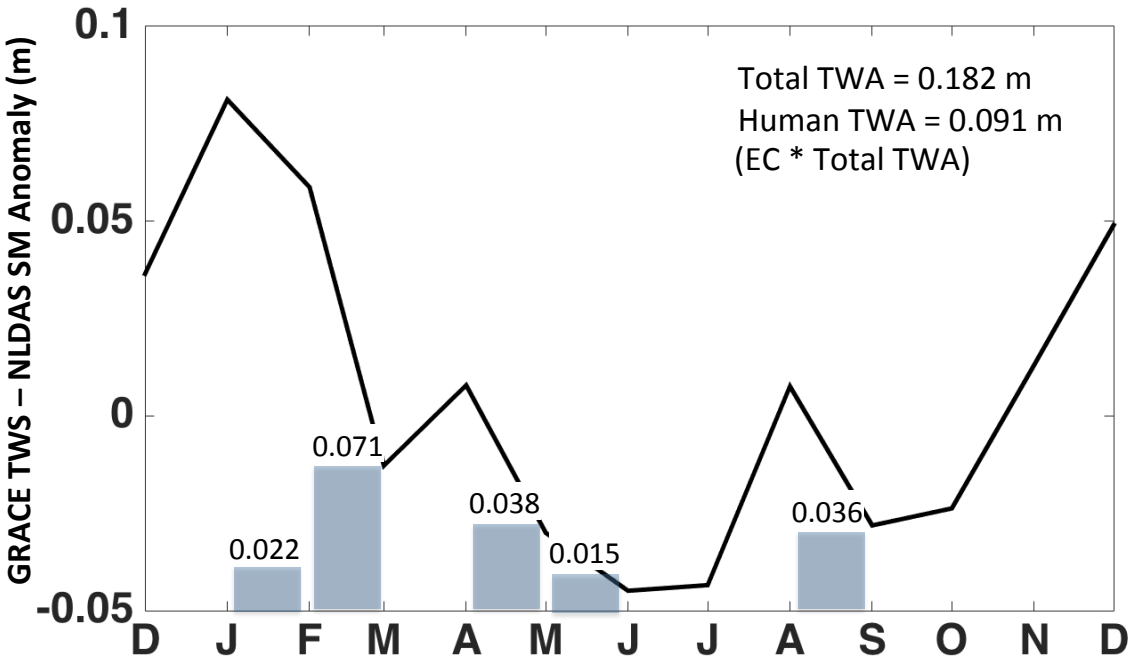

Figure 4.1: Conceptual diagram demonstrating how to determine Total Water Availability (TWA) from the difference in the GRACE total water storage (TWS) and NLDAS soil moisture (SM) anomaly. The total TWA encompasses all the active water available to a given area and is based on the cumulative month-to-month drop in monthly TWS (grey shaded areas). The human TWA represents the portion of the total water available to humans based on a Presumptive Standard (PS) value of 0.5. The remaining water must be left for the environment.

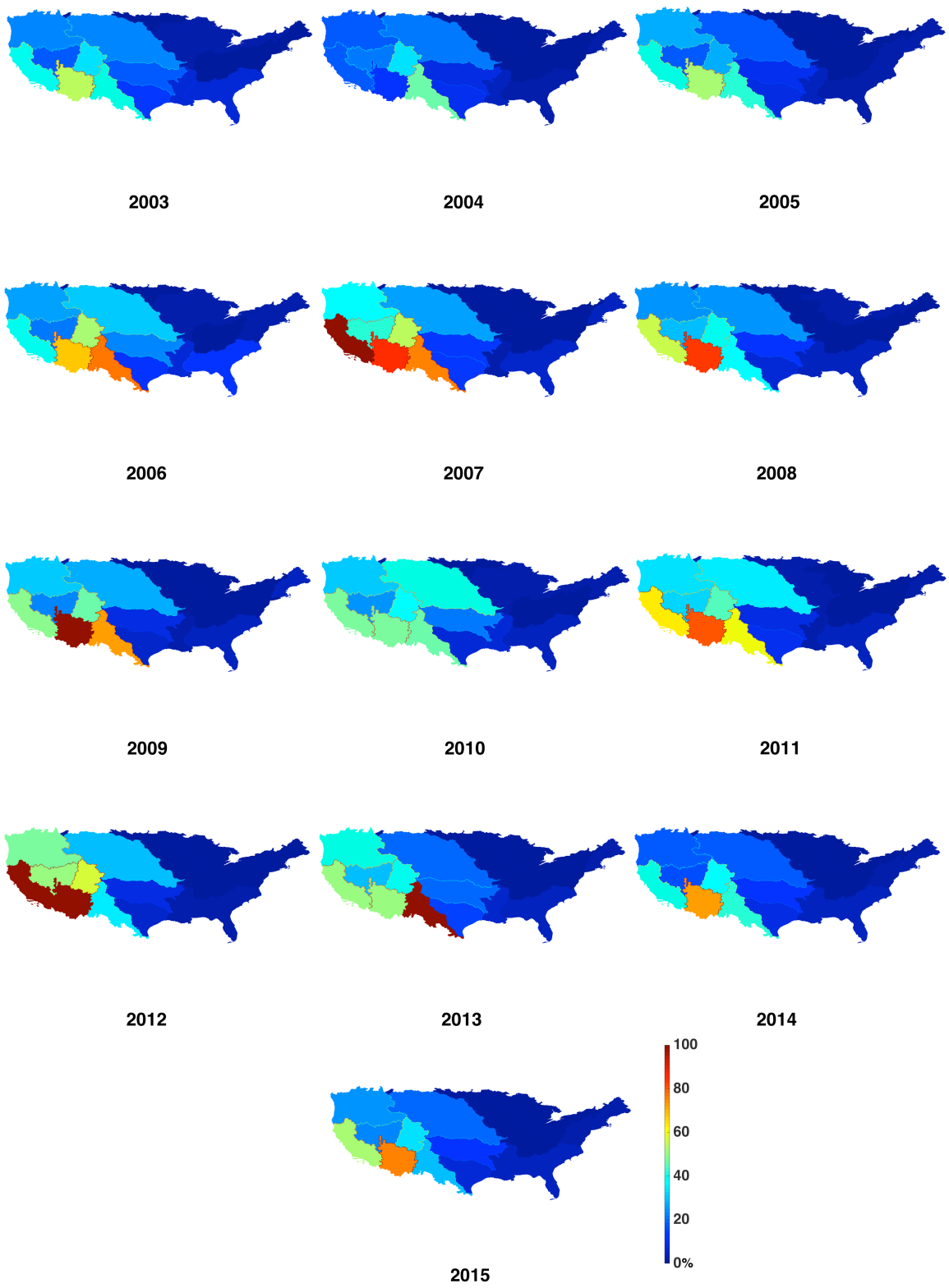

Figure 4.2: Annual 2003-2015 percent consumptive water use to availability ratios for the 18 two-digit HUC regions of the continental United States. Values shown represent results obtained when median environmental coefficient and irrigation efficiency parameters were used.

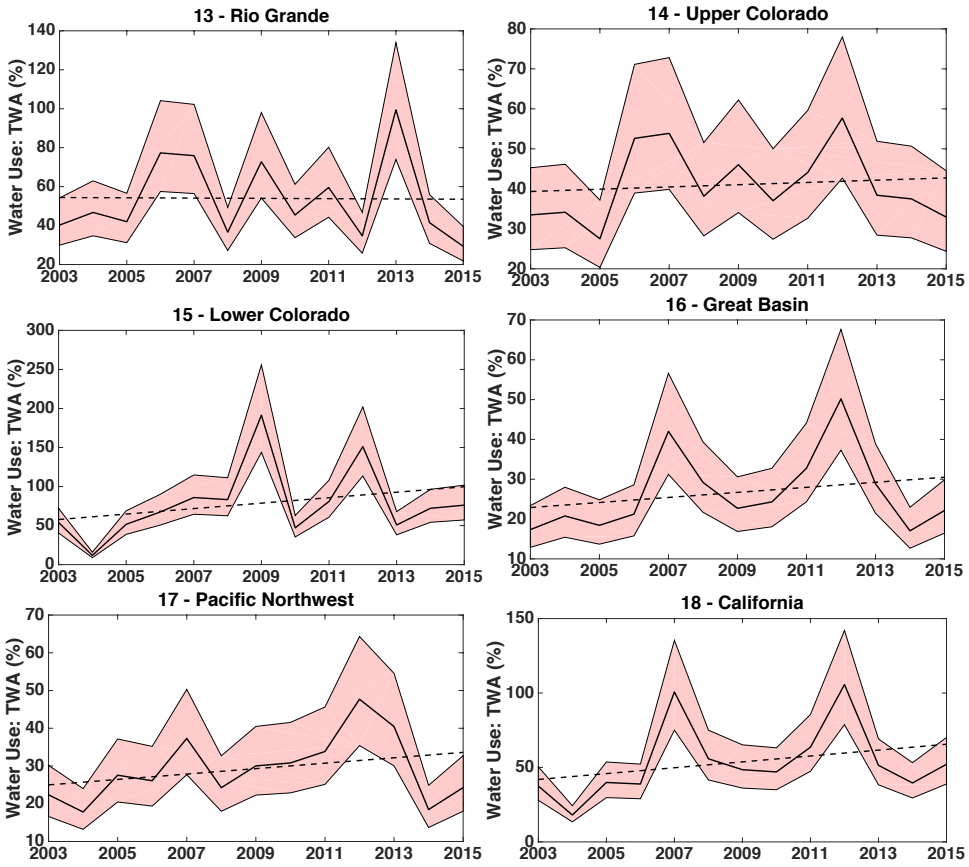

Figure 4.3: 2003-2015 time series of percent consumptive water use to availability ratios for the southwest two-digit HUC regions. Solid black line represents results obtained when median environmental coefficient of 0.5 and water efficiency ratio of 0.6 were used. Associated linear trends (dashed black line) in water use to availability fractions are as follows: 13 Rio Grande (-0.1% yr^{-1}, p-value = 0.96), 14 Upper Colorado (0.3% yr^{-1}, p-value = 0.70), 15 Lower Colorado (3.5% yr^{-1}, p-value = 0.33), 16 Great Basin (0.6% yr^{-1}, p-value = 0.41), 17 Pacific Northwest (0.7% yr^{-1}, p-value = 0.29), and 18 California (2.0% yr^{-1}, p-value = 0.30). Shaded regions indicate possible estimates given full range of parameter values.

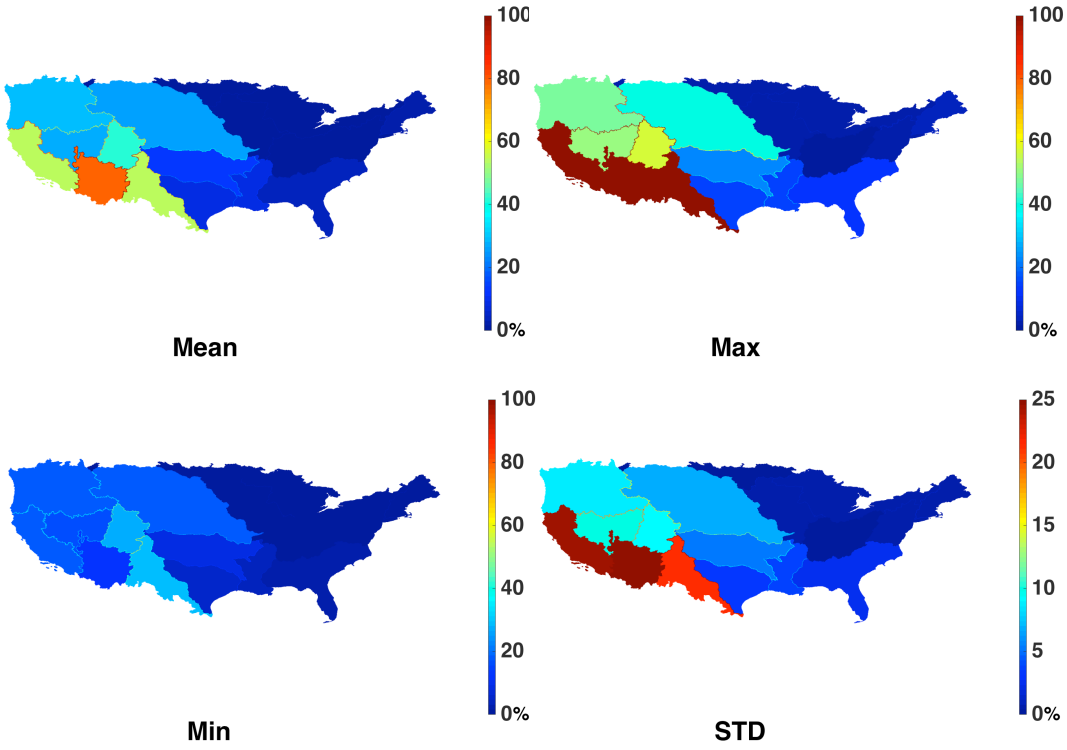

Figure 4.4: 2003-2015 mean (top-left), maximum (top-right), minimum (bottom-left), and standard deviation (bottom-right) percent consumptive water use to availability ratios for the 18 two-digit HUC regions of the continental United States. Values shown represent results obtained when median environmental coefficient and irrigation efficiency parameters were used.

Chapter 5

Conclusions

There are a lot of remaining unknowns requiring further investigation to fully understand the impacts of water resource management on the terrestrial water cycle and associated effects on the climate system. Although many observations of water storages and fluxes related to water resource management exist, the high spatial and temporal variability of these phenomena has made integration into Earth System models at the right space and time scales problematic. Given the global coverage and/or improvements in spatial or temporal resolution from previous similar missions, observations from NASA satellite missions such as GRACE and SWOT as well as advances in modeling show promise for closing this knowledge gam. We applied these tools here with this same goal in mind.

In this dissertation, I attempted to answer several key questions related to water management influence on the Earth system: 1) What are the impacts of reservoir management on the climate system and how do these vary in space and time? 2) Given the potential usefulness of data from the NASA SWOT mission to this work, how well can observations from this satellite be used to estimate changes in reservoir elevation and surface area? 3) And finally, does the existing water resource management system account for both human and environmental demands and can this be assessed with remote sensing? The comprehensive understanding gained from our exploration of these

questions is provided in the three preceding chapters, which we further summarize in the following section.

5.1 Summary of Results

The development of a reservoir management model for integration into a global LSM was described in Chapter 2. Although the model has yet to be fully coupled to an LSM to simulate the associated impacts on the climate, several intriguing results and model features make the model set-up ideal for its intended goal. Model performance metrics were used to select the minimum complexity set of equations based on the number of parameters and terms. Optimized parameter values were used to produce a generalized set of parameter equations, which resulted in simulated storage and outflow explaining an average of 67% of the variance in observations. By adding a climate-adaptive feature that allows parameter values to shift with warming temperatures to effectively mitigate the expected loss in storage, the developed model represents one of the first of its kind to explicitly account for a potential reservoir operator response to climate change. Although model performance dropped for reservoirs with a higher degree of management intensity (storage coefficient of variation or winter inflow to storage capacity ratio less than 0.22 or 2 x 10-7 s^{-1}), the strong model performance and climate adaptive component provides a great initial step towards incorporation in an LSM to examine reservoir impacts on the climate.

Expected global SWOT reservoir observation errors were described in Chapter 3. Results indicate aliasing due to the return interval of the satellite to be minimal, as reservoirs below 3 km^2 were found to have errors of up to 10% for a single observation

only for the lowest sampling frequencies. The spatial analysis tests over theoretical reservoirs suggest area and height errors of up to 21% and 20 cm, respectively for reservoirs below 1 km^2 and decrease exponentially above this size. Other theoretical and actual reservoir tests revealed that reservoir shape, orientation, topography, and partial swath coverage play a greater role than size in area and height errors for more extreme reservoir geospatial configurations. Although improvements to SWOTsim may lead to changes in some of the results shown here, by providing the first realistic estimate of anticipated SWOT reservoir results globally, our findings should serve as a template for future reservoir observations from SWOT upon launch. Furthermore, the findings are useful for improving data processing techniques in the instance of SWOT observations of reservoirs with extreme spatial characteristics. For example, reservoirs with a narrow shape that are oriented extremely parallel to orbit should be treated differently based on the results in the third chapter.

In the fourth chapter, I assessed the sustainability of current water management systems by comparing consumptive water use to total water availability derived from GRACE. Median parameter value results show sustainable water use to only be an issue for the southwest where mean consumptive water use was greater than 40% of total water availability and exceeded 200% in three of these basins. Moreover, maximum water use reductions of up to 67% were necessary to achieve sustainability in these areas. Despite the caveats mentioned for the parameters and spatial scale used for the analysis, the similarity in results to other studies and heavier reliance on remote sensing data indicate the established framework will be useful to improve consistency in future similar water scarcity studies, making for a more robust analysis.

5.2 Implications for Future Work

The first priority with future work for the research described in Chapter 2 is to include reservoirs in an LSM. As reservoirs have a major impact on the timing and magnitude of water fluxes across the land surface and to the atmosphere, such work is critical to better represent these exchanges in the model. Until this is achieved, the affects of existing reservoirs and those planned for the future on the local and regional climate will not be truly realized.

Given the spatiotemporal coverage of SWOT, which will be used to derive storage and discharge estimates worldwide on the order of approximately one observation per week, SWOT data will be ideal for use in different reservoir modeling applications at monthly timescales. Future SWOT reservoir data or the expected error characteristics in conjunction with reservoir observations are thus suitable for calibrating or running simulations with the newly developed reservoir model (or other reservoir models) once linked to an LSM in both a coupled and uncoupled context. This is particularly true for regions lacking in consistent reservoir observations, such as in developing countries or transboundary basins where monitoring networks and data sharing are limited. In this way, not only will the newly developed reservoir modeling system be used to evaluate reservoir management impacts of water exchanges with the land and atmosphere, but it will also demonstrate a new and important application of SWOT observations prior to launch.

Several improvements to the work described in Chapter 4 could enhance the robustness of the results. Parameter values used to determine consumptive water use and total water availability need to be better constrained both spatially and temporally.

Statistical downscaling methods could be applied to increase the spatial resolution of the estimates. Ideally, a greater number of irrigation records could be used to increase the variability in annual consumptive water use. Although not currently available for most countries at sub-national scales, models have been used for this purpose. Moreover, soil moisture data from the recently launched global Soil Moisture Active Passive (SMAP) mission provides a unique opportunity to derive high space- and time-resolution estimates of irrigation demands. The collective improvements would potentially enable a more robust comparison of consumptive water use to total water availability at smaller space and time scales. This work could be more useful to water resource managers by potentially highlighting regions with particularly chronic agricultural practices that require immediate change to increase water use sustainability including crop rotations or replacement or shifts in irrigation application techniques.

References

Akaike, H., 1974, A new look at the statistical model identification. IEEE Trans. Autom. Control. 19, 716-723.

Alcamo, J., P. Döll, T. Henrichs, F. Kaspar, B. Lehner, T. Rösch, and S. Siebert, 2003, Global estimates of water withdrawals and availability under current and future "business-as- usual" conditions. Hydrol. Sci. J., 48: 339–348.

Alcamo, J., M. Flörke, and M. Märker, 2007, Future long-term changes in global water resources driven by socio-economic and climatic changes, Hydrol. Sci. J., 52, 247–275.

Alsdorf, D. E., E. Rodriguez, and D. P. Lettenmaier, 2007, Measuring surface water from space, Reviews of Geophysics, 45.

Andreadis, K. M., E. A. Clark, D. P. Lettenmaier, and D. E. Alsdorf, 2007, Prospects for river discharge and depth estimation through assimilation of swath-altimetry into a raster-based hydrodynamics model, Geophys. Res. Lett., 34.

Barnett, T.P., Pierce, D.W., Hidalgo, H.G., Bonfils, H., Santer, B.D., Das, T., Govindasamy, B., Wood, A.W., Nozawa, T., Mirin, A.A., Cayan, D.R., Dettinger, M.D., 2008. Human-induced changes in the hydrology of the western United States. Science 319, 1080-1083.

Baros, N., J. J. Cole, L. J. Tranvik, Y. T. Prairie, D. Bastviken, V. L. M. Huszar, P. del Giorgio, and F. Roland, 2011, Carbon emission from hydroelectric reservoirs linked to reservoir age and latitude, 4, 593-596.

Bednarek, A. T., 2001, Undamming Rivers: A review of the ecological impacts of dam removal, Environ. Manage., 27, 803-814.

Biancamaria, S., K. M. Andreadis, M. Durand, E. A. Clark, E. Rodriguez, N. M. Mognard, D. E. Alsdorf, D. P., Lettenmaier, and Y. Oudin, 2010, Preliminary characterization of SWOT hydrology error budget and global capabilities, Journal of Selected Topics in Applied Earth Observations and Remote Sensing, 3: 6-19.

Biancamaria, S., F. Hossain, and D.P. Lettenmaier, 2011, Forecasting transboundary river water elevations from space. Geophysical Research Letters, 38: 1–5.

Biancamaria, S., D. P. Lettenmaier, and T. M. Pavelsky, 2015, The SWOT mission and capabilities for land hydrology, Surveys in Geophysics, 3269-3298.

Biemans, H., Haddeland, I., Kabat, P., Ludwig, F., Hutjes, R.W.A., Heinke, J., von Bloh, W., Gerten, D., 2011. Impact of reservoirs on river discharge and irrigation water supply during the 20th century. Water Resour. Res. 47, 1-15.

California Department of Water Resources (DWR), 2013, Brush, C.F., Dogrul, E.C., Kadir, T.N., Development and Calibration of the California Central Valley Groundwater-Surface Water Simulation Model (C2VSim), Version 3.02-CG.

Castle, S. L., B. F. Thomas, J. R. Reager, S. C. Swenson, M. Rodell, and J. S. Famiglietti, 2014, Groundwater depletion during drought threatens future water security of the Colorado River Basin, Geophys. Res. Lett., 41: 5904-5911.

Castle, S.L., J. T. Reager, B. F. Thomas, A. J. Purdy, M.-H. Lo, J. S. Famiglietti, and Q. Tang, 2015, Remote detection of water management impacts in the Colorado River Basin, in review, Geophys. Res. Lett 41.

Cayan, D. R., Maurer, E.P., Dettinger, M.D., Tyree, M., Hayhoe, K., 2008. Climate change scenarios for the California region. Clim. Change 87, 21-42.

Chao, B. F., Y. H. Wu, and Y. S. Li, 2008, Impact of artificial reservoir water impoundment on global sea level, Science, 320: 212-214.

Christensen, N. S., and D. P. Lettenmaier, 2007, A multimodel ensemble approach to assessment of climate change impacts on the hydrology and water resources of the Colorado River Basin, Hydrol. Earth Syst., 11: 1417–1434.

Cooke, G.D., E. B. Welch, S. A. Peterson, and S. A. Nichols (2005), Restoration and management of lakes and reservoirs, 3rd ed., Taylor and Francis, Boca Raton, FL, USA, 601 p.

Costanza, R., R. Arge, R. de Groot, S. Farber, M. Grasso, B. Hannon, K. Limburg, Naeem, R. V. O'Neill, J. Paruelo, R. G. Raskin, and P. Sutton, 1997, The value of the world's ecosystem services and natural capital, Nature, 387: 253–260.

Costanza, R., I. Kubiszewski, D. Ervin, R. Bluffstone, J. Boyd, D. Brown, H. Chang, V. Dujon, E. Granek, S. Polasky, V. Shandas, and A. Yeakley, 2011, Valuing ecological systems and services. F1000 Biol. Rep., 6: 1–6.

Crétaux, J.F., S. Biancamaria, A. Adalbert, M. Bergé-Hguyen, and B. Mélanie, 2015, Global surveys of reservoirs and lakes from satellites and regional application to the Syrdarya river basin., Environ. Res. Lett., 10, 1-13.

Cullen P., 2001, The future of flow restoration in Australia, WaterShed, September: 1-2.

Degu, A. M., F. Hossain, D. Niyogi, R. Pielke, J. M. Shepard, N. Voisin, and T. Chronis, 2011, The influence of large dams on surrounding climate and precipitation patterns, Geophys. Res. Lett., 38, L04405.

Döll, P., and S. Siebert, 2002, Global modeling of irrigation water requirements, Water Resources Research, 38: 1-10.

Döll, P., Hoffman-Dobrev, H., Portmann, F.T., Siebert, S., Eicker, A., Rodell, M., Strassberg, G., Scanlon, B.R., 2012. Impact of water withdrawals from groundwater and surface water on continental water storage variations. J. Geodyn. 59-60, 143-156.

Döll, P., H, M. Schmied, C. Schuh, F. T. Portmann, and A. Eicker, 2014, Global-scale assessment of groundwater depletion and related groundwater abstractions: combining hydrological modeling with information from well observations and GRACE satellites, Water Resour. Res., 50: 5698-5720.

Draper, A.J., A. Munevar, S.K. Arora, E. Reyes, N.L. Parker, F.I. Chung, and L.E. Peterson, 2004, CalSim: Generalized model for reservoir system analysis. J. Water Res. Plan. Manag. 130, 480-489.

Durand, M., K. M. Andreadis, D. E. Alsdorf, D. P. Lettenmaier, D. Moller, and M. Wilson, 2008, Geophys. Res. Lett., 35.

Durand, M., E. Rodriguez, D. E. Alsdorf, and M. Trig (2010), Estimating river depth from remote sensing interferometry measurements of river height, slope, and width, IEEE J. Sel. Topics Appl. Earth Observat. Remote Sens., 3: 20-31.

Eilander, D., F. O. Annor, L. Iannini, and N. van de Giesen, 2014, Remotely sensed monitoring of small reservoir dynamics: a Bayesian approach, Remote Sens., 6: 1191-1210.

Falkenmark, M., 1989, The massive water scarcity now threatening Africa: Why isn't it being addressed? Ambio, 18: 112–118.

Famiglietti, J. S., M. Lo, S. L. Ho, J. Bethune, K. J. Anderson, T. H. Syed, S. C. Swenson, C. R. de Linage, and M. Rodell, 2011, Satellites measure recent rates of groundwater depletion in California's Central Valley, Geophysical Research Letters, 38.

Famiglietti, J. S., 2014, The global groundwater crisis, Nat. Clim. Change., 4, 945-948.

Famiglietti, J. S., A. Cazenave, A. Eickler, J. T. Reager, M. Rodell and I. Velicogna, 2015, Satellites provide the 'big picture,' Science, August 14, 2015.

FAO, 2012, Irrigation water requirement and water withdrawal by country, K. Frenken and V. Gillet (authors), Food and Agriculture Organization of the United Nations, Rome, Italy., 263 p.

Fekete, B. M., Wisser, D., Kroeze, C., Mayorga, E., Bouwman, L. Wollheim, W.M., C.J. Vorosmarty, 2010, Millennium Ecosystem Assessment scenario drivers (1970 - 2050): Climate and hydrological alterations. Glob. Biogeochem. Cycles 24, 1-12.

Findlay, S., 1995, Importance of surface-subsurface exchange in stream ecosystems: The hyporheic zone, Limnol. Oceanogr.. 40, 159-164.

Fjørtoft, R., J-M. Gaudin, N. Pourthié, J-C. Lalaurie, A. Mallet, J-F. Nouvel, J. Martinot-Lagarde, H. Oriot, P. Borderies, C. Ruiz, and S. Daniel, 2014, KaRIn on SWOT: Characteristics of Near-Nadir Ka-Band Interferometric SAR Imagery, IEEE Trans. Geosci. Remote Sens., 52: 2172-2185.

Gao, H., C. Birkett, and D. P. Lettenmaier, 2012, Global monitoring of large reservoir storage from satellite remote sensing. Water Resour. Res. 48, 1-12.

Gleeson, T., Y. Wada, M. F. P. Bierkens, and L. P. H. van Beek, 2012, Water balance of global aquifers revealed by groundwater footprint, Nature, 400, 197-200.

Gleick, P.H., 1992, Environmental consequences of hydroelectric development: the role of facility size and type. Energy 17, 735-747.

Gleick, P. H., 2000, A look at twenty-first century water resources development, Water Int., 25, 127-138.

Google earth V. 7.1.5.1557. (July 10, 2013). 39°46'55.48"N 122° 20'44.42"W, eye alt 42,122 ft, http://www.earth.google.com [November 17, 2015].

Gordon, L. J., W. Steffen, B. F. Jönsson, C. Folke, M. Falkenmark, and Å. Johannessen, 2005, Human modification of global water vapor flows from the land surface, Proc. Nat. Acad. Sci., 102, 7612-7617.

Graf, W.L., 1999, Dam nation: A geographic census of American dams and their large-scale hydrologic impacts. Water Resour. Res. 35, 1305-1311.

Haddeland, I., Skaugen, T., Lettenmaier, D.P., 2006. Anthropogenic impacts on continental surface water fluxes. Geophys. Res. Lett. 33, 1-4.

Haddeland, I., et al., 2014, Global water resources affected by human interventions and climate change, Proc. Natl. Acad. Sci., 2014, 111: 3251-3256.

Hanasaki, N., S. Kanae, and T. Oki, 2006, A reservoir operation scheme for global river routing models. J. of Hydrol. 327, 22-41.

Hanasaki, N., S. Kanae, T. Oki, K. Masuda, K. Motoya, N. Shirakawa, Y. Shen, and K. Tanaka, 2008, An integrated model for the assessment of global water resources – Part 1: Model description and input meteorological forcing, Hydrol. Earth Syst. Sci., 12: 1007-1025.

Hayhoe, K., D.R. Cayan, C.B. Field, P.C. Frumhoff, E.P. Maurer, N.L. Miller, S.C. Moser, S.H. Schneider, K.N. Cahill, E.E. Cleland, L. Dale, R. Drapek, R.M. Hanemann, L.S. Kalkstein, J. Lenihan, C.K. Lunch, R.P. Neilson, S.C. Sheridan, and J.H. Verville, 2004. Emissions

pathways, climate change, and impacts on California. Proc. Natl. Acad. of Sci. 101, 12,422–12,427.
Hoekstra, A. Y., M. M. Mekonnen, A. K. Chapagain, R. E. Mathews, and B. D. Richter, 2012, Global monthly water scarcity: blue water footprints versus blue water availability, PLoS ONE, 7: 1–9.
Hossain, F., 2010, Empirical relationship between large dams and the alteration in extreme precipitation, Nat. Hazards, 11, 97-101.
Jelks, H. L., S. J. Walsh, N. M. Burkhead, S. Contreras-Balderas, E. Díaz-Pardo, D. A. Hendrickson, J. Lyons, N. E. Mandrak, F. McCormick, J. S. Nelson, S. P. Platania, B. A. Porter, C. B. Renaud, J. J. Schmitter-Soto, E. B. Taylor, and M. L. Warren, 2008, Conservation status of imperiled North American freshwater and diadromous fishes, Fisheries, 33: 372-407.
Jenkins, M.W., A.J. Draper, J.R. Lund, R.E. Howitt, S.K. Tanaka, R.S. Ritzema, G.F. Marques, S.M. Msangi, B.D. Newlin, B.J. van Lienden, M.D. Davis, K.B. Ward, 2001, Improving California water management: optimizing value and flexibility, CALFED Bay-Delta Program, Sacramento.
Kenny, J. F., N. L. Barber, S. S. Hutson, K. S. Linsey, J. K. Lovelace, and M. A. Maupin, Estimated use of water in the United States in 2005: U. S. Geological Survey Circular 1344, 52 p.
Krause, P., D.P. Boyle, and F. Base, 2005, Comparison of different efficiency criteria for hydrological model assessment. Adv. Geosci. 5, 89-97.
Kuczera, G., and M. Mroczkowski, 2010, Assessment of hydrologic parameter uncertainty and the worth of multiresponse data. Water Resour. Res. 34, 1481-1489.
Kumar, S. V., C. D. Peters-Lidard, J. A. Santanello, R. H. Reichle, C. S. Draper, R. D. Koster, G. Nearing, and M. F. Jasinski, 2015, Evaluating the utility of satellite soil moisture retrievals over irrigated areas and the ability of land data assimilation methods to correct for unmodeled processes, Hydrol. Earth Syst. Sci. Discuss., 12, 5967-6009.
Kustu, M. D., Y. Fan, and A. Robock, 2010, Large-scale water cycle perturbation due to irrigation pumping in the US High Plains: A synthesis of observed streamflow changes, J. Hydrol., 390, 222-244.
Lee, H., M. Durand, H. C. Jung, D. E. Alsdorf, C. K. Shum, and Y. Sheng, 2014, Characterization of surface water storage changes in Arctic lakes using simulated SWOT measurements, International Journal of Remote Sensing, 31: 3931-3953.
Lehner, B., C. R. Liermann, C. Revenga, C. J. Vorosmarty, B. Fekete, P. Crouzet, P. Doll, M. Endejan, K. Frenken, J. Magome, C. Nilsson, J. C. Robertson, R. Rödel, N. Sindorf, and D. Wisser, 2011, High-resolution mapping of the world's reservoirs and dams for sustainable river-flow management. Front. Ecol. Environ. 9, 494-502.
Liermann, C. R., J. Robertson, and R. Y. Ng, 2012, Implications of dam obstruction for global freshwater fish diversity, BioSci., 62, 539-548.
Lo, M-H., and J. S. Famiglietti, 2013, Irrigation in California's Central Valley strengthens the southwestern U.S. water cycle, Geophys. Res. Lett., 40.
Long, D. B. R. Scanlon, L. Longuevergne, A. Y. Sun, D. N. Fernando, H. Save, 2013, GRACE satellite monitoring of large depletion in water storage in response to the 2011 drought in Texas, Geophysical Research Letters, 40: 3395-3401.

Maupin, M. A., J. F. Kenny, S. S. Hutson, J. K. Lovelace, N. L. Barber, and K. S. Linsey, 2014, Estimated use of water in the United States in 2010: U. S. Geological Survey Circular 1405, 56 p.

Meigh, J. R., A. A. McKenzie, and K. J. Sene, 1999, A grid-based approach to water scarcity estimates for eastern and southern Africa, Water Resour. Manage., 13: 85-115.

Merrit, D. M., and N. L. Poff, 2010, Shifting dominance of riparian Populus and Tamarix along gradients of flow alteration in western North American rivers, Ecol. Appl., 20, 135-152.

Milly, P. C. D., J. Betancourt, M. Falkenmark, R. M. Hirsch, Z W. Kundzewicz, D. P. Lettenmaier, and R. J. Stouffer, 2008, Stationarity is dead: Whither water management? Science, 319, 573-574.

Minear, J.T., Kondolf G.M., 2009, Estimating reservoir sedimentation rates at large spatial and temporal scales: A case study of California. Water Resour. Res., 45, 1-8.

Mitchell, K. E., D. Lohmann, P. R. Houser, E. F. Wood, J.C. Schaake, A Robock, B.A. Cosgrove, J. Sheffield, Q. Duan, L. Luo, R. W. Higgins, R. T. Pinker, J. D. Tarpley, D. P. Lettenmaier, C H. Marshall, J. K. Entin, M. Pan, W. Shi, V. Koren, J. Meng, B. H. Ramsay, and A. A. Bailey, 2004, The multi-institution North American Land Data Assimilation System (NLDAS): Utilizing multiple GCIP products and partners in a continental distribtuted hydrological modeling system, J. Geophys. Res., 109, D07S90.

Moller, D., K. Andreadis, E. Rodriguez, X. Wu, and D. Alsdorf, 2010, A virtual mission to estimate discharge using assimilation of high-resolution simulated SWOT data: initial results over the Ohio River, Proceedings SPIE, 7826.

Mote, P., 2006, Climate-driven variability and trends in mountain snowpack in western North America. J. Climate, 19, 6209-6220.

Moyle, P. B., J. V. E. Katz, and R. M. Quiñones, 2011, Rapid decline of California's native inland fishes: A status assessment, Biol. Conserv., 144: 2414-2423.

Munier, S., A. Polebistki, C. Brown, G. Belaud, and D. P. Lettenmaier, 2015, SWOT data assimilation for operational reservoir management on the upper Niger River Basin, Water Resources Research, 51: 554-575.

Nash, J.E., and J.V. Sutcliffe, 1970, River flow forecasting through conceptual models part I – A discussion of principles. J. Hydrol., 10, 282-290.

Nazemi, A., Wheater, H.S., 2015a, On inclusion of water resource management in Earth System models – Part 1: Problem definition and representation of water demand, Hydrol. Earth Syst. Sci., 19: 33-61.

Nazemi, A., Wheater, H.S., 2015b, On inclusion of water resource management in Earth System models – Part 2: Representation of water supply and allocation and opportunities for improved modeling, Hydrol. Earth Syst. Sci., 19: 63-90.

Nelder, J.A., R. Mead, R., 1965. A simplex method for function minimization. Computer Journal, 7, 308-313.

NOAA National Climatic Data Center, State of the Climate: Drought for March 2014, published online April 2014, retrieved on September 8, 2014 from http://www.ncdc.noaa.gov/sotc/drought /2014/3.

Oki, T., and S. Kanae, 2006, Global hydrological cycles and world water resources, Science, 313: 1068–1072.

Pahl-Wostl, C., A. Arthington, J. Bogardi, S. E. Bunn, H. Hoff, L. Lebel, E. Nikitina, M. Palmer, L. N. Poff, K. Richards, M. Schlüter, R. Schulze, A. St-Hillaire, R. Tharme, K. Tockner,

and D. Tsegai, 2013, Curr. Opin. Environ. Sustain., Environmental flows and water governance: managing sustainable water uses, 5: 341-351.

Pavelsky, T. M., M. T. Durand, K. M. Andreadis, R. E. Beighley, R. C. Paiva, G. H. Allen, and Z. F. Miller, 2014, Assessing the potential global extent of SWOT river discharge observations, J. Hydrol., 519, 1516-1525.

Peral, E., E. Rodriguez, D. Moller, M. McAdams, M. Johnson, K. Andreadis, D. Arumugam, 2012, SWOT L1b Hydrology Simulator User Guide, Version 2.1, Jet Propulsion Laboratory, Pasadena, CA.

Poff, N. L., and J. K. H. Zimmerman, 2010, Ecological responses to altered flow regimes: a literature review to inform the science and management of environmental flows, Freshwater Biol., 55, 194-205.

Pokhrel, Y., N. Hanasaki, S. Koirala, J. Cho, P.J.-F. Yeh, H. Kim, S. Kanae, and T. Oki, 2012, Incorporating anthropogenic water regulation modules into a land surface model, J. Hydrometeor., 13, 255-269.

PRISM Climate Group, Oregon State University, http://prism.oregonstate.edu, created 4 Feb 2004.

Revenga, C., I. Campbell, R. Abell, P. de Villiers, and M. Bryer, 2005, Prospects for monitoring freshwater ecosystems towards the 2010 targets. Philos. Trans. Royal Soc. Biol. Sci. 360, 397-413.

Richey, A. S., B. F. Thomas, M.-H. Lo, J. T. Reager, K. A. Voss, M. Rodell, S. Swenson, and J. S. Famiglietti, 2015, Quantifying renewable groundwater stress with GRACE, Water Resour. Res., 51, 5217-5238.

Richter, B. D., J. V. Baumgartner, J. Powell, and D. P. Braun, 1996, A method for assessing hydrologic alteration within ecosystems, Conservation Biology, 1163–1174.

Richter, B. D., S. Postel, C. Revenga, T. Scudder, B. Lehner, A. Churchill, and M. Chow, 2010, Lost in development's shadow: the downstream human consequences of dams, Water Alt., 2010, 3, 14-42.

Rockström, J., M. Falkenmark, L. Karlberg, H. Hoff, S. Rost, and D. Gerten, 2009, Future water availability for global food production: the potential of green water for increasing resilience to global change. Water Resources Research, 45: 1–16.

Rodell, M., I. Velicogna, and J. S. Famiglietti, 2009, Satellite-based estimates of groundwater depletion in India, Nature, 460: 999-1002.

Rodell, M., and J. S. Famiglietti, 2001, An analysis of terrestrial water storage variations in Illinois with implications for the Gravity Recovery and Climate Experiment (GRACE), Water Resour. Res., 37, 1327-1339.

Rodriguez, E., and D. Moller, 2004, Measuring surface water from space, EOS Trans. AGU, 85, Fall Meet. Suppl., Abstract H22C-08.

Rodriguez, E., 2015, SWOT Science Requirements Document, JPL Document D-61923, http://swot.jpl.nasa.gov/files/SWOT_science_reqs_final.pdf, accessed 6 February 2016.

Rost, S., D. Gerten, A. Bondeau, W. Lucht, J. Rohwer, and S. Schaphoff, 2008, Agricultural green and blue water consumption and its influence on the global water system, Water Resour. Res., 44: 1-17.

Schewe, J., J. Heinke, D. Gerten, I. Haddeland, N. W. Arnell, D. Clark, R. Dankers, S. Eisner, B. Fekete, F. J. Colón-González, S. Gosling, H. Kim, X. Liu, Y. Masaki, F. T. Portmann, Y. Satoh, T. Stacke, Q. Tang, Y. Wada, D. Wisser, T. Albrecht, K. Frieler, F. Piontek, L.

Warszawski, P. Kabat, 2014, Multimodel assessment of water scarcity under climate change, Proceedings of the National Academy of Sciences, 111: 3245-3250.
Schneider, P., and S. J. Hook, 2010, Space observations of inland water bodies show rapid surface warming since 1985, Geophys. Res. Lett. 37 doi:10.1029/2010GL045059.
Smakhtin, V., C. Revenga, and P. Döll, 2004, A pilot global assessment of environmental water requirements and scarcity, Water International, 29: 3107-317, doi: 10.1080/02508060408691785.
Smakhtin, V., C. Revenga, and P. Döll, 2004b, Taking into account environmental water requirements in global-scale water resources assessments, Comprehensive Assessment Research Rep. 2, Comprehensive Assessment Secretariat, Colombo, Sri Lanka, 22.
Smith, L. and T. Pavelsky, 2009, Remote sensing of volumetric storage changes in lakes, Earth Surf. Process. Landforms, 34, 1353-1358.
Swain, D. L., M. Tsiang, M. Haugen, D. Singh, A. Charland, B. Rajaratnam, and N. S. Diffenbaugh, 2014, The extraordinary California drought of 2013/2014: Character, context, and the role of climate change, Bull. Am. Meteorol. Soc., 95: S3-S7.
Syed, T.H., J.S. Famiglietti, D.P. Chambers, J.K. Willis, and K. Hilburn, 2010, Satellite-based global-ocean mass balance estimates of interannual variability and emerging trends in continental freshwater discharge, Proc. Natl. Acad. Sci. USA, 42, 17,916 – 17,921.
Tapley, B. D., S. Bettadpur, J. C. Ries, P. F. Thompson, and M. M. Watkins, 2004, GRACE Measurements of mass variability in the Earth System, Science, 305: 21–24.
Tenant, D., 1976, Instream flow regimens for fish, wildlife, recreation and related environmental resources, Fisheries, 1: 6-10.
Thomas, A. C., J. T. Reager, J. S. Famiglietti, and M. Rodell, 2014, A GRACE-based water storage deficit approach for hydrological drought characterization. Geophysical Research Letters, 41: 1537–1545.
United States Geological Survey (USGS), 1983, National water summary 1983 – hydrologic events and issues, USGS Water-Supply Paper 2250, 243 p.
Villar, P. C., and W. C. Ribeiro, 2011, The agreement on the Guarani Aquifer: a new paradigm for transboundary groundwater management, Water Int., 36, 646-660.
Vanrheenen, N.T., A.W. Wood, R.N. Palmer, and D.P. Lettenmaier, D.P., 2004, Potential implications of PCM climate change scenarios for Sacramento-San Joaquin river basin hydrology and water resources. Clim. Change 62, 257-281.
Vörösmarty, C.J., K.P. Sharma, B.M. Fekete, A.H. Copeland, J. Holden, J. Marble, J.A. Lough, 1997, The storage and aging of continental runoff in large reservoir systems of the world. Ambio, 26, 210-219.
Vörösmarty, C. J., P. Green, J. Salisbury, and R. B. Lammers, 2000, Global Water Resources: Vulnerability from climate change and population growth, Science, 289: 284–289.
Vörösmarty, C. J., P. B. Mcintyre, M. O. Gessner, D. Dudgeon, A. Prusevich, P. Green, S. Glidden, S. E. Bunn, C. A. Sullivan, C. R. Leirmann, and P. M. Davies, 2010, Global threats to human water security and river biodiversity, Nature, 467: 555–561.
Voss, K. A., J. S. Famiglietti, M.-H. Lo, C. R. de Linage, M. Rodell, and S. C. Swenson, 2013, Groundwater depletion in the Middle East from GRACE with implications for transboundary water management in the Tigris-Euphrates-Western Iran Region, Water Resour. Res., 49: 904-914.

Vrugt, J.A., Gupta, H.V., Bastidas, L.A., Bouten, W., Sorooshian, S., 2003, Effective and efficient algorithm for multiobjective optimization of hydrologic models. Water Resour. Res., 39, 1214.

Wada, Y., L. P. H. van Beek, D. Viviroli, H. H. Dürr, R. Weingartner, and M. F. P. Bierkens, 2011, Global monthly water stress: 2. Water demand and severity of water stress, Water Resour. Res., 47: 1-17.

Wada, Y., and M. F. P. Bierkens, 2014, Sustainability of global water use: past reconstruction and future projections. Environmental Research Letters, 9: 1–17, doi: 10.1088/1748-9326/9/10/104003.

Wheater, H., Gober, P., 2013, Water security in the Canadian Prairies: science and management challenges, Phil. Trans. R. Soc. A., 371: p. 20120409.

Wild, T. B., and D. P. Loucks, 2014, Managing flow, sediment and hydropower regimes in the Sre Pok, Se San, and Se Kong Rivers of the Mekong basin, Water Resour. Res., 50, 5141-5157.

Williamson, C.E., J. E. Saros, and D. W. Schindlerm, 2009, Sentinels of change, Science, 323: 887-888.

Willis, A.D., Lund, J.R., Townsley, E.S., Faber, B.A., 2011, Climate change and flood operations in the Sacramento Basin, California, San Francisco Estuary and Watershed Science. 1-18.

Wisser, D., Fekete, B.M., Vorosmarty, C.J., Schumann, A.H., 2010, Reconstructing 20th century global hydrography: a contribution to the Global Terrestrial Network – Hydrology (GTN-H). Hydrol. Earth Syst. Sci. Discuss. 14, 1-24.

Wisser, D., Frolking, S., Hagen, S., Bierkens, M.F.P., 2013, Beyond peak reservoir storage? A global estimate of declining water storage capacity in large reservoirs. Water Resour. Res. 49, 1-8.

World Commission on Dams, 2000, Dams and development: a framework for decision making. Earthscan Publications: London, UK.

Yates, D., Sieber, J., Purkey, D., Huber-Lee, A., 2005, WEAP21 - A demand-, priority-, and preference-driven water planning model. Water Int. 30, 487-500.

Yeh, P. J. F., S. C. Swenson, J. S. Famiglietti, and M. Rodell, 2006, Remote sensing of groundwater storage changes in Illinois using the Gravity Recovery and Climate Experiment (GRACE), Water Resour. Res., 42.

Yoon, Y., and E. Beighley, 2014, Simulating streamflow on regulated rivers using characteristic reservoir storage patterns derived from synthetic remote sensing data, Hydrol. Process., 29: 2014-2026.

Zarfl, C., A. E. Lumsdon, J. Berlekamp, L. Tydecs, K. Tockner, 2014, A global boom in hydropower dam construction, Aquat. Sci., 77, 161-170.

Zhang, J., K. Xu, Y. Yang, L. Qi, S. Hayashi, and M. Watanabe, 2006, Measuring water storage fluctuations in Lake Dongting, China, by TOPEX/POSEIDON satellite altimetry, Environmental Monitoring and Assessment, 115: 23-37.

APPENDIX A

Table A1 SWOTsim Instrument Simulator Settings and Parameters

Setting or Parameter	Value
RESOLUTION GEOMETRY	
Azimuth Spacing (m)	30
Swath Width (m)	140,000
Ground Spacing (m)	30
Number of Landtypes	2 (water and land)
Near Range (m)	895,810
Number of Interferogram Pixels	3,860
RADAR PARAMETERS	
Peak Transmit Power (W)	1,500
Receive Noise Figure (dB)	8.
System Loss (dB)	4.5
Point Target Response Range Length (m)	3
Operational Mode	NPP
BEAM PARAMETERS	
Wavelength (m)	0.0084
Pulse Repetition Frequency (PRF) [Hz]	4,420
Pulse Duration (us)	4.5
Signal Bandwidth (MHz)	200
Sampling Frequency (MHz)	200
Velocity (m/s)	7,415.3
Ground Velocity (m/s)	6,506.4
Percent Processing Pulse Repetition Frequency (PRF) bandwidth (%)	100
Integrated Sidlobe Ratio (ISLR) [dB]	13.0
Baseline (m)	10.0
Polarization	Horizontal
System Noise Temperature (K)	3,681.79